PhD Thesis

Institute of Physical Chemistry
Polish Academy of Sciences
Kasprzaka 44/52
01-224 Warsaw, Poland

PhD Thesis

Chemical sensors with molecularly imprinted polymers as recognition units for determination of selected compounds of health importance

Zofia Iskierko

Supervisor
Prof. Włodzimierz Kutner, Ph.D., D.Sc.

Auxiliary supervisor
Krzysztof Noworyta, Ph.D.

The dissertation prepared within the International Ph.D. in Chemistry Studies at the Institute of Physical Chemistry of the Polish Academy of Sciences in Warsaw in the Group of Molecular Films Research led by Prof. Włodzimierz Kutner

Warsaw, April 2017

“Może to wszystko
dzieje się w laboratorium?
Pod jedną lampą w dzień
i miliardami w nocy?”

Wisława Szymborska

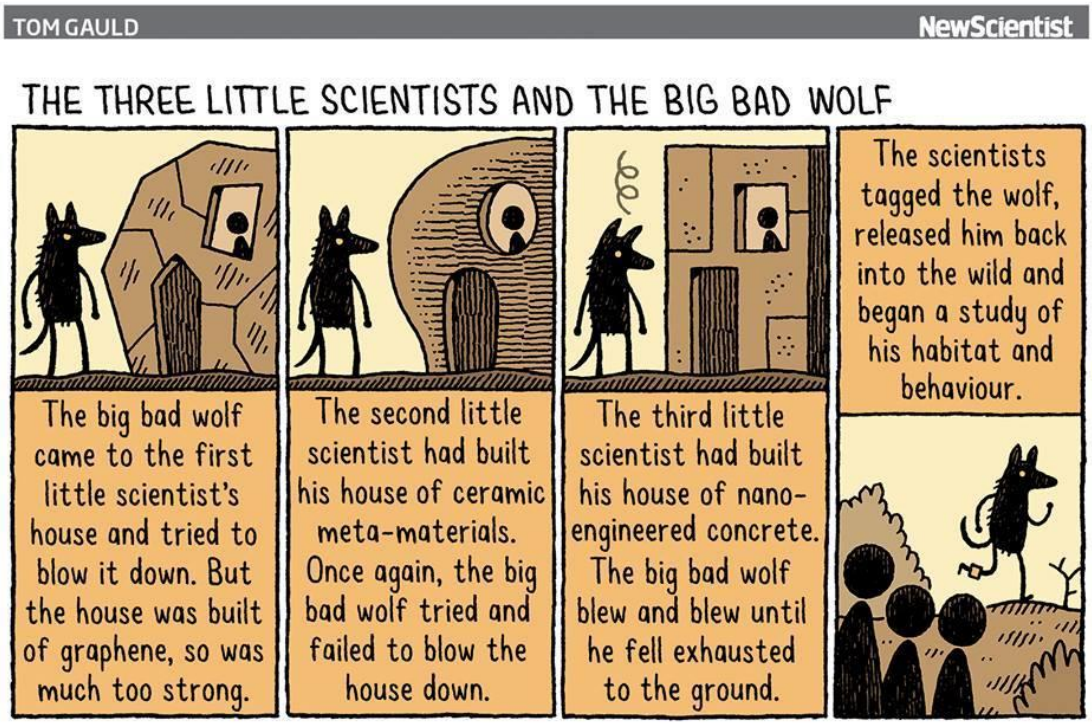

… and in the end The Three Little Scientists should prepare the house of molecularly imprinted polymers, which can selectively detect and determine the hazardous compounds of wolf's body fluids, so that they could diagnose all of his disorders and failures.

The end.

Podziękowania

Przede wszystkim chcę podziękować Michałowi, mojemu mężowi, który wspiera mnie zawsze we wszystkim i nieustannie mnie motywuje. Jestem bardzo wdzięczna swoim dzieciom, Rysiowi i Uli, dwóm najwspanialszym powodom, dla których żyję, za pozwalanie mi, od czasu do czasu, na pisanie tej pracy.

Ogromne podziękowania należą się mojej mamie, mojemu tacie i mojej teściowej, którzy zawsze chętnie pomagają nam w opiece nad dziećmi, i nie tylko, bez względu na wszystko.

Chciałabym zadedykować niniejszą pracę doktorską mojemu dziadkowi oraz teściowi, którzy czekali na moją obronę, jednak czas nie był dla nich łaskawy. Wierzę głęboko, że obydwaj wspierają mnie z góry.

Acknowledgements

First of all, I want to thank Michał, my husband, who always supports me and is my biggest motivation. I am greatly thankful to Rysio and Ula, two biggest reasons of my existence.

Big thanks are due to my mother, my father, and mother-in-law, who are always ready to help us, no matter what.

I would like to dedicate this dissertation to my grandfather and my father-in-law who were waiting for my defense, but time was too cruel for them. I truly believe, that both of them support me from above.

I would like to acknowledge gratefully my supervisors, Professor Włodzimierz Kutner, and Doctor Krzysztof Noworyta, for directing my research, valuable discussions, criticism, and patience.

I acknowledge strategic contribution of Doctor Piyush Sindhu Sharma, discussions of ideas and contributing to majority of my research activities.

I should also thank to Professor Andrzej Sadkowski, who encouraged me, in 2010, to apply for a PhD student position within International Doctoral Studies of the Institute of Physical Chemistry PAS.

Besides, I owe thanks to (in alphabetic order)

- Prof. Tiziana Benincori for providing cross-linking “T8” monomer **10**
- Prof. Alessandra Bossi for support and fruitful collaboration
- Dr. Paweł Borowicz for PM-IRRAS study
- Dr. Maciek Cieplak for helping with organic structures preparation, fruitful collaboration, and support
- Prof. Francis D’Souza for fruitful collaboration
- M.Sc. Marcin Dąbrowski for SEM imaging, support, especially in my beginnings in the new working place, and later fruitful collaboration
- Prof. Danek Elbaum for providing EG-FET system
- Dr. Krzysztof Fronc for providing EG-FET system, and explaining my first experiments with Keithley source-meter
- M.Sc. Karolina Gołębiewska for AFM imaging

- Grzegorz Krzyżewski for photography/artwork
- Dr. Agnieszka Pietrzyk-Le for fruitful collaboration and a lot of advices (also informal), she is the most friendly person I have ever met
- Dr. Daniel Prochowicz for providing MOF-5
- Dr. Anna Rola-Noworyta for great support
- Prof. Franco Sannicolò for providing cross-linking "T8" monomer **10**
- Dr. Marta Sosnowska for synthetizing functional monomers, **6**, **8**, **9**, and fruitful conversations
- Dr. Filip Stefaniak for docking simulations
- Jerzy Junosza Szaniawski for artwork
- Eng. Tadeusz Szałek for technical support
- M.Sc. Diana Toczydłowska for docking simulations
- M.Sc., Eng. Jan Zasłona for electronic technical support.

I am grateful to all members of the Group of Molecular Films Research for a great team spirit and support.

The present research was financially supported by the Polish National Science Centre, NCN, through

- Opus 1 Project „Chemosensors for selective determination of selected renal dysfunction biomarkers using molecularly imprinted polymers, deposited by electrochemical polymerization, as recognition layers", no. 2011/01/B/ST5/03796 (with Dr. Krzysztof Noworyta as the Principal Investigator) for devising chemosensors for selective determination of inosine and chemosensors for selective determination of human lipocalin-2 (NGAL), and
- Preludium 6 Project „Chemical sensors for selective determination of chosen amino acids of gluten proteins using molecularly imprinted polymers (MIPs) as recognition units", no. 2013/11/N/ST5/01907 (with me as the Principal Investigator) for devising of phenylalanine enantioselective chemosensors.

Moreover, I would like to acknowledge my participation in other projects, which broaden my knowledge in the field of molecular imprinting, namely

- „Kwantowe nanostruktury półprzewodnikowe do zastosowań w biologii i medycynie - Rozwój i komercjalizacja nowej generacji urządzeń diagnostyki molekularnej opartych o nowe polskie przyrządy półprzewodnikowe", no. POIG.01.01.02-00-008/08-00), 2008-2012, financially supported by The European Regional Development Fund
- „Selective determination of chosen oligonucleotides by synthetic polymer systems of molecular recognition" with Dr. Agnieszka Pietrzyk-Le as the Principal Investigator of the Pomost 6 project, no. POMOST/20/12-6/10, financially supported by the Foundation for Polish Science, FNP
- „Mesoporous films of molecularly imprinted conducting polymers as recognition units of chemosensors for selective determination of D-arabitol and L-arabitol – a modern tool for candidiasis diagnosis" with Marcin Dąbrowski as the Principal Investigator of the Preludium 1 grant no. 2011/01/N/ST4/03491, financially supported by the Polish National Science Centre, NCN
- „Chemical sensors for early diagnosis of autism in children" with Dr. Piyush Sindhu Sharma as the Principal Investigator of the Iuventus IV project no. IP/2014/041473, financially supported by the Ministry of Science and Higher Education of Poland, MNiSW, and
- „Determination of peptide lung cancer biomarkers by novel analytical platforms with imprinted polymers as selective recognition units" with Dr. Krzysztof Noworyta as the Principal Investigator of the Opus 8 project no. 2014/15/B/ST4/04642, financially supported by the Polish National Science Centre, NCN.

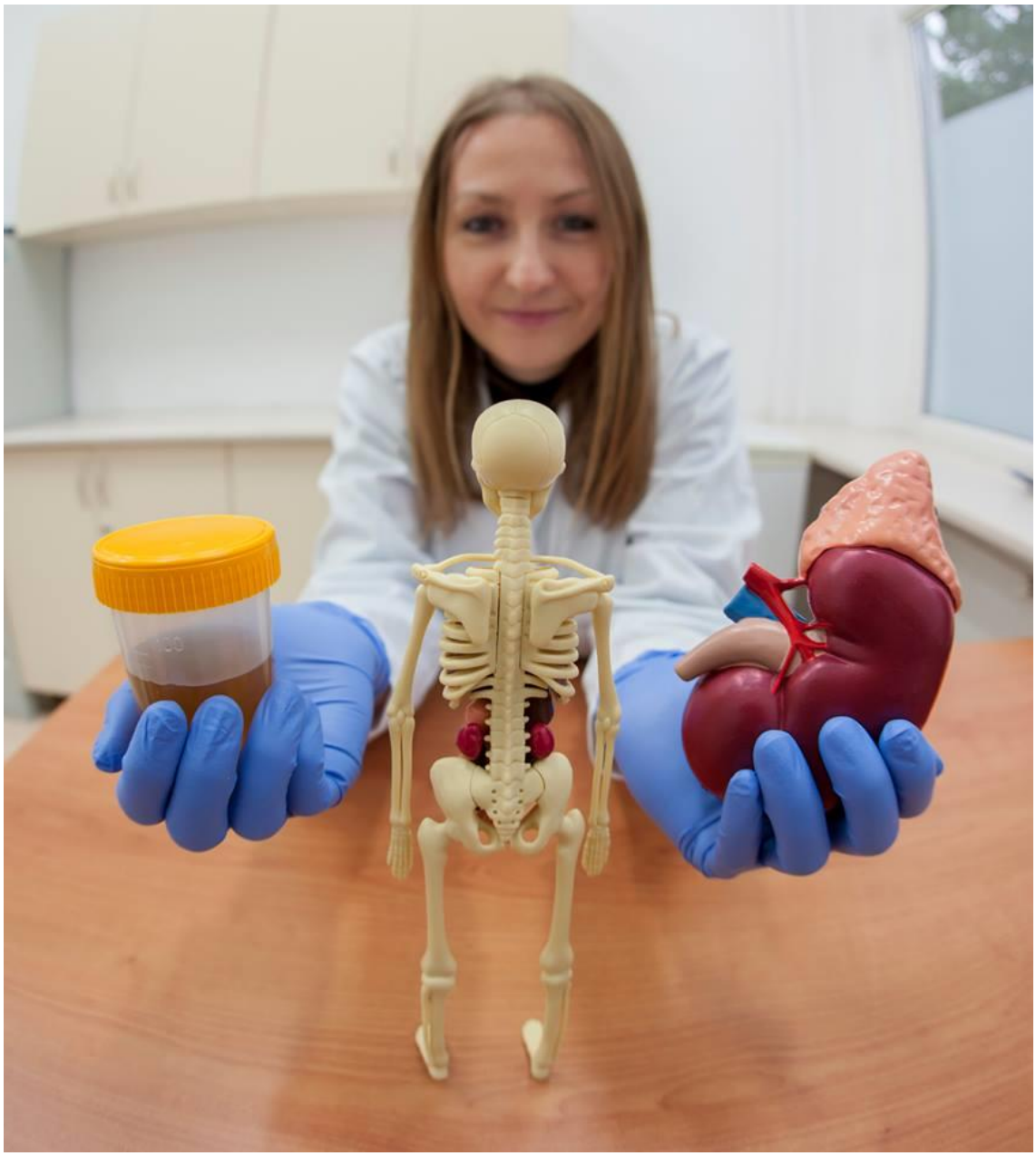

A photography by Grzegorz Krzyżewski for a press note of October 2016, http://naukawpolsce.pap.pl/aktualnosci/news,411589,nowy-polimer-ostrzeze-o-groznych-chorobach-nerek.html (in Polish), http://scienceinpoland.pap.pl/en/news/news,411868,diagnostics-of-the-future-new-polymer-warns-of-dangerous-kidney-disease.html (in English).

List of scientific achievements

Original papers included in the dissertation

(1) **Iskierko, Z.**, Sosnowska, M., Sharma, P. S., Benincori, T., D'Souza, F., Kamińska, I., Fronc, K., Noworyta, K., "Extended-gate field-effect transistor (EG-FET) with molecularly imprinted polymer (MIP) film for selective inosine determination", *Biosens. Bioelectron. 74*, **2015**, 526-533, 5-year impact factor, IF = 6.675, 9 citations.

(2) **Iskierko, Z.**, Sharma, P. S., Prochowicz, D, Fronc, K., D'Souza, F., Toczydłowska, D., Stefaniak, F., Noworyta, K., „Molecularly imprinted polymer (MIP) film with improved surface area developed by using metal-organic framework (MOF) for sensitive lipocalin (NGAL) determination", *ACS Applied Materials and Interfaces 8*, **2016**, 19860-19865, 5-year impact factor, IF = 7.145, 5 citations.

(3) **Iskierko, Z.**, Chęcińska, A., Sharma, P. S., Gołębiewska, K., Noworyta, K., Borowicz, P., Fronc, K., Bandi, V., D'Souza, F., Kutner, W., "Molecularly imprinted polymer based extended-gate field-effect transistor chemosensor for phenylalanine enantioselective sensing", *J. Mater. Chem. C 5*, **2017**, 969-977, 5-year impact factor, IF = 5.066, 1 citation.

Review papers included in the dissertation

(4) Sharma, P. S., **Iskierko, Z.**, Pietrzyk-Le, A., D'Souza, F., Kutner, W., "Bioinspired intelligent molecularly imprinted polymers for chemosensing: A mini review", *Electrochem. Commun. 50,* **2015**, 81-87, 5-year impact factor, IF = 4.820, 23 citations.

(5) **Iskierko, Z.**, Sharma, P. S., Bartold, K., Pietrzyk-Le, A., Noworyta, K., Kutner, W., "Molecularly imprinted polymers for separating and sensing of macromolecular compounds and microorganisms", *Biotechnol. Adv. 34,* **2016**, 30–46, 5-year impact factor, IF = 11.847, 10 citations.

Original papers not included in the dissertation

(6) Dąbrowski, M., Sharma, P. S., **Iskierko, Z.**, Noworyta, K., Cieplak, M., Lisowski, W., Oborska, S., Kuhn, A., Kutner, W., "Early diagnosis of fungal infections using piezomicrogravimetric and electric chemosensors based on polymers molecularly imprinted with D-arabitol", *Biosens. Bioelectron. 79,* **2016**, 627–635, 5-year impact factor, IF = 6.675, 7 citations.

(7) Sannicolò, F., Mussini, P. R., Benincori, T., Martinazzo, R., Arnaboldi, S., Appoloni, G., Panigati, M., Quartapelle Procopio, E., Marino, V., Cirilli, R., Kutner, W., Noworyta, K., Pietrzyk-Le, A., **Iskierko, Z.**, Bartold, K., "Inherently chiral spider-like oligothiophenes", *Chem. Eur. J. 22*, **2016**, 10839-10847, IF = 5.771, 5-year impact factor, IF = 5.731, 2 citations.

(8) Bartołd, K., Pietrzyk-Le, A., Huynh, T.-P., **Iskierko, Z.**, Sosnowska, M., Noworyta, K., Lisowski, W., Sannicolò, F., Cauteruccio, S., Licandro, E., D'Souza, F., Kutner, W., „Programmed transfer of sequence information into a molecularly imprinted polymer for hexakis(2,2'-bithien-5-yl) DNA analogue formation toward singe-nucleotide-polymorphism detection", *ACS Applied Materials and Interfaces 9*, **2017**, 3948–3958, 5-year impact factor, IF = 7.145, 0 citations.

(9) Sharma, P. S., **Iskierko, Z.**, Noworyta, K., Cieplak, M., Borowicz, P., Lisowski, W., D'Souza, F., Kutner, W., „Synthesis and application of a 'plastic antibody' in electrochemical microfluidic platform for oxytocin determination", *submitted manuscript*.

(10) Cieplak, M., Węgłowski, R., **Iskierko, Z.**, Węgłowska, D., Sharma, P. S., Noworyta, K., D'Souza, F., Kutner, W., „Optical chemosensor for protein determination with molecularly imprinted polymer recognition and birefringence liquid crystal detection", *submitted manuscript*.

Book chapters

(1) Sharma, P. S., **Iskierko, Z.**, D'Souza, F., Kutner, W., "Macromolecular Imprinting for Improved Health Security", chapter no. 7 in the book "Biosensors for Security and Bioterrorism Applications", p. 141-160, red. D. Nikolelis, Springer International Publishing Switzerland, 2016, ISBN 978-3-319-28924-3.

Patents awarded and patent applications

(1) **Iskierko, Z.**, Sosnowska, M., Sharma, P. S., D'Souza, F., Benincori, T., Noworyta, K., Polish Pat. Appl., No. P.408507, 11 June 2014, „Pochodne tiofenu i sposób ich otrzymywania, warstwa rozpoznającego polimeru przewodzącego wytworzonego metodą wdrukowywania molekularnego z zastosowaniem pochodnych tiofenu, sposób jej otrzymywania, jak również jej zastosowanie do selektywnego wykrywania i oznaczania inozyny.", awarded 12 December 2016 with No. 225836. (English translation of the patent title: „Derivatives of thiophene and method for obtaining them, layer of the identifying conducting polymer produced by molecular typing method using the thiophene derivatives, method for obtaining it, as well as its application for selective detection and determination of inosine").

(2) Dąbrowski, M., Sharma, P. S., Noworyta, K., Adamkiewicz, W., **Iskierko, Z.**, Heim, M., Kuhn, A., Kutner, W., Polish Pat. Appl., No. P.408290, 22 May 2014, „Warstwy rozpoznających polimerów przewodzących wytworzonych metodą wdrukowywania molekularnego i sposób ich otrzymywania, jak również ich zastosowanie do selektywnego wykrywania i oznaczania D- i L-arabitolu." (English translation of the patent title: „Layers of recognizing conducting polymers, produced by method of molecular printing and the method for obtaining them, as well as application for selective detection and determination of D- and L-arabitol").

(3) Bartołd, K., Pietrzyk-Le, A., Huynh, T.-P., **Iskierko, Z.**, Noworyta, K., Sosnowska, M., Lisowski, W., Kutner, W., D'Souza, F., Licandro, E., Sannicolò, F., Mussini, P. R., Polish Pat. Appl., No. P.409328, 29 August 2014, „Nowa sonda DNA zawierająca pochodne tiofenu i sposób jej wytwarzania, warstwa przewodzącego polimeru wdrukowywanego molekularnie z zastosowaniem tych pochodnych i sposób jej wytwarzania oraz zastosowanie tej sondy do selektywnego wykrywania i oznaczania oligonukleotydu TATAAA." (English translation of the patent title: „New DNA probe containing derivatives of thiophene and method for producing it, conductive layer of the polymer in-printed by molecular typing method using these derivatives and method for producing it, as well as the application of this probe for selective detection and determination of TATAAA oligonucleotide").

(4) **Iskierko, Z.**, Sosnowska, M., Sharma, P. S., Noworyta, K., D'Souza, F., Bandi, V., Benincori, T., Appoloni, G., Kutner, W., Polish Pat. Appl., No. P.417299, 24 May 2016, „Warstwa rozpoznająca epitop glutenu i jej otrzymywanie metodą wdrukowywania molekularnego z zastosowaniem pochodnych tiofenu, oraz zastosowanie tej warstwy do selektywnego wykrywania i/lub oznaczania glutenu występującego w zbożowych produktach spożywczych." (English translation of the patent title: „Recognition film for gluten epitope detection and method of producing of this recognition film of molecularly imprinted polymer using thiophene derivatives and application of thereof for selective detection and/or determination of gluten in cereal food products").

(5) Łach, P., Cieplak, M., Sharma, P. S., **Iskierko, Z.**, D'Souza, F., Kutner, W., Polish Pat. Appl., No. P.417300, 24 May 2016, „Chemosensor z molekularnie wdrukowanym polimerem do selektywnego oznaczania *N*-nitrozo-L-proliny." (English translation of the patent title: „Chemical sensor with molecularly imprinted polymer for selective determination *N*-nitrozo-L-proline").

(6) Cieplak, M., Węgłowski, R., **Iskierko, Z.**, Węgłowska, D., Sharma, P. S., Noworyta, K., Kutner, W., Polish Pat. Appl., No. P.418746, 19 September 2016, „Nowy selektywny czujnik optyczny do oznaczania stężenia białek, w szczególności ludzkiej albuminy, z zastosowaniem polimerów wdrukowanych molekularnie i wykorzystaniem dwójłomności ciekłych kryształów." (English translation of the patent title: „The new, selective, optical chemosensor for determination of proteins, especially human albumin, using molecularly imprinted polymers and the birefringence of the liquid crystals").

(7) Sharma, P. S., **Iskierko, Z.**, Noworyta, K., Cieplak, M., Borowicz, P., Lisowski, W., D'Souza, F., Kutner, W., ., Polish Pat. Appl., No. P.419678, 5 December 2016, „Pochodna tiofenu i sposób jej otrzymywania, warstwa rozpoznająca oksytocynę i sposób jej wytwarzania metodą wdrukowania molekularnego z zastosowaniem tej pochodnej, jak również jej zastosowanie w elektrochemicznej, mikroprzepływowej platformie." (English translation of the patent title: „Thiophene derivative and its application for preparation of selective recognition layer for oxytocin through molecular imprinting, as well as its application in electrochemical microfluidic platform for selective detection and determination of oxytocin").

Active participation in international scientific events

Oral presentations

(1) **Iskierko, Z.**, Sharma, P. S., Noworyta, K., Fronc, K., Kutner, W., „Czujniki chemiczne do oznaczania glutenu z molekularnie wdrukowywanymi polimerami (MIP) jako selektywnymi warstwami rozpoznającymi", *I Interdyscyplinarne Sympozjum Doktorantów ICHF PAN i MIBMiK*, 23-25 April 2015, Otrębusy, Poland, Institute of Physical Chemistry PAS and International Institute of Molecular and Cell Biology in Warsaw.

(2) **Iskierko, Z.**, Chęcińska, A., Sharma, P. S., Noworyta, K., Kutner, W., „Czujniki chemiczne z molekularnie wdrukowywanymi polimerami (MIP) jako warstwami rozpoznającymi do enancjoselektywnego oznaczania D- i L-fenyloalaniny", *59 Zjazd Polskiego Towarzystwa Chemicznego*, 19-23 September 2016, Poznań, Poland.

(3) **Iskierko, Z.**, Sharma, P. S., Zembrzuska, D, D'Souza, F., Kutner, W., "Molecularly imprinted polymer (MIP) as recognition unit in chemosensor for selective melatonin determination", *XXth International Winter School on Coordination Chemistry*, University of Wrocław, 5-9 December 2016, Karpacz, Poland.

Poster presentations

(1) **Iskierko, Z**., Sosnowska, M., Sharma, P. S., D'Souza, F., Noworyta, K., "Development of inosine-imprinted polymer as a recognition unit in chemosensors for early detection of renal dysfunctions", *The Sixth International Workshop on Surface Modification for Chemical and Biochemical Sensing SMCBS 2013*, Institute of Physical Chemistry PAS, 8-12 November 2013, Łochów, Poland.

(2) Bartołd, K., Huynh, T.-P., Sosnowska, M., **Iskierko, Z.**, Ciesielczuk, A., Pietrzyk-Le, A., "A molecularly imprinted polymer approach to detection of TATAAA oligonucleotide", *The Sixth International Workshop on Surface Modification for Chemical and Biochemical Sensing SMCBS 2013*, Institute of Physical Chemistry PAS, 8-12 November 2013, Łochów, Poland.

(3) **Iskierko, Z.**, Sosnowska, M., Sharma, P. S., D'Souza, F., Noworyta, K., "Early Detection of Renal Disfunctions: Development of Inosine-Imprinted Polymer as a Recognition Unit in the Extended-Gate Field-Effect Transistor Sensors", *15th International Conference of Electroanalysis ESEAC 2014*, 11-15 June 2014, Malmö, Sweden.

(4) **Iskierko, Z.**, Dąbrowski, M., Sharma, P. S., Noworyta, K., Fronc, K., Elbaum, D., Kutner, W., "Selective Determination of D-arabitol using Molecularly Imprinted Polymer based Extended-Gate Field-Effect Transistor (EG-FET) Chemosensor", *65th Annual Meeting of the International Society of Electrochemistry*, 31 August - 5 September 2014, Lausanne, Switzerland.

(5) Pietrzyk-Le, A., Bartołd, K., Huynh, T.-P., **Iskierko, Z.**, Noworyta, K., Sosnowska, M., Kutner, W., D'Souza, F., Sannicolò, F., Mussini, P. R., Licandro, E., "Determination of the TATAAA oligonucleotide via hybridization of the electrosynthesized molecularly imprinted polymer (MIP) bearing complementary adenine and thymine nucleobases", *65th Annual Meeting of the International Society of Electrochemistry*, 31 August - 5 September 2014, Lausanne, Switzerland.

(6) **Iskierko, Z.**, Sosnowska, M., Sharma, P. S., D'Souza, F., Noworyta, K., "Development of Inosine-Imprinted Polymer as a Recognition Unit in the Extended-Gate Field-Effect Transistor Sensors", *2nd Cambridge-Warsaw Young Scientists Meeting CWM 2014*, Cambridge University, 13-16 September 2014, Cambridge, United Kingdom.

(7) **Iskierko, Z.**, Sharma, P. S., Prochowicz, D., Fronc, K., Noworyta, K., "Molecularly imprinting polymer (MIP) as the artificial receptor in a chemosensor for lipocalin-2 determination", *Frontiers in polymer science*, Elsevier, 20-22 May 2015, Riva del Garda, Italy.

(8) **Iskierko, Z.**, Chęcińska, A., Sharma, P. S., Noworyta, K., Fronc, K., Kutner, W., "Extended-gate field-effect transistor (EG-FET) as the transducer in a chemosensor for stereoselective D- and L-phenylalanine determination", *17th Topical Meeting of the International Society of Electrochemistry*, 31 May - 3 June 2015, Saint-Malo, France.

(9) Chęcińska, A., **Iskierko, Z.**, Sharma, P. S., Noworyta, K., Fronc, K., D'Souza, F., Kutner, W., "Extended-gate field-effect transistor (EG-FET) as the transducer in a chemosensor for stereoselective D- and L-phenylalanine determination", *The Seventh International Workshop on Surface Modification for Chemical and Biochemical Sensing SMCBS 2015*, Institute of Physical Chemistry PAS, 6-10 November 2015, Pułtusk, Poland.

(10) **Iskierko, Z.**, Sosnowska, M., Sharma, P. S., D'Souza, F., Fronc, K., Noworyta, K., Kutner, W., "Chemical sensor for selective determination of gluten proteins using molecularly imprinted polymers (MIPs) as recognition units", *The Seventh International Workshop on Surface Modification for Chemical and Biochemical Sensing SMCBS 2015*, Institute of Physical Chemistry PAS, 6-10 November 2015, Pułtusk, Poland.

(11) **Iskierko, Z.**, Sharma, P. S., Prochowicz, D., Fronc, K., D'Souza, F., Noworyta, K, „Molecularly imprinted polymer films with increased surface for the determination of macromolecular compounds", *The 9th International Conference on Molecular Imprinting (MIP2016)*, 26-30 June 2016, Lund, Sweden.

List of abbreviations

AAm – acrylamide

ACN – acetonitrile

AEMA – 2-aminoethyl methacrylate hydrochloride

AFM – atomic force microscopy

AIF – apparent imprinting factor

AMPSA – 2-acrylamido-2-methyl-1-propanesulfonic acid sodium salt

ARF – acute renal failure

ATP – adenosine triphosphate

Au-QCR – Au-coated quartz crystal resonator

BSA – bovine serum albumin

CE – capillary electrophoresis

CNT – carbon nanotube

CS – celiac sprue

ChemFET – chemosensitive field-effect transistor

CL – chemiluminescence

CM – cross-linking monomer

CV – cyclic voltammetry

D – drain

DFT – density functional theory

DMF – dimethylformamide

DMSO – dimethyl sulfoxide

L-DOPA – levodopa, L-3,4-dihydroxyphenylalanine

DPV – differential pulse voltammetry

EG – extended gate

EG-FET – extended-gate field-effect transistor

EGDMA – ethylene glycol dimethacrylate

EIS – electrochemical impedance spectroscopy

ENFET – enzyme-modified field-effect transistor

EQCM – electrochemical quartz crystal microbalance

FET – field-effect transistor

FIA – flow-injection analysis

FM – functional monomer

FTIR – Fourier transformed infrared spectroscopy

G – gate

GOx – glucose oxidase

HEMT – high-electron-mobility transistor

HIV – human immunodeficiency virus

HSA – human serum albumin

IF – imprinting factor

ISFET – ion-selective field-effect transistor

IUPAC – International Union of Pure and Applied Chemistry

LOD – limit of detection

LOQ – limit of quantification

MAA – methacrylic acid

MIP – molecularly imprinted polymer

MIPM – molecularly imprinted polymeric micelle

MOF – metal-organic framework

MOSFET – metal-oxide semiconductor field-effect transistor

NGAL – neutrophil gelatinase-associated lipocalin, *aka* human lipocalin-2

NIP – non-imprinted polymer

NNMBA – *N*,*N'*-methylene*bis*acrylamide

OFET – organic field-effect transistor

PM – piezoelectric microgravimetry

PM-IRRAS – polarization-modulation infrared reflection-absorption spectroscopy

PMMA – poly(methyl-methacrylate)

PVC – poly(vinyl chloride)

PXRD – powder X-ray diffraction

RE – reference electrode

R.T. – room temperature

S – source

SAM – self-assembled monolayer

SPAM – smart plastic antibody material

SPE – screen-printed electrode

SPR – surface plasmon resonance

St.dev. – standard deviation

T – template

(TBA)ClO_4 – tetra-*n*-butylammonium perchlorate

TL – toluene

TnT – human cardiac troponin

TMA – thiomalic acid

TPA – terephthalic acid

QCR – quartz crystal resonator

VEGF – vascular endothelial growth factor

WE – working electrode

XPS – X-ray photoelectron spectroscopy

List of symbols

A – electrode surface area, cm^2

A_{acoust} – acoustically active area of the resonator, cm^2

α_a – charge transfer coefficient of an anodic process

α_c – charge transfer coefficient of a cathodic process

c – concentration, M

D – diffusion coefficient, $cm^2\ s^{-1}$

E – potential, V *vs.* reference electrode

E_i – initial potential, V *vs.* reference electrode

E_f – final potential, V *vs.* reference electrode

E_{pa} – anodic peak potential, V *vs.* reference electrode

E_{pc} – cathodic peak potential, V *vs.* reference electrode

E_v – vertex potential, V *vs.* reference electrode

ε – molar absorptivity, $M^{-1}\ cm^{-1}$

f_0 – fundamental frequency of the resonator, MHz

Δf – change of resonant frequency, s^{-1}

ΔG – change of Gibbs free energy, kJ mol^{-1}

I_D – drain current, A

I_{pa} – anodic current, A

I_{pc} – cathodic current, A

K_M – Michaelis-Menten constant, M

λ – wavelength, nm

L – length, cm

μ_q – shear modulus of quartz, $g\ s^{-2}\ cm^{-1}$

ρ_q – quartz density, $g\ cm^{-3}$

R^2 – correlation coefficient

R_D – dynamic resistance, Ω

S/N – signal-to-noise ratio

t – time, s

v – potential scan rate, $mV\ s^{-1}$

V_D – drain voltage, V

V_G – gate voltage, V

V_R – voltage applied to the reference electrode, V

V_T – threshold voltage

W/L – width-to-length ratio

Abstract (in English)

The present Ph.D. thesis describes research on development, preparation, and characterization of four chemosensors for selective determination of chosen compounds of health importance. These compounds are, namely, inosine, human lipocalin-2 (NGAL), as well as D- and L-phenylalanine. In these chemosensors thin films of molecularly imprinted polymers (MIPs) were applied as recognition units, while extended-gate field-effect transistors (EG-FETs) served as transduction units. Stability of pre-polymerization complexes of templates/analytes with dedicated functional monomers were first estimated. For that, the Gibbs free energy gains due to complex formation were calculated using quantum chemistry computing with the density functional theory (DFT) at the B3LYP level of approximation and the 3-21G* or 6-31G* data basis set. All the functional and cross-linking monomers were derivatives of *bis*(2,2'-bithienyl)methane. Chosen monomers were electrochemically polymerized under potentiodynamic conditions in the presence of templates to form recognition units dedicated to one of the above mentioned compounds of health importance. After the polymerization, templates were extracted from MIPs. In order to prove the template removal, such techniques were applied as differential pulse voltammetry (DPV), UV-vis spectroscopy, and polarization-modulation infrared reflection-absorption spectroscopy (PM-IRRAS). Morphology of deposited MIP films were characterized and imaged with AFM and SEM spectroscopy. Such analytical parameters of chemosensors were estimated as sensitivity, selectivity, and limit of detection (LOD), as well as, in case of D- and L-phenylalanine chemosensors, also enantioselectivity. Moreover, the influence of surface enhancement with sacrificial metal-organic frameworks (MOFs) on analytical chemosensor performance was investigated for the NGAL chemosensor. Sensitivity of resulting chemosensors was sufficiently high to determine the chosen analytes of health importance in body fluids. Selectivity of the resulting chemosensors reached allowed discriminating the analytes from their common interferences as well as compounds with similar chemical structures.

Abstract (in Polish)

Przedmiotem rozprawy doktorskiej było zaprojektowanie, wytworzenie i zbadanie właściwości czterech chemoczujników do selektywnego oznaczania wybranych związków chemicznych odgrywających istotną rolę w prawidłowym funkcjonowaniu ludzkiego organizmu. Związkami tymi były inozyna, ludzka lipokalina-2 (NGAL) oraz D- i L-fenyloalanina. Elementami rozpoznającymi tych chemoczujników były cienkie warstwy polimerów wdrukowanych molekularnie (ang. molecularly imprinted polymers, MIPs), a przetwornikami sygnału tranzystory polowe z rozszerzonymi bramkami (ang. extended-gate field-effect transistors, EG-FETs). W celu przygotowania warstw rozpoznających MIPów wybrano odpowiednie monomery funkcyjne i za pomocą modelowania kwantowo-chemicznego zbadano ich oddziaływania z analitami/szablonami posługując się metodą wykorzystującą teorię funkcjonału gęstości (ang. density functional theory, DFT), na poziomie przybliżeń B3LYP z bazą danych 3-21G* lub 6-31G*. Zarówno monomerami funkcyjnymi, jak i sieciującymi były pochodne *bis*(2,2'-bitienylo)metanu. Warstwy rozpoznające czujników osadzono za pomocą polimeryzacji elektrochemicznej, w warunkach potencjodynamicznych, wybranych monomerów funkcyjnych i sieciujących w obecności analitów, które na tym etapie badań spełniały rolę szablonów. Po polimeryzacji, szablony te usunięto z warstw MIPów. W celu potwierdzenia całkowitego usunięcia szablonów zastosowano woltamperometrię pulsową różnicową (ang. differential pulse voltammetry, DPV), spektroskopię UV-vis i spektroskopię odbiciowo-absorpcyjną o modulowanej polaryzacji w podczerwieni (ang. polarization-modulation infrared reflection-absorption spectroscopy, PM-IRRAS). Morfologię osadzonych warstw scharakteryzowano i zobrazowano za pomocą mikroskopii sił atomowych (atomic force microscopy, AFM) i skaningowej mikroskopii elektronowej (ang. scanning electron microscopy, SEM). Wyznaczono, m.in. takie parametry analityczne wytworzonych chemoczujników jak czułość, wykrywalność i selektywność, a w przypadku czujników do oznaczania D- i L-fenyloalaniny, również enancjoselektywność. Ponadto zbadano wpływ rozwinięcia powierzchni pracującej chemoczujników z zastosowaniem materiałów metaloorganicznych (ang. metal-organic frameworks, MOFs) na ich sprawność analityczną. Okazało się, że wykrywalność chemoczujników była wystarczająco wysoka

do wykrywania wybranych analitów w ludzkich płynach ustrojowych. Chemosensory te były na tyle selektywne, że umożliwiły rozróżnienie wybranych analitów od typowych substancji przeszkadzających i związków chemicznych o podobnej budowie.

Contents

Introduction and research goals

The amazing sensing functions of human body inspire scientists in designing artificial sensors. In all five main senses (sight, hearing, smell, touch, and taste) the sensing mechanism is similar. This is, a receptor (eye, ear, skin, nose, and tongue) recognizes the object, and then the recognition signal is transmitted via neutrons to the central transduction unit (brain). In effect, the signal is perceived. Our research goal, as researchers, is to mimic these processes by constructing artificial selective chemosensing systems.

Among others, the researcher role is to devise, fabricate, and characterize selective recognition systems that will significantly contribute to early clinical diagnosis and, in consequence, will help saving human lives.

To complete the research goal of the present dissertation, four compounds of health importance have been chosen as templates for designing four different artificial recognizing systems of the future. These compounds include inosine and human lipocalin-2 (NGAL), known as biomarkers of acute renal failure (ARF). This failure is a common and potentially devastating problem in clinical nephrology with a high mortality rate. Two other compounds are D- and L- enantiomers of phenylalanine, selected to demonstrate the engagement of MIP-based chemosensors in chiral recognition. Chemical structures and properties of the chosen compounds will be described in Chapter 1.1. This chapter will be followed by a brief literature survey considering "Bioinspired artificial recognition materials" and then "MIP-based FET chemosensors" in Chapters 1.2 and 1.3, respectively.

After this survey, the "Experimental part" section will be provided in Chapter 2 including description of chemicals used (Chapter 2.1), "Instrumentation and procedures" (Chapter 2.2), and "Experimental techniques" (Chapter 2.3).

Chapter 3, "Results and discussion", will present chemical sensor designing and determination procedure developing. Moreover, performance of the devised systems

engaging MIPs as recognition units and EG-FETs as transduction units for selective determination of chosen compounds of health importance will be tested. These results have already been published in Biosensors and Bioelectronics in 2015, ACS Applied Materials and Interfaces in 2016, and Journal of Materials Chemistry C in 2017.

Chapter 1

Literature review

1. 1 Compounds of health importance

1.1.1 Inosine

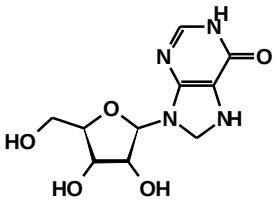

Scheme 1.1-1. Structural formula of inosine, template **1**.

Inosine **1** (Scheme 1.1-1) is a purine nucleoside composed of hypoxanthine and D-ribose. It is a main degradation product of adenosine with potential immuno-modulatory and neuroprotective effects. It is used as a drug to relieve symptoms of several diseases.[1] Moreover, it has been identified as a potential early-warning biomarker of renal dysfunctions[2] as well as of gout and asymptomatic hyperuricemia.[3] Besides, its increased level has been determined in critically ill patients with sepsis.[4] Together with its nucleotides, inosine plays an important role in human body. It correlates with the sclerosis symptoms on the one hand,[5] and it protects an organism against inflammation[6,7] on the other. Furthermore, inosine is one of the biomarkers in diabetic nephrophathy.[2] It is estimated that the rate of death caused by renal disease is 17 times higher in diabetics than in nondiabetics.[8] In addition, diabetic nephrophathy is associated with considerably increased risk and mortality of cardiovascular disease. The inosine concentration in blood of healthy patients is in the range of 0 to 0.75 μM.[2,3] However, this concentration in patients with developed diabetic nephropathy can be as high as 2.4 μM.[2] Moreover, in patients with diagnosed gout or asymptomatic

hyperuricemia, the blood concentration of this compound reached 2.4–2.9 μM.[3] Furthermore, the urinary inosine level can reach 25 μM in individuals after physical exercise.[9]

Considering the above issues, devising a diagnostic tool and developing a procedure for rapid and efficient early inosine determination in humans is important from the clinical analysis point of view. Up to now, inosine is determined using mainly flow analytical techniques, such as capillary electrophoresis (CE)[10,11] or high performance liquid chromatography (HPLC),[12] or techniques using enzymatic reactions.[13-15] Enzymatic reaction systems combined with flow-injection analysis (FIA)[13] and systems with enzymes immobilized directly on electrodes[15,16] or membranes[14] are used for this purpose. However, chromatographic techniques are time-consuming, expensive, and a qualified personnel is needed for their operation. Reproducibility of techniques based on enzymatic reactions is usually low and, moreover, their sensitivity is unsatisfactory for real biological systems. Therefore, many other procedures for selective inosine determination have been developed. These procedures mainly involve oxidation of inosine and their nucleotides on different carbon electrodes, including carbon fiber microelectrodes,[17] carbon paste electrodes modified with $La(OH)_3$ nanowires,[18] pyrolytic graphite electrodes coated with one-dimensional carbon nanorods,[19] or glassy carbon electrodes modified with 3-amine-5-mercapto-1,2,4-triazole.[20] Sensitivity of these electroanalytical procedures is sufficient for determination of inosine in biological systems.[20] However, their drawback consists in instability caused by chemical reactions of electro-oxidation products of purine nucleobasis on electrode surfaces.[21] Additionally, these systems are usually not selective and, moreover, they require application of a relatively high potential.

In view of these points, a novel chemosensor capable of selective sensing of inosine is reported in Chapter 3.1. In this chemosensor, thin polymer film molecularly imprinted with inosine and the extended-gate field-effect transistor (EG-FET) play the role of a recognition and signal transduction unit, respectively. The chemical recognition unit introduces desired selectivity into the sensor whereas the EG-FET provides the sensitivity of the integrated chemosensor device. Up to now, no other MIP-based inosine chemosensor has been reported.

1.1.2 Human lipocalin-2, NGAL

Scheme 1.1-2. Simplified crystal structure of neutrophil gelatinase-associated lipocalin, NGAL, template **2**.

Neutrophil gelatinase-associated lipocalin, NGAL, (Scheme 1.1-2) is a ~25 kDa protein of the lipocalin superfamily.[22] Lipocalins comprise a class of proteins that are characterized by eight β-strands of amino acids forming a β-barrel defining a calyx. The calyx binds and transports low-molecular-weight molecules. Recent reports confirmed that this transport protein is a novel early biomarker for acute renal failure, ARF.[23,24] The ARF, secondary to ischemic injury, remains as a common and potentially devastating problem in clinical nephrology with a high mortality rate.

Typically, NGAL is determined by sandwich ELISA method[24] offering limit of detection (LOD) at the level of 2-80 nM. However, ELISA methods suffer from costly antigen preparation and, moreover, their stability is limited. An MIP-based surface plasmon resonance (SPR) method of NGAL determination has recently been reported with nanomolar detectability.[25,26] Therefore, there is a great need for a low-cost or disposable chemosensor capable of determining this biomarker protein with high detectability. Moreover, this chemosensor should be selective with respect to common interfering proteins present in real samples of body fluids. For a highly sensitive chemosensor, it is important to transduce interactions of an analyte with a recognition unit into a detectable signal.[27] A conducting polymer-based recognition unit appeared suitable for this purpose.[27] Combination of an electronic signal transduction with a conducting polymer recognition helped to devise a chemosensor of a high operational merit.[28]

A novel chemosensor capable of selective NGAL sensing is reported in Chapter 3.2. In this chemosensor, a thin polymer film molecularly imprinted with the inosine template and the EG-FET play the role of the recognition and signal transduction unit, respectively. Additionally, a sacrificial underlayer of metal-organic framework (MOF) was engaged to enlarge the working surface of the transducer. Therefore, a big protein molecule of NGAL was imprinted via the "surface imprinting" approach. This approach allowed increasing the chemosensor signal significantly.

1.1.3 Phenylalanine

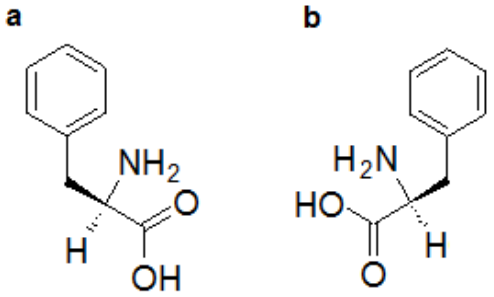

Scheme 1.1-3. Structural formulas of (a) D-phenylalanine, template **3**, and (b) L-phenylalanine, template **4**.

L-Phenylalanine is an essential amino acid. Human body transforms it into tyrosine and some neurotransmitters or their precursors, such as L-3,4-dihydroxyphenylalanine (L-DOPA), adrenalin, and noradrenalin.[29] If the body lacks the enzyme responsible for L-phenylalanine transformation, this amino acid is highly accumulated. This metabolic disorder is called phenylketonuria. In contrast to L-phenylalanine, the D-phenylalanine enantiomer is not found in food. Importantly, only the D-phenylalanine enantiomer was proposed, out of the two enantiomers, as a chronic pain reliever.[30] Some animal studies confirmed the D-phenylalanine use to cure depression associated with Parkinson's disease.

Various efforts were undertaken to imprint phenylalanine (Table 1.1-1).[31-37] However, most of the reported MIP chemosensors for phenylalanine could not discriminate between its enantiomeric forms. Moreover, both selectivity and sensitivity of these chemosensors were not appreciable. Additionally, most of the prepared MIPs were devised to serve as materials for phenylalanine separation. In contrast, Chapter 3 proposes an easy and effective way of preparation of MIP films and their use as

recognition units, integrated with EG-FET transducers, to devise chemosensors for highly selective and sensitive determination of D- and L-phenylalanine. Selective molecular cavities were generated in MIPs by using carboxy derivatized *bis*(bithienyl)-methane as the functional monomer. The EG-FET gate surface, coated with either the D- or L-phenylalanine-templated MIP film, rapidly and selectively responded to D- or L-phenylalanine enantiomer analyte, respectively. Advantageously, these chemosensors discriminated between analytes of a homologous series differing by a single atom and between enantiomers differing only in their three-dimensional structure.

Table 1.1-1. MIP-based analytical methods developed for the determination of phenylalanine.

Functional monomer/cross-linking monomer/porogen	Form of prepared MIP	MIP application	Enantiomer separation	Analytical parameter	Ref.
Methacrylic acid/EGDMA/toluene	Bead (diameter 28 µm)	Separation	Yes	Low enantioselectivity (1.28)	31
Methacrylic acid/EGDMA/ACN	Bulk	Separation	No	Phenylalanine separation from other amino acids	32
Acrylonitrile/acrylic acid/DMSO	Film	PM sensor	No	LOQ: 50 - 500 mg L^{-1}, LOD: 45 mg L^{-1}	33
Polystyrene-co-polyethylene	Film	SPR sensor	No	LOD: 0.5 mM	34
Acrylamide/EGDMA/ethanol	Bead (diameter ~0.2 to 1 µm)	Optical sensor	No	LOQ: 1.3 µM - 0.5 mM, LOD: 0.6 µM	35
β-cyclodextrin derivatized vinyl carboxylic acid/*N*,*N*'-methylene bisacrylamide/water	Polymer prepared in spaces between beads of self-assembled polystyrene colloidal crystal	Optical sensor	Yes	LOQ: 10 - 100 nM, LOD: 0.6 nM	36
Poly(ethylene-co-vinylalcohol)	Core-shell bead (100 – 300 nm diameter) with a magnetic core	Optical sensor	No	Binding to catecholamine hormones, the isotherm study from ~25 to 100 µg mL^{-1}	37

ACN, acetonitrile; DMSO, dimethyl sulfoxide; EGDMA, ethylene glycol dimethacrylate; LOD, limit of detection; LOQ, limit of quantification; PM, piezoelectric microgravimetry; SPR, surface plasmon resonance.

1. 2 Bioinspired artificial recognition materials

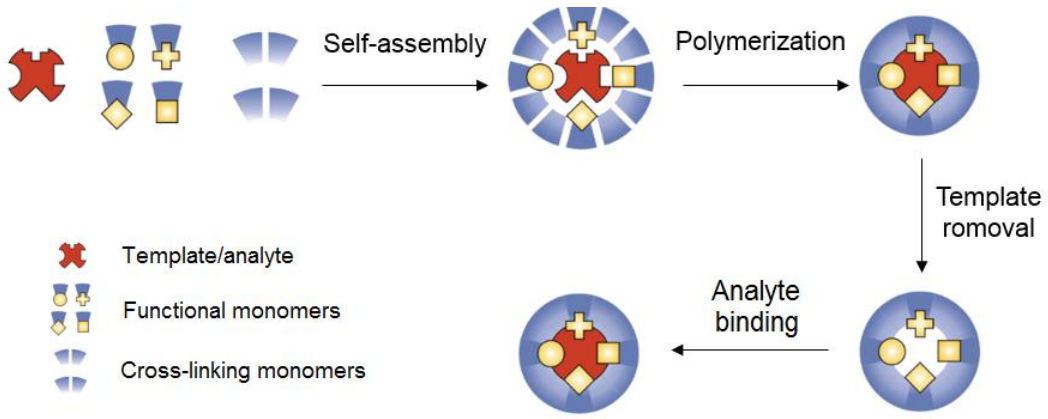

Scheme 1.2-1. A sketch of consecutive steps of preparation of a molecularly imprinted polymer (MIP).

The principal role of recognition materials is to selectively distinguish between the target analyte and its interferences. This selectivity is afforded by complementary binding of the recognition unit of a sensor with the analyte.[38, 39] This unit can be either artificial or natural. The former includes synthetic organic or inorganic materials whereas the latter most often engage surface immobilized proteins (antibodies, enzymes, or histons) and nucleic acids (DNA, RNA, and aptamers).[38] Biomacromolecules of these compounds frequently self-organize into well-arranged compact shapes for their dedicated biological functions. However, these systems suffer from several deficiencies, including limited stability because of poor tolerance to extreme determination conditions.

To overreach these drawbacks, there have been several attempts to develop procedures for preparation of recognition materials of selectivity similar to that of the corresponding biomacromolecular compounds. Frequently, nature guides designing these materials. Inspired by nature, the structure of recognition cavities of receptors of the biological origin can be mimicked to devise synthetic smart materials for chemical sensing.[40] By choosing a starting material of proper recognition functionalities, one may succeed in fabricating synthetic materials with molecular cavities with the desired selectivity.[41]

Nowadays, more and more selective receptors using target analytes or their surrogates as templates are synthesized according to the procedure of molecular

imprinting in polymers,[42] resulting in bioinspired artificial materials called molecularly imprinted polymers (MIPs). These MIPs are readily applied as recognition units in chemosensors. Stability constants of formation of complexes of these artificial receptors with analytes are often similar to those of the biological receptors.[43] Generally, the procedure of molecular imprinting (Scheme 1.2-1) involves polymerization of a pre-polymerization complex in solution of functional monomers with a template in the presence of cross-linking monomers. Subsequent removal of the template leaves in the resulting polymer molecular cavities complementary in their size, shape, and orientation of recognition sites to those of the binding sites of template molecules.[44, 45]

In a traditional MIP preparation procedure, mostly acrylic derivatives served as both functional and cross-linking monomers. Photopolymerization of these monomers produced bulk blocks of MIPs. These blocks, after grinding, well suited as column packing materials for liquid-solid separations, such as chromatography[46] and solid-phase extraction.[47] However, MIPs in a form of bulk materials were not much suitable for direct application in chemosensors. Therefore, finely ground MIP particles were directly integrated with surfaces of different transducers in some initial attempts of chemosensor preparation.[48-51] Towards that, MIP particles were surface immobilized within, e.g., an agarose[50] or chitosan[52,53] film, or a conducting polymer film deposited by electropolymerization[54] on an electrode surface for immediate signaling any event of binding an analyte molecule by an MIP cavity. Noticeably, these attempts were considered as preliminary steps towards the fabrication of real electrochemical chemosensors.

The requirement of an intimate contact of the MIP films with the transducer surfaces for chemosensor fabrication initiated the development of the procedures for growing MIP films directly on these surfaces. Towards that, templates were imprinted into conducting polymer films.[55,27]

Apart from the above-mentioned procedures of MIP preparation directly on the transducer surfaces, several other strategies were developed, including drop or spin coating:

- from a solution of the pre-prepared polymer
- of a composite containing a conducting scaffold material, e.g., carbon nanotubes graphite, or carbon black), MIP particles, and a binder, e.g., poly(vinyl chloride) PVC
- of a complex of a functional monomer with a template, formed in solution, followed by chemical polymerization of this complex to form a thin MIP film.

1.2.1 Conductivity of molecularly imprinted recognition units

A wide range of different functional monomers, varying from those capable of formation of non-conducting acrylic and silane polymers as well as self-assembled monolayers (SAMs) to conducting-polymer-forming functional monomers were used for preparation of MIP-based recognition units of chemosensors.[27,56]

Literature survey of the last few years shows that the application of MIPs in chemosensing is not limited to electrochemical sensors. Other transduction techniques are used to prepare convenient and easy to operate chemosensors as well. From the recent year reports on the "chemical sensor" topic, it follows that over half of the contributions involve acrylic-based monomers, thus outstripping the conducting-polymer-forming functional monomers (Figure 1.2-1a).

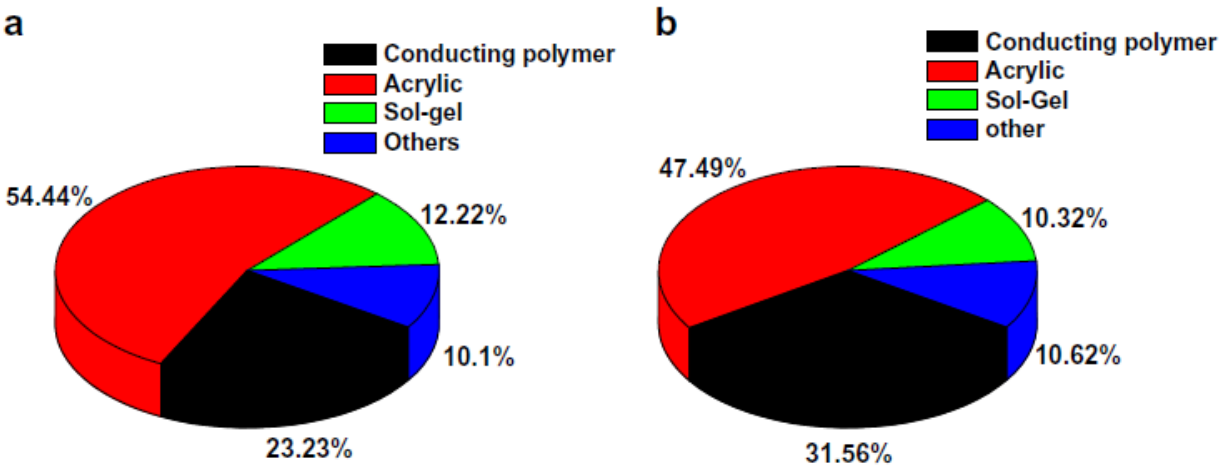

Figure 1.2-1. Contribution of different functional monomers for preparation of the (a) all MIP-based chemosensors and (b) electrochemical MIP-based sensors. This survey covers a 5-year span, between 2010 and 2014.[57,58]

Similarly, switching to the topic of "electrochemical sensor", a similar survey once again reveals more contributions of acrylic-based MIPs (Figure 1.2-1b). Initially, it seemed difficult to fabricate an electrochemical sensor with the acrylic-based MIPs

because of lack of a direct path for electron conduction from the recognition sites of molecularly imprinted cavities to the electrode surface.[59] The integration of these non-conducting films with different conducting scaffolds, mostly carbon allotropes, aided in circumventing these difficulties.[60-64] Moreover, the exploration of different transduction techniques not really requiring the recognition unit to be a conducting film, e.g., capacitance, increased the number of applications of the acrylic-based MIPs in electrochemical sensors.[65]

Apparently, the number of publications on the MIP-based chemical sensors has grown over the last few years, and conducting polymers are still being more and more widely exploited for this purpose (Figure 1.2-2). The application of conducting polymers in the mass and optical chemosensors is increasing as well. Popularity of electropolymerizing monomers in imprinting is growing because of an easy one-step procedure of preparation of conducting polymers executed. Thickness of the resulting MIP film is readily controlled by the charge passed during the electropolymerization. Moreover, removal of a template from MIP films is easy to control, which is particularly important if MIPs are to be applied to trace analysis.

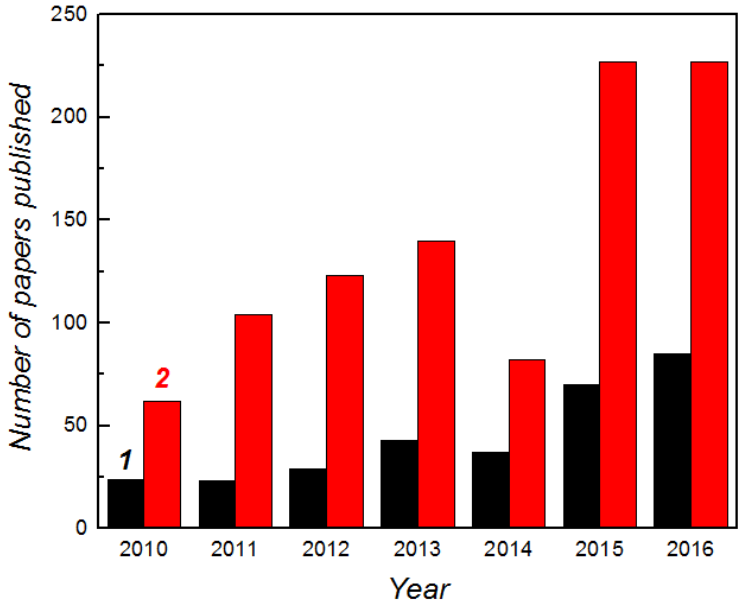

Figure 1.2-2. Number of papers published on MIP chemosensors during the last few years. (*1*) Conducting polymers and (*2*) other polymers.[57, 58]

1.2.2 Selectivity of molecularly imprinted recognition units

Importantly, the specificity of bioreceptors is incurred by their molecular cavities, in which different recognition sites are positioned in a well-defined manner to provide definite chemical microenvironment for reversible binding of target analyte molecules. To this end, enormous progress has been made during the recent few years in the area of molecular imprinting. Several new artificial receptors have been constructed showing strong, reversible, and selective binding of compounds of small molecules and even those of macromolecules.[41,42] Designing molecular cavities in MIPs in a fashion of an "enzyme active center," is now accomplished with the use of derivatized functional monomers.[66-69] Noticeably, the formation of a stable pre-polymerization complex is important for preparation of a highly selective MIP. This complexation is afforded by self-assembling complex components by virtue of

- non-covalent interactions, such as hydrogen bonding, ion-pairing, molecular inclusion, or the hydrophobic, van der Waals, or dipole–dipole interactions, or
- reversible covalent bonding[70]
- semi-covalent bonding.[71]

The possibility of the complex formation in solution of analytes with dedicated functional monomers has firstly been estimated by quantum-chemistry calculations since decades.[72] Advantageously, software development along with the increase of the computing power of computers has made the use of molecular simulations based upon mathematical modeling possible.[73] Hence, the imprinters can estimate now the Gibbs free energy gains due to complex formation with the density functional theory (DFT) at different approximation levels and different basis sets. Higher negative gain in this energy is indicative of higher possibility of the formation of a stable pre-polymerization complex. With this preliminary screening step, the strongest binding functional monomers can be selected and, hence, favorably used for imprinting a given target analyte. This preliminary modeling step of MIP preparation saves time and money for chemicals.

As mentioned above, the monomer functionalities are important, firstly, for preparing a pre-polymerization complex in solution, and then for analyte recognition by reversible interactions. These recognition functionalities are chosen on the grounds of complementarity to the binding sites of the template. For instance, if the target analyte

bears a carboxylic group, then an amine functionalized monomer can be the monomer of choice, and vice versa. Various reviews present lists of functional monomers forming non-conducting (acrylic or silane[56]), and conducting[27,74] polymers. These lists prevailingly include commercially available monomers. However, very often commercially available conducting polymer forming monomers lack recognizing functionalities. Therefore, the selectivity of the resulting MIPs is low. To circumvent this deficiency, complementary interactions between the functional monomer and the template were introduced by considering the point that the larger the number of complementary template-(functional monomer) interactions, the stronger is the binding and fidelity of recognition of the resulting MIP.[75] So, although each interaction is weak, all these interactions concertedly result in quite strong pre-polymerization complexes. Towards that, only derivatized thiophenes and carbazoles were used as functional monomers up to now.[27,76] Actually, a whole "library" of the functionalized thiophene and carbazole-based monomers allowing for a high number of complementary interactions has already been designed and synthesized.[27,57]

The newly designed functional monomers are capable of multiple non-covalent interactions with analytes. The application of these monomers, in comparison to the use of either more than one functional monomers or excess of a functional monomer, seems advantageous for designing a selective molecular cavity.[77] This is because excessive randomly polymerized functional monomer molecules may result in nonspecific recognition sites in MIPs. Moreover, multiple or excessive functional monomers can generate steric crowding during the formation of a pre-polymerization complex. Unfortunately, an additional synthesis step, necessary to be accomplished before MIP preparation, limits a widespread use of these tailored functional monomers.[57]

1.2.3 "Enzyme-like" molecularly imprinted recognition units

Another approach to preparation of highly selective MIPs is to mimic enzyme active centers. Accordingly, the active center of the tyrosinase enzyme was mimicked for preparation of selective, durable, and robust chemosensors for targeting dopamine[59] and phenol[78] analytes. The active center of this enzyme contains two copper atoms, that interact with dioxygen of catechol, thus resulting in catalytic degradation of the

latter. These two copper atoms are coordinated with three histidine residues. Similar cavity was formed using the functional monomer of urocanic acid ethyl ester, and the copper-metal ions during phenol imprinting.[78] In another similar approach, the resulting MIP chemosensor revealed the Michaelis-Menten kinetics with respect to oxidation of catechol and dopamine. The Michaelis-Menten constant, K_M, value for catechol and dopamine was 0.049 and 0.093 mM, respectively.[59]

A similar MIP with high affinity to the carbonic anhydrase inhibitor, such as acetazolamide and ethoxzolamide, was designed by mimicking the active center of carbonic anhydrase. This center consisted of a cone-shaped cavity containing Zn(II) tetrahedrally coordinated by three histidine residues with a solvent molecule as the fourth ligand.[79] Therefore, functional monomers bearing chemical groups, similar to those of histidine moieties building the natural center structure, were synthesized to prepare biomimetic hydrogels.[80] The zinc ions were introduced in the form of methacrylate salt, the hydroxyl- and amino- groups were incorporated in the form of 2-hydroxyethyl methacrylate and *N*-hydroxyethyl acrylamide, respectively, while 4-vinylimidazole resembled histidine. The ability of the resulting MIP to accumulate, retain, and then release acetazolamide and ethoxzolamine was high. A higher amount of these analytes was loaded and their release was controlled by this biomimetic network better than by a conventionally synthesized *N*-hydroxyethyl acrylamide hydrogel.[80]

1.2.4 Recognition of macromolecular compounds of health importance

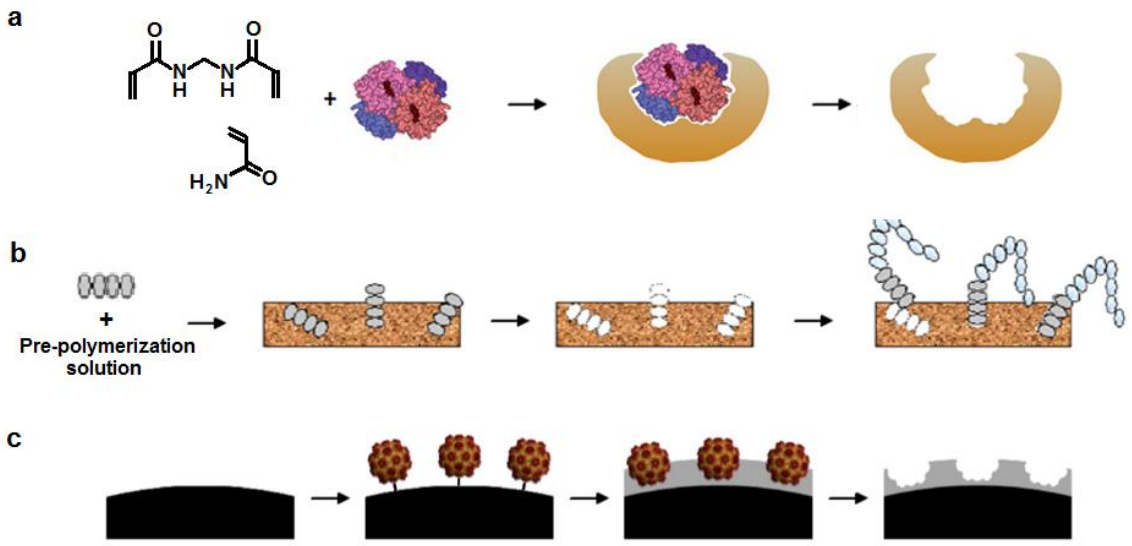

Scheme 1.2-2. An illustration of three main strategies for protein imprinting (a) "bulk" imprinting,[81] (b) "epitope" imprinting,[83] and (c) "surface" imprinting.[82]

Proteins are macromolecular compounds composed of sequences of different amino acids. The rapidly growing field of proteomics requires the use of simple and sensitive protein determination systems. Besides, quantification of different proteins, e.g., bovine serum albumin (BSA), lysozyme, or myoglobin, is important in clinical diagnostics. Determination of the concentration of these proteins in body fluids helps diagnosing various diseases at their very early stages of development.

The main three strategies (Scheme 1.2-2) are used for protein imprinting, namely, "bulk" imprinting, "epitope" imprinting, and "surface" imprinting.[84] The first approach (Scheme 1.2-2a) consists in trapping a whole protein macromolecule inside an MIP film.[85] Then, both template releasing and analyte binding is difficult. Therefore, this procedure is rarely applied in sensor development and will not be discussed herein. The second approach (Scheme 1.2-2b) proposes imprinting only a short, surface exposed, peptide fragment, called "epitope", of a big protein molecule. The third approach (Scheme 1.2-2c) involves protein immobilization on a solid substrate surface before imprinting in thin film.[84,44]

With the epitope imprinting, a biomimetic chemosensor for determination of the human immunodeficiency virus type 1 (HIV-1) related protein (glycoprotein 41) was

fabricated.[86] For this fabrication, dopamine was used as the functional monomer, and then electropolymerized on a quartz crystal resonator (QCR) surface. A subsequent piezomicrogravimetric (PM) measurement showed that not only affinity towards the template peptide of the resulting MIP film was high but also the corresponding glycoprotein 41 protein was bound selectively. The LOD of this determination was appreciable reaching 2 ng mL^{-1}.

Similarly, an interesting procedure of preparation of MIPs with enhanced affinity to cells[87-89] involved the use of an epitope analog for imprinting.[90,91] For that, the polymer surface was imprinted with a protein exposed on the surface of the biological entity, such as a cell. Interaction between this polymer surface and the cell led to specific binding. In one example, fibronecin, a cell-adhesive protein, was adsorbed on the surface of silica beads and used as the "stamp" to imprint a biocompatible polymer containing 2-methacryloyloxyethyl phosphorylcholine units.[87] Fibronectin binding a cell culture greatly enhanced adhesion of L929 cells. Other extensively used polymer matrices for imprinting whole cells included polydimethylsiloxane[92-94] and polyurethane.[95]

In the example of surface imprinting, the protein template molecules were covalently immobilized on the surface of a solid substrate for preparation of a sensitive electrochemical chemosensor (Scheme 1.2-3).[96] This approach enabled imprinting proteins insoluble in the pre-polymerization solution. Moreover, it minimized aggregation of proteins, thus leading to the formation of more homogeneous recognizing sites. However, this approach required proper tuning of thickness of the MIP film. Growth of this film over the protein template could lead to permanent protein entrapment.

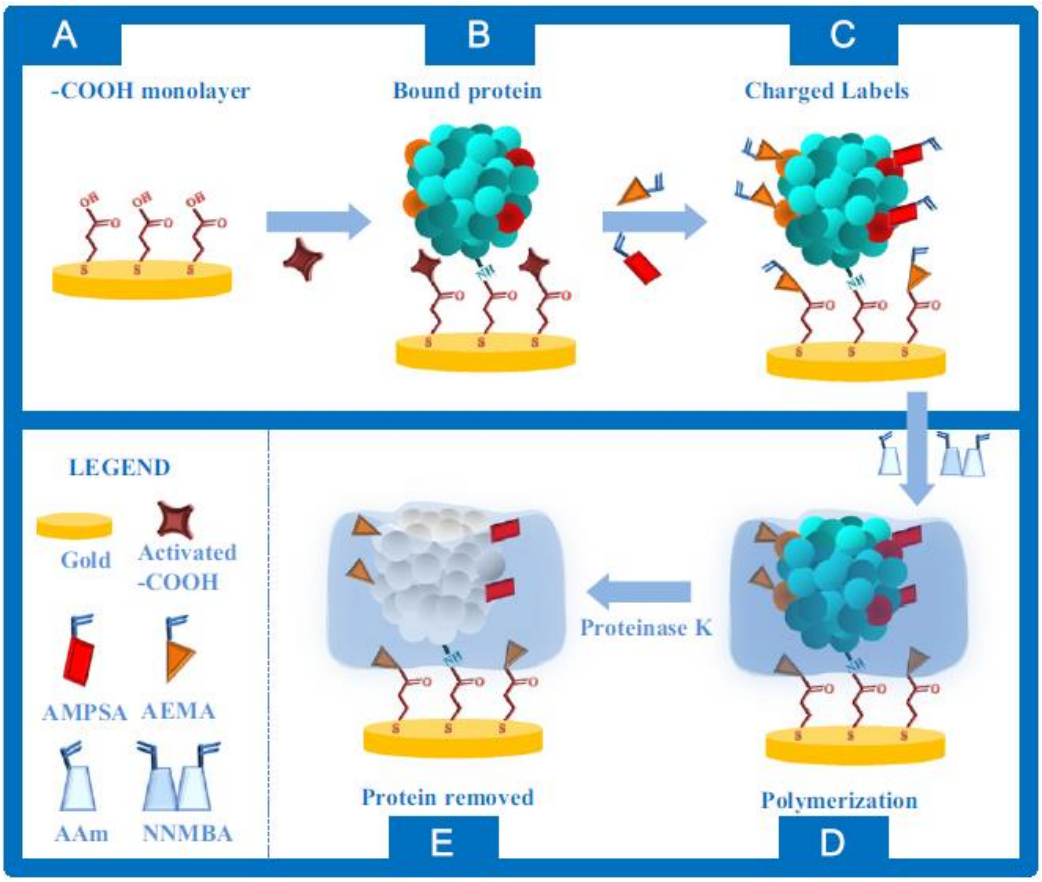

Scheme 1.2-3. A sketch of the smart plastic antibody, SPAM, synthesis. (A) A gold screen-printed electrode (SPE) modified with thiomalic acid (TMA) and producing a carboxylic layer. (B) Myoglobin immobilized on the activated carboxyl groups of Au-SPE/TMA. (C) Charged-monomers in position and blocked carboxyl functions that remained active. (D) Polymerization with neutral monomer structures around the template. (E) Recognizing sites formation by template removal with proteinase K. Abbreviations AMPSA, AEMA, AAm, and NNMBA, stand for 2-acryl amido-2-methyl-1-propanesulfonic acid sodium salt, 2-aminoethyl methacrylate hydrochloride, acrylamide, and *N*,*N'*-methylene*bis*acrylamide, respectively. (Adapted from[96])

In a common sensing practice, an electroactive surface area is enlarged with high surface area materials, e.g., carbon nanotubes (CNTs), for enhancement of analytical signals. Towards that, few reports described the preparation of thin conducting MIP films on CNTs.[97-99] The resulting composite MIPs provided a nanogram level detectability of the BSA protein determination. From the point of view of such surface development, MOF utilization also appeared promising.[100-102]

Worth mentioning, protein-imprinted polymers, in the hydrogel form, were prepared to decrease the cross-linking density and rigidity of the MIP structure. The lower density of cross-linking in the hydrogel MIP appeared favorable for the in-and-out

mass transfer of bulky proteins in the polymer matrix. Unfortunately, these bulk imprinted gels needed an additional supporting membrane for their immobilization on a transducer surface.[103]

To devise an MIP-based chemosensor for the human cardiac troponin (TnT) protein, a biomarker for myocardial infection combined with potentiometric[104] and cyclic voltammetry (CV) transductions were used.[105] The TnT detectability of both resulting chemosensors was high. That is, a potentiometric chemosensor was prepared by coating a metal wire with a mixture of MIP particles with PVC and a plasticizer forming a membrane. Although this approach used a composite of CNTs and MIP, detectability of the resulting chemosensor was higher[104] than that of the MIP prepared with the 1,2-phenylenediamine functional monomer.[105]

Some chemosensors for NGAL detection and determination have been devised.[25,26] In one, localized SPR spectroscopy was used as the transduction technique and LOD of 13 nM NGAL was reached. This detectability surpassed that offered by traditional techniques, such as piezoelectric microgravimetry (PM) at a quartz crystal microbalance (QCM) and liquid chromatography,[106] and was suitable for the detection of many proteins at clinical concentrations. However, the challenge remained to approach the performance of natural antibodies in a comparable detection platform.[107]

1.2.5 Recognition of small-molecule compounds of health importance

In human body, the determination of not only macromolecular compounds but also several of those small-molecule compounds regulating important metabolism paths is crucial in order to detect early stages of diseases. Therefore, another topic of interest for artificial sensor designers is sensing relatively small biorelevant compounds, such as hormones (e.g., testosterone[108]), neurotransmitters (e.g., histamine[66] or adrenaline[67]), and monosaccharides (e.g., glucose[109-112]). In our body, hormones play an important role of chemical messengers. They control many metabolic processes, including growth and reproduction. A laboratory can determine the hormone levels in body fluids, such as blood, urine, and saliva. However, improvement of hormone determination in medical healthcare is still needed[113] because the hormone disorder is dangerous.

Towards that, an MIP chemosensor was devised for the impedimetric determination of testosterone, an endogenous steroid hormone with strong androgenic

and anabolic effects.[108] To fabricate this chemosensor, a solution of the pre-polymerization complex of methacrylic acid (MAA) and ethylene glycol dimethacrylate (EGDMA) was prepared in the presence of the testosterone template. Next, the electrode surface was spin-coated with this mixture, and then the mixture photopolymerized. The LOD of the resulting chemosensor was 103 ng/L testosterone.

Adrenaline is a well-known neurotransmitter hormone involved in the etiology and symptomatology of several neurological and psychiatric disorders. The suitability of the devised functional monomer forming a conducting polymer was demonstrated by imprinting this hormone.[67] That is, the carboxyl and crown ether derivatized *bis*(bithiophene)-based functional monomers were synthesized to match binding sites available on the adrenaline template. For signal transduction, the resulting MIP film was integrated with an electrode of a QCR for simultaneous electrochemical and PM chemosensing. Importantly, the detectability of the electrochemical transduction reached down to 2 nM adrenaline. Because of the presence of dedicated molecular cavities, these chemosensors were appreciably selective to adrenaline in the presence of common interferences.

A histamine neurohormone triggers several allergic reactions. Therefore, a PM MIP chemosensor was devised for selective histamine determination.[66] As the recognition unit, the chemosensor contained an MIP film, deposited by potentiodynamic electropolymerization, and a QCR as the signal transducer. Selective molecular cavities were generated with the crown ether and dioxaborane derivatives of *bis*(2,2'-bithiophene) functional monomers. Here, again, the choice of monomers was made by considering available binding sites on the histamine template. Under flow-injection analysis (FIA) conditions, the chemosensor detected histamine at the concentration as low as 5 nM.

Various other transducers integrated with MIPs that used acrylic-based functional monomers[114, 115] were engaged in histamine sensing with the micromole detectability.[114] Interestingly, the selectivity of these MIPs was quite similar to that of the (conducting polymer)-based MIP.[66] However, the detectability of the latter was higher because of more extensive preconcentration of the analyte in the dedicated MIP.

For several decades, the fabrication of glucose biosensors has received considerable attention because of importance of glucose determination in clinical

analysis. Most of glucose biosensing systems use the glucose oxidase (GOx) enzyme for glucose quantification. For that, proper GOx immobilization and close proximity of the GOx active center to the electrode surface are important for successful biosensor operation. Therefore, easy to prepare and robust MIP-based recognition units of chemosensors were devised. In one study, a thin film of an MIP of non-conducting poly(1,2-aminophenol) was deposited on an electrode surface for selective glucose sensing.[109] Different voltammetric glucose chemosensors were prepared.[110] For that, molecularly imprinted polymeric micelles (MIPMs) were engaged. That is, a film was in situ formed on the electrode surface by deposition of the MIPM by electropolymerization. Sensitivity and selectivity toward glucose of the resulting chemosensor were high. The chemosensor linear dynamic concentration response ranged from 0.2 to 8 mM indicating the presence of numerous effective recognition sites embedded in the polymer matrix because of the large surface area of the MIPMs. Moreover, both stability and reversibility of this chemosensor were high.

Furthermore, different pre-prepared polymers were cross-linked to result in MIP films as recognition units for devising chemosensors for glucose.[111,112] These polymers were rich in hydrogen bond forming groups, such as carbonyl, carboxyl,[111] or amino[112] groups, for possible interactions with the glucose template. Then, these interactions helped to pre-concentrate glucose in the MIP emptied cavities for amplification of the detection signal.

An attention should be paid to MIP-based chemical sensors dedicated to detection of such small-molecule compounds of health importance as inosine and phenylalanine. However, MIP-based chemosensor for inosine has not been much studied yet.[116] This analyte was detected and determinated with a sophisticated procedure involving ultra-performance liquid chromatography-photodiode array detection.[117] The water-compatible MIP was synthesized using theophylline as the so-called “dummy-template” and acrylamide as the functional monomer. In this approach inosine, together with hypoxanthine, were investigated as the degradation products of adenosine triphosphate (ATP) derivatives in fish samples, because ATP degradation products are used as freshness indexes for assessment of fish quality. The solid samples were blended together with an extracted MIP in a matrix solid-phase dispersion. This procedure resulted in the sample disruption and subsequent adsorption of the

products on the MIP. Afterwards, the MIP was washed with *n*-hexane and chromatograms were obtained using aqueous solution of ammonium hydroxide (pH = 9.0) as the eluent. Linearity for both hypoxanthine and inosine was high with the correlation coefficient (R^2) of 0.9987 and 0.9986, respectively.

In contrast to scarce inosine MIP chemosensors, those for detection and determination of phenylalanine were broadly investigated[58] (Table 1.1-1). One of these chemosensors involved the application of superparamagnetic nanoparticles.[37] In this study, determination of phenylalanine in urine using magnetic MIP composite nanoparticles was combined with optical sensing to improve sensitivity. Poly(ethylene-co-vinyl alcohol) was employed as the polymer matrix. Fluorescence spectrophotometry was used to determine both the target and interferences binding to molecular cavities of the MIP. Apparently, functional groups of phenylalanine dominated the selectivity of the synthesized MIPs. Finally, the composite nanoparticles were used to separate and determine the target phenylalanine in urine by Raman scattering microscopy.

Another MIP-based chemosensor for L-phenylalanine determination was integrated with chemiluminescence (CL) transducer.[35] The MIP imprinted with L-phenylalanine enantiomer was synthesized using acrylamide (AAm) as the functional monomer and ethylene glycol dimethacrylate (EGDMA) as the cross-linking monomer. Then, the synthesized MIP was employed as the recognition unit by packing it into a flow cell in order to devise a flow-injection analysis (FIA) CL chemosensor. The luminol-H_2O_2-(L-phenylalanine) intensity linearly responded to the analyte concentration in the range of 1.30×10^{-6} to 5.44×10^{-4} M with the LOD of 6.23×10^{-7} M. The chemosensor was successfully applied to L-phenylalanine determination in real samples.

1. 3 MIP-based FET chemosensors

Devising and fabricating sensors for such physical phenomena as light, heat, or pressure is relatively simple. However, these become more complicated if signals originate from atoms or molecules. These sensors are often referred to as chemical sensors (chemosensors) or biochemical sensors (biosensors).[118]

According to the International Union of Pure and Applied Chemistry (IUPAC) a chemosensor, or a chemical sensor, is a device that transforms information, ranging from the concentration of a specific sample component to total composition analysis, into the analytically useful signal. The chemical information, mentioned above, may originate from a chemical reaction of the analyte or from a physical property of the system investigated.[119] On the other hand, biosensor is a device that uses specific biochemical reactions mediated by isolated enzymes, immune-systems, tissues, organelles or whole cells to detect chemical compounds, usually by electrical, thermal or optical signals.[120] In other words, a chemosensor is a device in which chemical interaction between recognition unit and the molecule of the analyte is needed to turn it into a measureable signal by a transducer (Scheme 1.3-1), and a biosensor is an analytical device involving biological recognition element whose interaction with an analyte is turned into a measurable signal by a transducer.[121]

Typically for a chemo- or biosensor, the recognition element, containing artificial or natural receptor sites, respectively, is assembled on a transducer surface to generate an output detection signal. In a biosensor, the molecular preferential treatment or recognition is accomplished by integrating a transducing element with either biological system, such as *in vitro* tissues, microorganisms, organelles or cells, or biological macromolecular compounds, such as antibodies, enzymes, proteins, nucleic acids, histones, etc.[122] Preferential binding of the analyte by the receptor sites induces changes in the physicochemical properties of the sensing system. Those changes are detected using proper signal transducers. Typically, the binding of the target analyte by selective recognition units are transduced by an optical,[50,123] piezoelectric,[124,125] or electric signals.[126] Among the latter, the area of FET-based MIP chemosensors is rapidly growing (Table 1.3-1).

Chemical and biochemical sensor preparation involves an interdisciplinary research. As the number of applications of these sensors is growing, their market demand increases.[38] Nowadays, this demand is not only limited to sensing systems for small-molecule analytes but that of macromolecular compounds sensing is enormously growing as well. Detection and quantification of the latter analytes in clinical analysis, e.g., in routine blood testing[38] is very costly. Moreover, the importance of these sensors is appreciated in several other fields including biological and chemical security,[127] environmental protection,[128,129] and food safety.[130] For the last few decades, chemical and biological sensors have attracted considerable attention because of their perceived ability to constitute sensing systems selective for determination of target analytes.

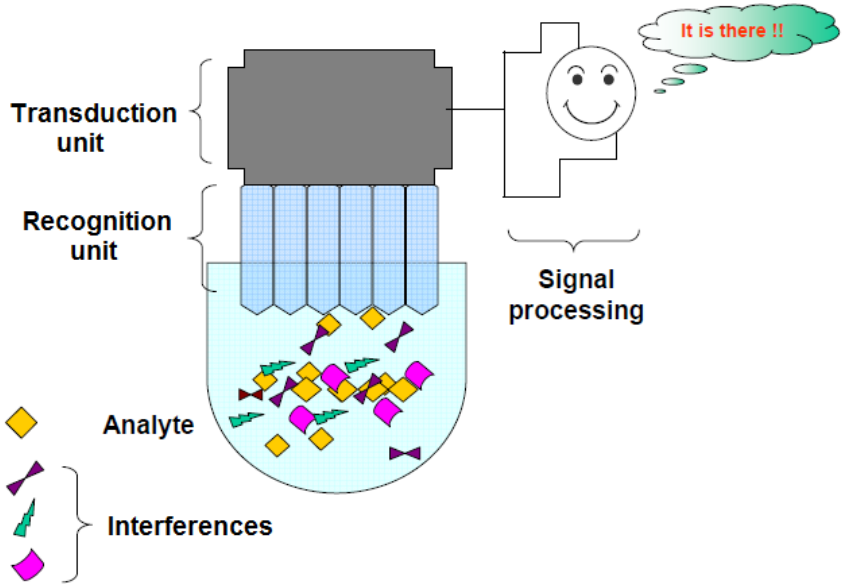

Scheme 1.3-1. An illustration of a chemo- or biosensor.[118]

For several decades, modified metal-oxide-semiconductor field-effect transistor (MOSFET) devices have been applied for chemosensing.[131] Among them, ion-sensitive field-effect transistors (ISFETs) were initially devised and used. After the first successful application of ISFETs,[132] various reports have described similar devices for determination of different analytes of interest.[133,134] Depending on the type of modification, devices are named,[135] e.g., ChemFETs, if the charge on the gate electrode is applied by a chemical process, ENFETs, if devices are dedicated to specific recognition of biomolecules using enzymes, or OFETs, if the transistor channel consists of an organic

semiconductor. As an improvement involving isolation of the FET from the chemical environment, an extended-gate field-effect transistor (EG-FET) was also devised.[136-138] Because the S-D current flow is controlled by the electrical field produced by the gate, all these devices have common term of "field-effect transistors" (FETs).[139]

Such numerical criteria as sensitivity, detectability, linear dynamic concentration range, and selectivity should be considered before devising a bio- or chemosensor. Bioreceptors, such as immobilized proteins (antibodies, enzymes, or histones), nucleic acids (DNA, RNA or aptamers), intracellular receptors, cell receptors, microorganisms, living plants, and even whole animal tissues, serve efficiently as recognition units in biosensing.[38]

In recent years, we can witness a rapid progress in devising label-free biosensors engaging the aptamer technology conjugated with the FET transduction.[140] Aptamers, in brief, are relatively short single strands of synthetically designed DNA oligonucleotides that self-assemble into unique molecular recognition units in order to entrap different proteins specifically at high affinity.[140] As an example, vascular endothelial growth factor (VEGF), a cancer biomarker, was in vitro electrochemically detected with a biosensor using an aptamer for recognition and a FET for transduction.[141] This high-performance FET chemosensor detected as low as 400 fM of the VEGF analyte. Its recognition unit contained an anti-VEGF RNA aptamer tethered to carboxylated polypyrrole nanotubes.

However, biosensors suffer from a major drawback, i.e., the bioreceptors employed are often comprised of several sub-units, which degrade during immobilization under conditions different from their natural environment. Another deficiency includes limited stability because of low tolerance of extreme solution acidity or basicity, temperature, some organic solvents, and exposure to external fields (e.g., electromagnetic or ultrasonic). Moreover, lifetime of bioreceptors is usually short, their availability is low, their cost is high (because of the necessity of tedious purification) analyte determination and reproducibility is inadequate. For instance, the activity of the same enzyme, purchased from the same manufacturer but of a different batch, may be different. To overcome these drawbacks, artificial recognition units capable of binding target compounds with affinity similar to that of the corresponding bioreceptors are being devised and fabricated extensively.[57,118]

One of examples showing an artificial recognition unit integrated with the FET can be the dopamine chemosensor.[142] The sensing element of this device was located at the (Au-gate)-(aqueous solution) interface by means of a SAM composed of cysteamine and 4-formylphenyl boronic acid. The covalent and selective adsorption of dopamine induced a surface dipole potential, which shifted the electrode work function and modulated the double-layer capacitance. As a result, the device was capable to detect dopamine down to picomolar concentration with sensitivity higher than that revealed by other methods. However, the selectivity of this chemosensor was not investigated.

To provide selectivity, a tailor-made recognition unit should carefully be considered and designed. In many instances, affinity and selectivity of MIPs are as good as that of natural receptors.[118] Like most polymer materials, MIPs are processable. That is, they are compatible with the fabrication techniques and engineering conditions like micromachining, laser ablation, and surface patterning. Therefore, the use of MIPs opens up the possibility for integration of the chemosensors with the electromechanical systems. Evidently, the low manufacturing cost and inexpensive preparation have made MIPs interesting for fabrication of so-called “plastic antibodies”. In recent years, the field of MIPs has attracted significant interest, revealed in several reviews.[44, 118, 143, 144]

Table 1.3-1. Chemical sensors with molecularly imprinted polymers (MIPs) as recognition units integrated with field-effect transistors (FETs) as transduction units, reported in literature since 2001, in chronological order.

Year	Template/analyte	Type of polymer/ imprinting matrix	Recognition sites of MIP (functionalities)	pH	Concentration range	Limit of detection	Biological concen-tration reached?	Real sample measurement?	Type of the transistor (or electronic transduction)	Ref.
2001	4-Chlorophenoxy acetic acid 2,4-Dichlorophenoxy acetic acid	Metal oxide (TiO_2)	-OH	7.2	0.5 – 6 mM 0.1 – 9.0 mM	$(5 \pm 2) \times 10^{-4}$ M $(1.0 \pm 0.2) \times 10^{-5}$ M	-	-	ISFET	145
2002	Adenosine 5′-monophosphate Guanosine 5′-monophosphate Cytosine 5′-monophosphate Uridine 5′-monophosphate Glucose	Acrylic polymer	$–B(OH)_2$	7.0	$3 \times 10^{-5} – 5 \times 10^{-3}$ mM $4 \times 10^{-5} – 2 \times 10^{-3}$ mM $2 \times 10^{-6} – 5 \times 10^{-4}$ mM $1 \times 10^{-5} – 5 \times 10^{-3}$ mM $1 \times 10^{-6} – 8 \times 10^{-4}$ mM	1.5×10^{-5} mM 1.5×10^{-5} mM 8.0×10^{-7} mM 2.0×10^{-5} mM 8.0×10^{-7} mM	Yes	-	ISFET	146
2003	NAD+ NADP+ NADH NADPH	Acrylic polymer	$–CONH_2$ $–B(OH)_2$	7.2	$5 \times 10^{-4} – 8 \times 10^{-2}$ mM $3 \times 10^{-4} – 7 \times 10^{-2}$ mM $1 \times 10^{-4} – 5 \times 10^{-2}$ mM $2 \times 10^{-4} – 1 \times 10^{-1}$ mM	4×10^{-4} mM 2×10^{-4} mM 1×10^{-4} mM 2×10^{-4} mM	-	Yes	ISFET	147
2007	NAD+ NADP+ NADH NADPH	Acrylic polymer	$–CONH_2$ $–B(OH)_2$	7.3	$5 \times 10^{-4} – 8 \times 10^{-2}$ mM $3 \times 10^{-4} – 7 \times 10^{-2}$ mM $1 \times 10^{-4} – 5 \times 10^{-2}$ mM $2 \times 10^{-4} – 1 \times 10^{-1}$ mM	4×10^{-4} mM 2×10^{-4} mM 1×10^{-4} mM 2×10^{-4} mM	-	-	ISFET MSFET	148
2009	cAMP	Acrylic polymer	Thiourea moiety	8.0	0.1 – 1.0 mM	0.1 mM	-	-	ISFET	149
2009	Theophylline	Acrylic polymer	-COOH	-	The binding experiments to MIP were performed with three theophylline	-	-	-	CNT-FET	150

					concentrations of 10, 15 and 20 μg/ml					
2010	Creatinine	Acrylic polymer	-OH	-	0.2 – 1.3 mg/mL	0.2 mg/mL	Yes	-	ISFET CMOS	151
2011	Diphenyl phosphate	Acrylic polymer	Thiourea moiety	-	10 – 40 μM	10 μM	-	-	ISFET	152
2013	Ethanol	Acrylic polymer	-COOH	-	0.65 – 45.0 ppm	0.5 ppm	Yes	The sensor response to ethanol was not influenced significantly up to relative humidity of 45%.	Resistor	153
2015	Inosine*	Conducting thiophene polymer	$–B(OH)_2$, –N, and $–NH_2$	-	0.5 – 50 μM	0.62 ±0.01 μM	Yes	-	EG-FET	116
2016	D-Arabitol	Conducting thiophene polymer	$–B(OH)_2$	-	0.12 – 1.00 mM	0.12 mM	Yes, suitable for early diagnosis of fungal infections	-	EG-FET	45
2016	NGAL**	Conducting thiophene polymer	–OH groups of catechol moieties	-	0.1 – 0.9 μM	120 nM	Yes	-	EG-FET	154
2016	TATAAA	Conducting thiophene polymer	Thymine and adenine moieties, Watson-Crick pairing	-	0.1 – 7.5 μM	0.1 μM	-	-	EG-FET	155

2016	Phosphate ions ($Na_3PO_4 \times 12\ H_2O$)	Acrylic polymer	$-CH_3$, -Cl	5.0	0.02 – 20 mg L^{-1}	1.97 μg L^{-1}	-	-	AlGaN/GaN HEMT	156
2016	Urea	Acrylic polymer	-COOH	4.0, 7.0, 10.0	1.0×10^{-4} – 1.0 M	1.0×10^{-4} M	Yes	No	ISFET	157
2016	PSA	Polydopamine	-OH, -N	7.4	10^{-2} – 10^{8} pg mL^{-1} (linear 0.1 pg mL^{-1} – 1 ng mL^{-1} PSA)	0.1 pg mL^{-1}	Yes	Yes	EG-FET	158
2017	D-Phenylalanine and L- phenylalanine***	Conducting thiophene polymer	-COOH	3.0	13 – 100 μM	13 μM	Yes	Yes	EG-FET	125

cAMP – cyclic adenosine 3',5'-cyclic monophosphate

NAD+ – β-nicotinamide adenine dinucleotide
NADP+ – β-nicotinamide adenine dinucleotide phosphate
NADH – 1,4-dihydro-β-nicotinamide adenine dinucleotide

NADPH – 1,4-dihydro-β-nicotinamide adenine dinucleotide phosphate
PSA – prostate specific antigen,

Articles labeled with *, **, ***, stand for papers already published but they constitute the content of the present thesis in Chapters 3.1, 3.2, and 3.3, respectively. Comparing them with other MIP-based FET chemosensors in this table may emphasize contribution of the present research to this field of science.

The first attempt to integrate molecularly imprinted material with the FET transducer dates back to 2001.[145] That is, SiO_2 gates of ISFETs were functionalized with TiO_2 films, which contained molecular cavities imprinted with 4-chlorophenoxyacetic or 2,4-dichlorophenoxyacetic acid as templates. It occurred that these two functionalized devices revealed an impressive selectivity in sensing the analytes/templates being imprinted. The LOD of the first chemosensor was $(5 \pm 2) \times 10^{-4}$ M and the concentration range was 0.5 to 6.0 mM (Table 1.3-1). The LOD of the other chemosensor was $(1.0 \pm 0.2) \times 10^{-5}$ M and the concentration range was 0.1 to 9.0 mM. The equilibration time of the devices was 5 min. Although the TiO_2 is not a polymer but a metal oxide, the reported research was the first to attempt integrating an artificial recognition unit with an electric FET transduction unit.

In a subsequent report,[147] cavities for recognition of the NAD(P)+ and NAD(P)H cofactors were imprinted in a cross-linked acrylamide-acrylamidophenylboronic acid copolymer film. The transduction signal of the functionalized ISFET devices was a potentiometric output that originated from the generation of a boronate complex of functional monomer with template. This was the result of binding of the analyte to the recognition cavities and of the change in the local pH at the gate-polymer interface. The imprinted polymer films integrated with the ISFETs allowed determining respective analytes with high detectability (Table 1.3-1). The ISFET devices functionalized with the NADH or NADPH imprinted films were employed in the analysis of the biocatalyzed oxidation of lactic acid and ethanol in the presence of lactate dehydrogenase and alcohol dehydrogenase, respectively. This work was repeated and published again in 2007 with further explanation of properties of the chemosensors with the structure of the nucleotides and the composition of the films.[148]

In 2009, a biomimetic chemosensor for adenosine-3',5'-cyclic monophosphate (cAMP), which is an important intracellular regulator of many cellular processes, was fabricated in combination with an ISFET as the transducer and a cAMP-imprinted polymer as the recognition material.[149] The cAMP-imprinted polymer was prepared using 1-allyl-2-thiourea as the functional monomer. This monomer interacted with both the adenine and cyclic phosphate binding site of cAMP, and the recognizing site of the thiourea moiety in the cAMP-imprinted cavity distinguished between the chemical structure of adenine and cyclic phosphate of cAMP. The binding of cAMP by the

imprinted polymer enabled electronic transduction onto the ISFET electrode, and cAMP in the concentration range of 0.1 to 1.0 mM (Table 1.3-1) was determined in aqueous solutions.

Other publications describing MIPs integrated with FET sensors involve selective determination of creatinine,[151] diphenyl phosphate,[152] and ethanol.[153] In all of these studies the transistor gates were coated with a non-conducting acrylic MIP matrix. Performance of these acrylic MIP materials is superior in many applications, however, they often suffer from the presence of nonhomogeneous molecular cavities, slow response time, and low binding reproducibility.[57] Application of electropolymerizable functional monomers generating electrochemically conducting polymers often avoids these undesired effects. These monomers enable easy controlling the MIP film morphology.[159]

In order to provide higher conductivity and controlled morphology to the recognition MIP unit in the EG-FET sensing system, a conducting polymer was for the first time utilized in 2015.[116] In this work, a derivatized polythiophene was deposited by potentiodynamic electropolymerization directly on the extended gate of FET. Although EG-FET was used as the transducer before,[136-138, 160] this work was the first successful attempt to engage this transducer modification also with an MIP recognition unit. The experimental setup prepared that way was allowed for the flexibility in the gate shape.[160] After publishing on the MIP-inosine EG-FET chemosensor, other chemosensors were similarly devised for detection and determination of D-arabitol,[45] human lipocalin-2 (NGAL),[154] oligonucleotide with the thymine-adenine-thymine-adenine-adenine-adenine (TATAAA)[155] sequence of nucleobases, as well as D- and L-phenylalanine.[125] Herein, development of four of these chemosensors, namely, for inosine, NGAL, as well as D- and L-phenylalanine is discussed below in Chapters 3.1, 3.2, and 3.3, respectively, thus indicating the contribution of the present dissertation to the chemosensing field of analytical chemistry.

One of the main clinical goals in devising chemosensors with artificial recognition units is to improve early medical diagnosis. Nowadays, many of known biomarkers of dangerous diseases can be detected only when it is already too late for the proper, successful treatment. Therefore, devising not only selective but also very sensitive tools for this diagnosis is important. One of the ways to improve the chemosensor response

is to enlarge its working surface area. This approach was also used for improving performance of MIP-FET-based chemosensors. The first attempt involved engagement of carbon nanotubes and semiconductor nanowire FETs[97-99] for improvement chemosensor sensitivity. Eventually, however, the chemosensor performance was not examined in these studies. Another example of MIP-FET working surface development comprised utilization of a sacrificial MOF underlayer for lipocalin sensing.[154] In this example, it was possible to reach the LOD as low as 120 nM lipocalin. Results of this study is described in details in Chapter 3.2.

A sound improvement to FET-based MIP chemosensors was made by devising an extended-gate system. In an EG-FET, the chemically sensitive unit is deposited as a thin film on surface of the gate extending from a FET. The experimental setup prepared that way shows major advantage of flexibility in the gate shape.[160] Advantageously, with the use of neither expensive instruments nor reagents, minute changes in potential at the gate surface generated by the presence of charged analytes are transduced into detectable electric signals. Additionally, the stability of FET characteristics in the ambient environment is greatly improved. Importantly, packing and transporting this setup for measurements in field is relatively easy.[116]

Although various reports described different applications of FET-based chemosensors, the combination of EG-FET transduction with MIP-based recognition has so far not been explored deeply,[116] despite that it offers numerous advantages. Firstly, MIP selectivity combined with signal amplification by the FET leads to highly sensitive chemosensors selective to chosen analytes. Moreover, MIP recognition films integration with the EG-FET is much easier than with classical FETs because it does not require complicated and costly processing. The EG-FET can easily be adapted to operate in both organic and water solutions, which is important from the point of view of chemosensor fabrication and its practical application. Moreover, the EG-FETs offer an excellent possibility of chemosensor miniaturization.

Great advantage of integrating an MIP with an EG-FET in one device is providing to the sensing system high selectivity on the one hand and high sensitivity on the other. The latter can easily be tuned by changing the gate voltage. Then, LOD as low as 0.1 pg/mL is reached.[158] In this latter study, polydopamine imprinted with prostate specific antigen (PSA) was used as the recognition unit and a commercial MOSFET with

EG was applied as the transducer. The devised chemosensor was ready to detect PSA at a very low concentration in real samples of human plasma.

Another promising step into further development of the (MIP-FET)-based chemosensors is the use of AlGaN/GaN high-electron-mobility transistors (HEMTs)[156,161] as transducers. Recently, chemosensors were constructed successfully with these HEMTs. This is because in HEMTs the conducting channel of the two-dimensional electron gas is located very close to the semiconductor surface. Therefore, a HEMT is extremely sensitive to adsorption of analytes.[162] Because of sufficiently high chemical and physical stability in water,[163,164] ion-sensitive AlGaN/GaN HEMTs appeared advantageous for ion detection. Their application to determination of ions in solutions can be considered as the first step towards constructing more advanced sensing systems. It is envisioned that in the near future HEMTs will be applied as transducers to detect and determine more complex analytes.

Chapter 2

Experimental part

2. 1 Chemicals

Table 2.1-1. Templates/analytes.

No.	Name	Structural formula	Source
1	Inosine	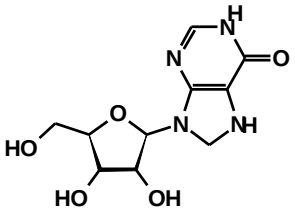	Sigma-Aldrich
2	Human lipocalin-2 (NGAL)		Sigma-Aldrich
3	D-Phenylalanine	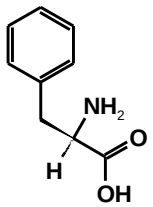	Sigma-Aldrich
4	L-Phenylalanine	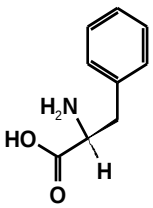	Sigma-Aldrich

Table 2.1-2. Functional monomers.

No.	Name	Structural formula	Source
5	2,2’-Bithiophene-5-boronic acid	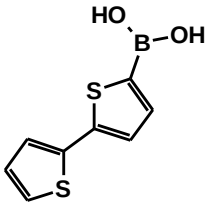	Sigma-Aldrich
6	2-(Cytosin-1-yl)ethyl *p-bis*(2,2’-bithien-5-yl)methylbenzolate	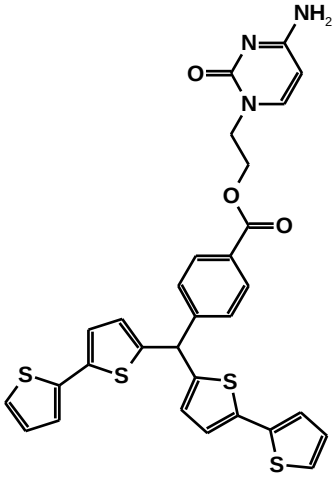	Synthesized at the University of North Texas
7	2,2’-Bithiophene-5-carboxylic acid	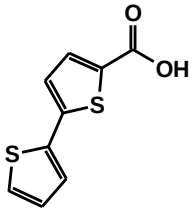	Sigma-Aldrich
8	*p-bis*(2,2'-Bithien-5-yl)methyl-o-catechol	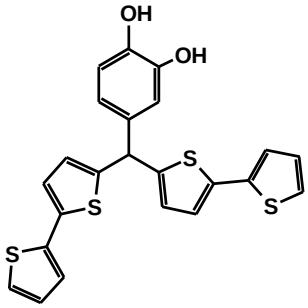	Synthesized at the University of North Texas[165]
9	*p-bis*(2,2'-Bithien-5-yl)methylbenzoic acid	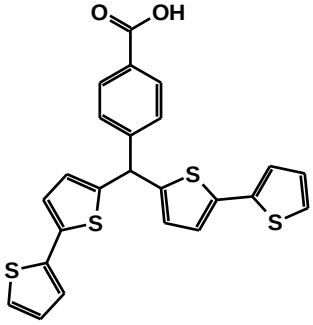	Synthesized at the University of North Texas[67]

Table 2.1-3. Cross-linking monomers.

No.	Name	Structural formula	Source
10	2,4,5,2′,4′,5′-*hexa*(Thiophen-2-yl)-3,3′-bithiophene	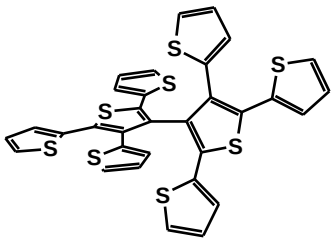	Synthesized at the University of Insubria[155]
11	2,2′-Bithiophene	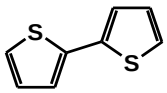	Sigma-Aldrich

Table 2.1-4. Interferents.

No.	Name	Structural formula	Source
12	Adenosine	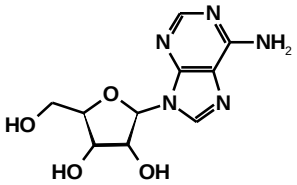	Sigma-Aldrich
13	Guanosine	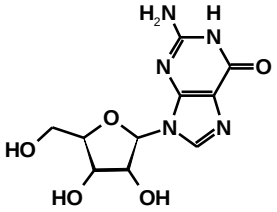	Sigma-Aldrich
14	Glucose	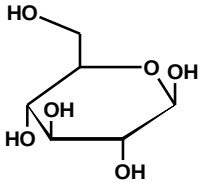	Sigma-Aldrich
15	Thymine	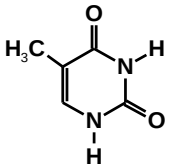	Sigma-Aldrich

16	HAS	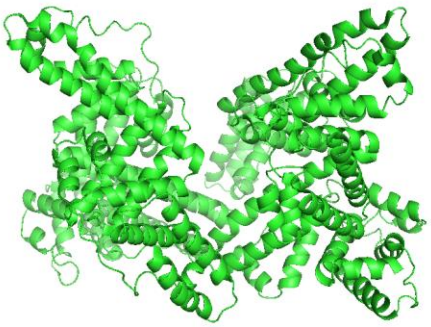	Sigma-Aldrich
17	D-Alanine	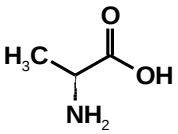	Sigma-Aldrich
18	D-Proline	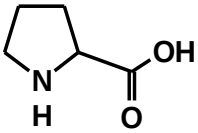	Sigma-Aldrich
19	D-Tyrosine	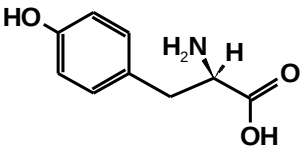	Sigma-Aldrich

Table 2.1-5. Solvents.

Solvent (CAS)	**Source**	**Purity**	**Function**
Acetonitrile, ACN (75-05-8)	Sigma-Aldrich	99.8%, anhydrous	Main solvent for all MIP films preparation
N,*N*-Dimethylformamide, DMF (68-12-2)	Sigma-Aldrich	99.8%, anhydrous	Solvent for MOF-5 preparation
Isopropanol, *i*-PrOH (67-63-0)	CHEMPUR	99.7%	Solvent for cleaning Au-glass slides
Methanol, MeOH (67-56-1)	STANLAB	analytical grade	Solvent for cleaning Au-QCRs
Toluene, TL (08-88-3)	Sigma-Aldrich	99.8%, anhydrous	Solvent for the NGAL in preparation MIP-**2**
Trichloromethane (chloroform), $CHCl_3$ (67-66-3)	Sigma-Aldrich	≥99.0%, anhydrous	Solvent for MOF-5 preparation

Other chemicals

- Hydrochloric acid, HCl, CAS 7647-01-1, 31-38%, CHEMPUR
- Sodium phosphate monobasic, NaH_2PO_4, CAS 10049-21-5, 99%, CHEMPUR
- Sodium hydroxide, NaOH, CAS 1310-73-2, 99%, POCH
- Terephthalic acid, TPA, CAS 100-21-0, 98%, Sigma-Aldrich
- Tetra-*n*-butylammonium perchlorate, $(TBA)ClO_4$, CAS 1923-70-2, ≥99%, Fluka

All the chemicals were used as received.

2. 2 Instrumentation and procedures

2.2.1 Computational calculations and simulations

All quantum-chemical calculations were performed on the workstation with four Intel dual-core processors and Gaussian09 software installed (Gaussian, Inc., CT, USA).[166] Structures of the monomers and the pre-polymerization complexes were optimized using the density functional theory (DFT) with the B3LYP functional and 6-31G* or 3-21G* basis set. The change of the Gibbs free energy, ΔG, of complex formation was obtained from frequency calculation.

The simulation of ligand docking was conducted using Autodock Vina[167] (version 1.1.2) with exhaustiveness parameter set to 64 with the 16×18×20 box size. The center of the box was set to the geometric center of 4-methylcatechol (native ligand).

2.2.2 Preparation of Au-glass slides

Au-glass slides (size 7×21 mm) were prepared in the Institute of Electronic Materials Technology (Warsaw, Poland) by sputtering a thin (100 nm) Au layer over a thin (15 nm) Ti underlayer. These slides were used as supports for deposition of polymer films, and then applied for further investigations, i.e., AFM, SEM, and PM-IRRAS studies. Before each film deposition, Au-glass slides were cleaned with isopropanol in ultrasonicated (160 W power IS-3R of InterSonic, Olsztyn, Poland) for 30 min. Moreover, Au-glass slides coated with respective MIP films were used as extended gates of EG-FET systems.

2.2.3 Preparation of an MOF-5 underlayer for surface developed film molecularly imprinted with human lipocalin-2

In order to obtain a carboxy-terminated Au-glass slide (Scheme 2.2-1) capable of initiating growth of the MOF, an electrochemical polymerization of 2 mM 2,2'-bithiophene-5-carboxylic acid **7** in 0.1 M $(TBA)ClO_4$, ACN solution was performed under potentiodynamic conditions with the scan rate of 50 mV s^{-1}. Just one potentiodynamic cycle was used for thin polymer film deposition. In the next step, the carboxy-terminated Au electrode was placed in a solution of 1.12 mM $Zn(NO_3)_2 \times 6H_2O$ and 0.25 mM TPA in 5 mL DMF to deposit a film of MOF-5.[168] The above mixture was heated

for 6 h at 120 °C, and then the temperature was raised to 150 °C until crystallization began. Finally, the sample was repeatedly washed with DMF, then $CHCl_3$, and then dried.

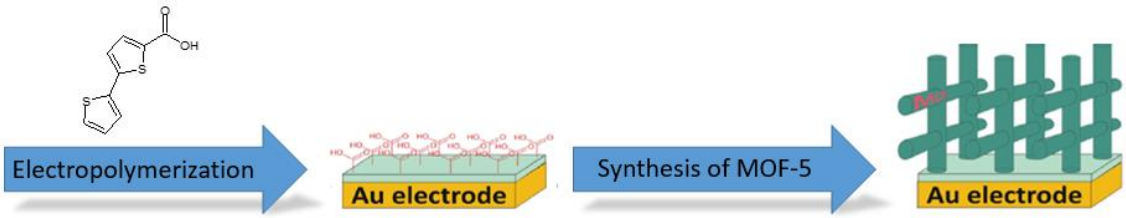

Scheme 2.2-1. Consecutive steps of the procedure utilized herein, which led to preparation of an Au-glass slide with the MOF crystal film deposited.[154]

2.2.4 Preparation of molecularly imprinted polymer and non-imprinted polymer thin films

In the present thesis, four molecularly imprinted polymer (MIP) films were separately prepared and examined. These are, as follows.

MIP-**1** – polymer molecularly imprinted with inosine,

MIP-**2** – polymer molecularly imprinted with human lipocalin-2, NGAL,

MIP-**3** – polymer molecularly imprinted with D-phenylalanine,

MIP-**4** – polymer molecularly imprinted with L-phenylalanine.

Each of the above MIP films were investigated in comparison to respective non-imprinted polymer (NIP) films. Control NIP films were prepared by deposition from the template-free solutions using the same electropolymerization procedures as those for MIPs.

2.2.4.1 Instrumentation

An AUTOLAB computerized electrochemistry system of Eco Chemie (Utrecht, The Netherlands), equipped with expansion cards of the PGSTAT12 potentiostat and the FRA2 frequency response analyzer, and controlled by GPES v.4.9 software of the same manufacturer, was used for the potentiodynamic deposition of thin MIP-**1**, MIP-**3**, and MIP-**4** films, as well as respective NIP films. Electrochemical deposition experiments for MIP-**2** were performed using Autolab PGSTAT20 potentiostat/galvanostat driven by dedicated GPES v.4.3 software.

A three-electrode electrochemical cell (Scheme 2.2-2) was applied for all MIP film depositions on 1-mm diameter Pt disk electrodes or Au-glass slides. The MIP films were deposited by potentiodynamic electropolymerization in the potential range of 0.50 to 1.40 V vs. Ag/AgCl for MIP-**1**, 0 to 1.40 V for MIP-**2**, and 0.50 to 1.25 for MIP-**3** and MIP-**4**. The scan rate was 50 mV s^{-1}. Sufficient solution conductivity was afforded by a 0.1 M (TBA)ClO_4 supporting electrolyte. Thickness of the MIP films was controlled by the number of the potential cycles and, therefore, by the amount of charge passed.

The same instrumentation setup was used for differential pulse voltammetry (DPV) measurements.

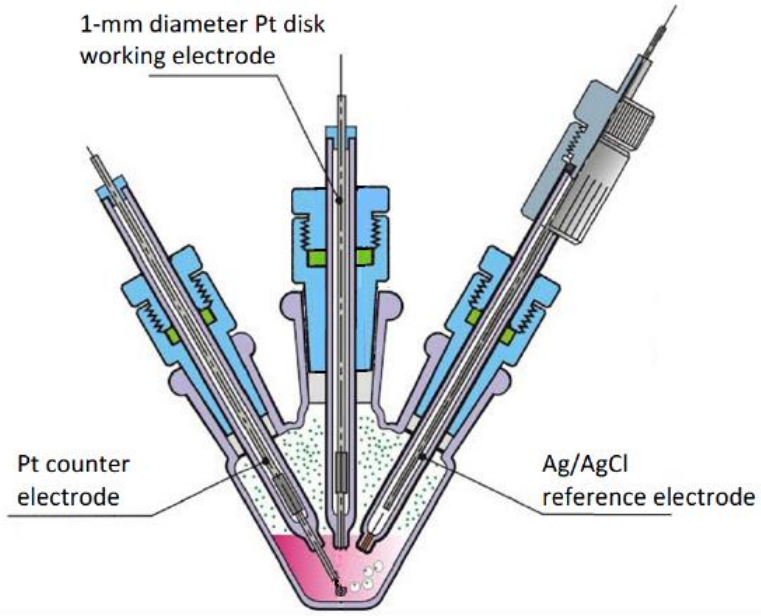

Scheme 2.2-2. The sketch of a three-electrode electrochemical mini cell.

2.2.4.2 General procedure of polymer preparation

A general procedure of preparation of MIP and NIP films (Scheme 2.2-3) was completed in 5 steps.

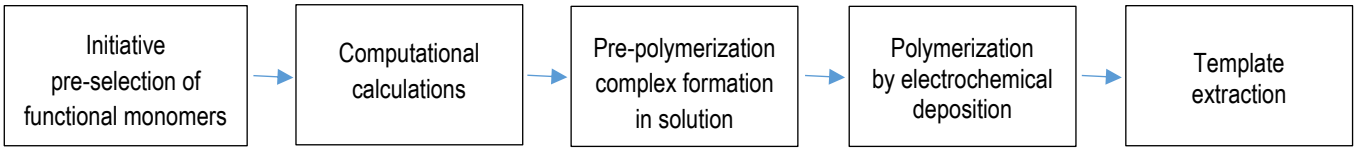

Scheme 2.2-3. Flow chart of consecutive steps of a general MIP film preparation procedure.

MIPs and NIPs preparation procedure was initiated by pre-selection of functional monomers. This step was based on experience, chemical intuition and literature survey.

The second step involved computational calculations of stability of the pre-polymerization complex and its structure optimization. For that, structures of a template molecule, functional monomer molecules, and their complexes were optimized separately. Next, Gibbs free energy changes (ΔG) corresponding to formation of optimized complex molecules were calculated. These ΔG values for complexes of different compositions and stoichiometry were compared in order to select those most promising for the MIP formation. This is why complexes of the most negative ΔG values were chosen for the next step.

After computational calculations, the selected functional monomers were dissolved in a suitable solvent (or in a solvent mixture) together with the template and cross-linking monomers to form spontaneously the pre-polymerization complex in solution.

In the fourth step, these complexes were polymerized, under potentiodynamic conditions, and the resulting polymer film was deposited on the surface of electrodes (i.e., Au-glass slides, 1-mm diameter Pt disk electrode) in the supporting electrolyte solution. The potentiodynamic technique used allowed for controlling roughness and thickness of the MIP films deposited. After the deposition, the MIP films were rinsed with abundant solvent to remove excess of the supporting electrolyte and non-polymerized functional monomers.

The fifth step involved template extraction. This step was dependent on the type of analyte-film interactions. It led to emptying the molecular cavities imprinted in the MIPs. The MIP films, prepared that way on electrodes, formed recognition units of chemical sensors and were ready for analyte selective detection and determination.

2.2.4.3 Preparation of a polymer molecularly imprinted with inosine

Thin MIP-**1** film was prepared by dissolving the inosine **1** template together with functional 2,2'-bithiophene-5-boronic acid **5**, 2-(cytosin-1-yl)ethyl *p-bis*(2,2'-bithien-5-yl)methylbenzolate **6**, and crosslinking 2,4,5,2',4',5'-*hexa*(thiophen-2-yl)-3,3'-bithiophene **10** monomers in ACN. The molar ratio of the template to functional monomers was 1 : 1 : 1, as inferred from the quantum-chemical calculations. Concentrations of inosine and both functional monomers were kept at 0.1 mM. To provide accessible molecular cavities in the resulting MIP, an excess of the cross-linking monomer **10** was

used, so that the template-to-cross-linker molar ratio was 1 : 4. The template was removed by sample washing in 0.1 M HCl.

2.2.4.4 Preparation of a polymer molecularly imprinted with human lipocalin-2

The solution for polymerization leading to preparation of MIP-**2** was prepared by dissolving the functional *p-bis*(2,2'-bithien-5-yl)methyl-*o*-catechol **8** and crosslinking 2,2'-bithiophene **11** monomers together with the NGAL **2** template at the molar ratio of 100 : 400 : 1, respectively. The mixed TL and ACN solvent solution at the volume ratio of 7 : 3 was used to dissolve the monomers and the template. For preparation of a structured MIP film, the Au-glass slide coated with MOF-5 crystals[168] (Scheme 2.2-4) was immersed in the solution for pre-polymerization for 1 h. After the polymerization, the protein template was removed together with MOF by sample washing for 1 h in 0.1 M HCl. Direct electropolymerization carried out using the same pre-polymerization solution, on the Au-glass slide without MOF deposited, led to deposition of a non-structured thin MIP film.

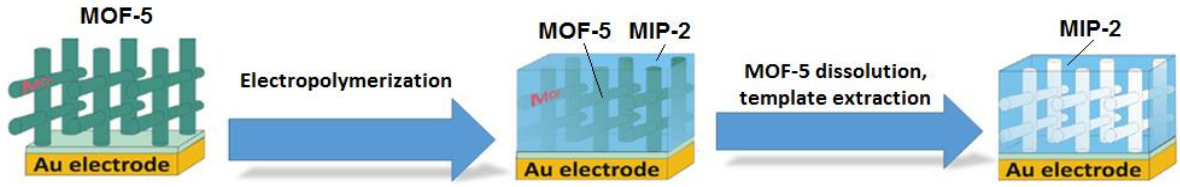

Scheme 2.2-4. Consecutive steps of the procedure leading to preparation of an MIP-**2** structured film.[154]

2.2.4.5 Preparation of polymers molecularly imprinted with D- or L-phenylalanine

Thin films of MIP-**3** and MIP-**4** were separately imprinted with D-phenylalanine **3** and L-phenylalanine **4**, respectively. An ACN-water mixed solvent solution of the 9 : 1 volume ratio was used. For preparation of solutions for electropolymerization, template **3** or **4** along with the *p-bis*(2,2'-bithien-5-yl)methylbenzoic acid **9** functional monomer were dissolved in these mixtures. Quantum chemistry calculations suggested the 1 : 2 optimum molar ratio of the template to the functional monomer. Moreover, crosslinking 2,4,5,2',4',5'-*hexa*(thiophen-2-yl)-3,3'-bithiophene monomer **10** at the molar ratio of 1 : 1 to template was used to generate molecular cavities in MIP accessible for the analyte molecules. Templates **3** or **4** were then extracted from the films by liquid-solid extraction with 10 mM NaOH at R.T. for 90 min.

2.2.5 Extended-gate field-effect transistor chemosensor measurements

The EG-FET sensing setup (Scheme 2.2-5) consisted of two main units. Its recognition unit was made of the Au-glass slide coated with a film of respective extracted MIP or NIP, and, in the case of the NGAL chemosensor, also with the surface enlarged MIP-**2** on MOF film. The working surface area of the extended recognition unit was 21 mm^2. This unit was electrically connected to the transduction unit, i.e., the gate of a commercial MOSFET model CD4007UB. A Keithley 2636A (Keithley Instruments, Inc. OH, USA) dual-channel source meter was used for deriving the transistor characteristics. These characteristics were determined under stagnant-solution conditions using a conical glass electrochemical mini cell filled with 1 mL of water (for MIP-**1** and MIP-**2**) or 10 mM NaH_2PO_4 (for MIP-**3** and MIP-**4**). The gate coated with an MIP film was mounted parallel to the Pt reference electrode. Distance between these electrodes was kept constant at ~10 mm.

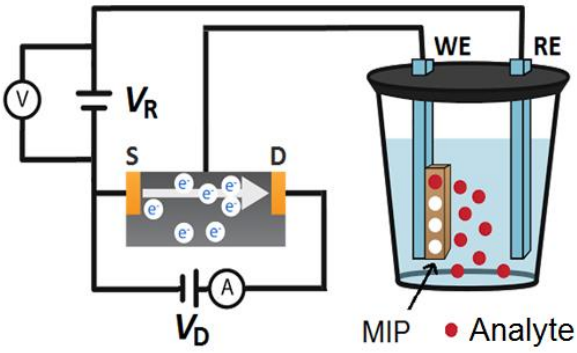

Scheme 2.2-5. Experimental setup based on the EG-FET design, using Au-glass slide with the deposited extracted MIP or NIP film as the gate (working electrode, **WE**), and a Pt plate as the reference electrode (**RE**). **D** and **S** stand for the drain and source components of the FET structure, respectively.

2.2.6 Piezoelectric microgravimetry (PM) measurements

Piezoelectric microgravimetry (PM) measurements were carried out with a Model 5710 electrochemical quartz crystal microbalance of IPC PAS.[169] The resonant frequency change was measured with 1-Hz resolution using a 14-mm diameter, plano-plano quartz crystal resonators (Au-QCRs) of 10-MHz resonant frequency with 5-mm in diameter and 100-nm thick Au film electrodes vapor deposited over a 10-nm thick Ti underlayer on both resonator faces. For electropolymerization, which was performed under stagnant-

solution conditions, electrochemical quartz-crystal microbalance (EQCM) 5710 was interfaced with the EP-20 potentiostat, both of IPC PAS, and its quartz crystal holder was mounted horizontally with the Au-QCR facing upward in order to use as low volume of the sample solution as 100 µL. The resonators were cleaned for 5 min with MeOH before electropolymerization. For PM measurements under flow injection analysis (FIA) conditions, a flow-through EQCM 5610 holder of IPC PAS [170] was used. For experiments using MIP-**1,** distilled water was used as the carrier solution pumped with the 35 µL/min flow rate and for experiments with the MIP-**3** 10 mM NaH_2PO_4 was engaged as the carrier solution pumped with the same flow rate.

2.2.7 Other instrumentation and procedures

The UV–visible spectra were recorded with 0.1-nm resolution by using a UV 2501-PC recording spectrophotometer of Shimadzu Corp (Tokyo, Japan).

Polymer surfaces were imaged with atomic force microscopy (AFM) using a Multimode 8 microscope equipped with the Nanoscope V controller both of Bruker. Tapping™ and ScanAsyst Mode™ imagining was performed. For the ScanAsyst Mode™ mode, a silicon tip, mounted on a nitride cantilever of 70 kHz resonant frequency, was used. For the Tapping™ mode, a silicon tip, mounted on a silicon cantilever of 270 KHz resonant frequency, was used. For this imaging, the polymer films were deposited on the (7×4) mm^2 strips of the Au-glass slides. For determining average film thickness, some parts of the films were carefully removed in few different places from the electrode surface, i.e., scratched with a Teflon™ spatula, under an optical microscope. Subsequently, these scratches were imaged with AFM. Then, heights of the resulting steps were measured by averaging the number of points on both sides of the step (sufficiently far from its partially detached front). The difference of the average values of points on the step and at its foot determined the height of the step. Finally, step heights measured for different scratches were averaged to get an average value of film thickness.

SEM images of polymers deposited on Au-glass slides were recorded with Nova NanoSEM 450 microscope of FEI (USA).

Powder X-ray diffraction (XRD) data were collected on Empyrean diffractometer (PANalytical, The Netherland). Diffraction measurements employed Ni-filtered Cu Kα

radiation of a copper sealed tube, charged with 40 kV voltage and 40 mA current, and Bragg-Brentano geometry with beam divergence of 1 degree in the scattering plane. Diffraction patterns were measured in the range of 4-50 degrees of scattering angle by step scanning with step of 0.02 degree.

Infrared (IR) spectra were measured with a Vertex 80v Fourier Transform IR (FTIR) computer-controlled Bruker spectrophotometer equipped with Opus 6.5 software of the same manufacturer. In order to measure an IR signal from thin polymer films, the PMA50 module was used. This module enables carrying out polarization-modulation infrared reflection-absorption spectroscopy (PM-IRRAS) measurements with 2-cm^{-1} resolution. For each spectrum, 1024 scans were recorded. For the measurements, polymer films were deposited on Au-glass slides. The experimental IR spectra were compared with those theoretically generated. Theoretical vibration frequencies of normal modes were calculated with the DFT method within harmonic approximation. Positions of the bands in experimental spectra were determined with the procedure implemented in the Opus 6.5 software package. Calculated normal modes were assigned to experimental bands in two steps. The first Vibrational Energy Distribution Analysis (VEDA) step calculated normal modes expressed in terms of local modes (vibrations of internal coordinates: bonds, i.e., bond angles, and dihedral angles).[171,172] In the second step, the spectra calculated were fitted to experimental data by means of linear regression. That way, the unharmonic factor was phenomenologically introduced to calculated frequencies. The calculated frequencies were scaled with the SPESCA program.[173]

2. 3 Experimental techniques

2.3.1 Measurements involving extended-gate field-effect transistors (EG-FETs)

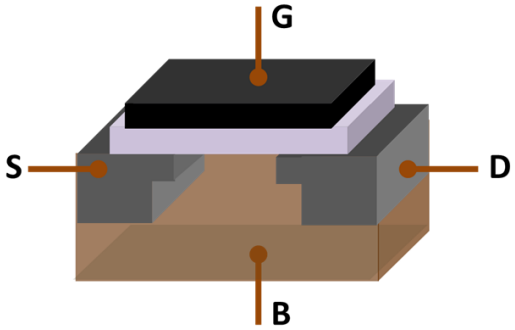

Scheme 2.3-1. Metal-oxide semiconductor field-effect transistor (MOSFET) showing gate (G), body (B), source (S) and drain (D) terminals. The gate is separated from the body by an insulating layer (white area). B is connected to the source terminal making it a three-terminal device like other FETs.[139]

The structure of a MOSFET is shown in Scheme 2.3-1. The MOSFET consists of a small piece of a p-type silicon (substrate, or body, B) with two n-type regions called source (S), and drain (D). The surface is coated with an insulating layer (for example, SiO_2) and a thin metal layer is deposited on top of it to form a gate. If the gate is positively charged, current flows between S and D (the channel).

From the point of view of electronics, the MIP-film coated Au-glass slides (see Chapter 2.2.2), used in the present thesis, are in fact simple extensions of the classical FET gates. So, all changes of potential at the Au-glass slide were transferred to the transistor gate leading to changes of the S – D current, exactly as if the potential changes occurred on the gate itself. In order to open or close the gate, there is also a need to apply certain voltage across the solution/polymer/Au-glass interfaces. For that purpose, the additional electrode is immersed in the test solution, which was polarized herein by using a source meter. At constant applied gate voltage (V_G), drain voltage (V_D) was varied and the resulting drain current (I_D) was measured. When the analyte was sorbed in the MIP film, the effective gate voltage was changed leading to the I_D change, which was proportional to the amount of the analyte sorbed in the film (Scheme 2.3-2). Therefore, the operation of the EG-FET was very similar to that of a typical MOSFET,

except that an additional sensing structure in the form of an extended gate was immersed in the test solution.

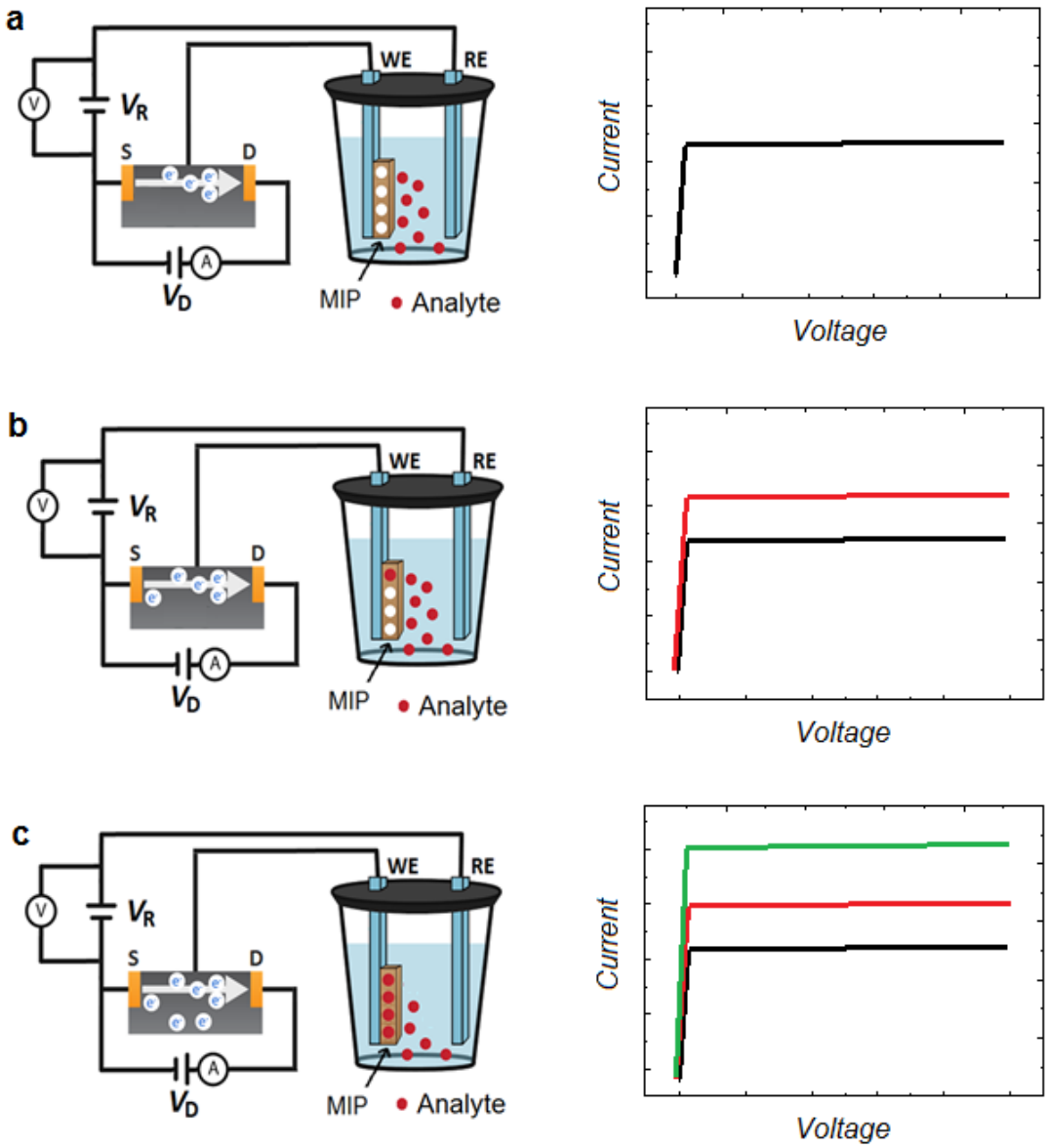

Scheme 2.3-2. Performance of a simplified setup, based on the EG-FET design, using an extended gate coated with a template-extracted MIP film as the working electrode, **WE** (a) before the analyte binding, (b) after binding some portion of the analyte by the MIP, (c) after filling with the analyte molecules all molecular cavities in MIP. **D** and **S** stand for the drain and source components of the FET structure, respectively. Current changes caused by the analyte binding to the MIP are shown with the EG-FET characteristics (on the right-hand side of each scheme). **RE** stands for the reference electrode. V_D and V_R stand for the drain voltage and reference voltage, respectively.

2.3.2 Cyclic voltammetry (CV)

CV is one of the most frequently used electroanalytical techniques where variation of current with the potential, applied to the working electrode, is measured. This potential is linearly changed with time from the initial value of E_i to the final value of E_f, through the vertex potential, E_v (Scheme 2.3-3).

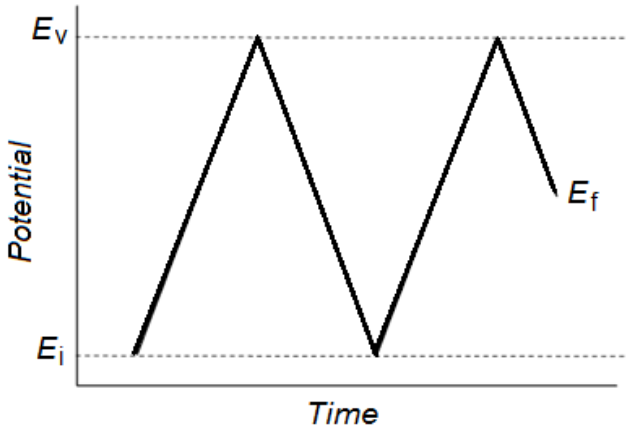

Scheme 2.3-3. The potential change with time of the working electrode in cyclic voltammetry, CV.

In a typical cyclic voltammogram (a curve of $I = f(E)$), recorded for a solution containing a red-ox active analyte, current peaks are observed. With the increase of the working electrode potential, current increases (A-B in Scheme 2.3-4) until the analyte concentration at the electrode surface drops to zero (B in Scheme 2.3-4). Then, the anodic current peak, I_{pa}, is formed at the anodic peak potential, E_{pa}. Afterwards, current decreases as the concentration of the analyte is depleted in the electrode vicinity (B-C in Scheme 2.3-4). If the red-ox couple is reversible, then negative current will grow during the opposite potential scan until the cathodic peak potential, E_{pc}, of the oxidized species is reached (C-D in Scheme 2.3-4). This cathodic peak, I_{pc}, is formed because of depletion of the oxidized species in the electrode vicinity.

For a reversible red-ox process, the peak current is described by the Randles-Ševčik equation (Equation 2.3-1)[174] if the process is diffusion controlled.

$$i = 2.72 \times 10^5 n^{2/3} D^{1/2} A v^{1/2} c \qquad \text{(Equation 2.3-1)}$$

In this equation *n* is the number of electrons exchanged in the elementary electrode process, *A* is the electrode surface area in cm^2, *D* is the diffusion coefficient of a red-ox species in cm^2/s, *v* is the potential scan rate in V/s, and *c* is the red-ox species concentration in bulk of the solution, in M.

Moreover, the anodic-to-cathodic peak separation for this process is described by Equation 2.3-2,[174]

$$\Delta E = E_{\mathrm{pa}} - E_{\mathrm{pc}} = \frac{0.059}{n}\ [V] \qquad \text{(Equation 2.3-2)}$$

The situation is different for a quasi-reversible process, that is the process controlled by both the rate of the electrode process and the rate of diffusion. In this case, the peak separation is larger. For an irreversible process, solely controlled by the rate of the electrode process, the anodic and cathodic peak separation is even higher or, in many cases, only one peak is seen on the cyclic voltammogram. For an irreversible oxidation, the peak of anodic current is described by Equation 2.3-3

$$i_{\mathrm{pa}} = 2.72 \times 10^5 \alpha_{\mathrm{a}}^{1/2} D^{1/2} A v^{1/2} c \qquad \text{(Equation 2.3-3)}$$

where α_{a} is the charge transfer coefficient of an anodic process.

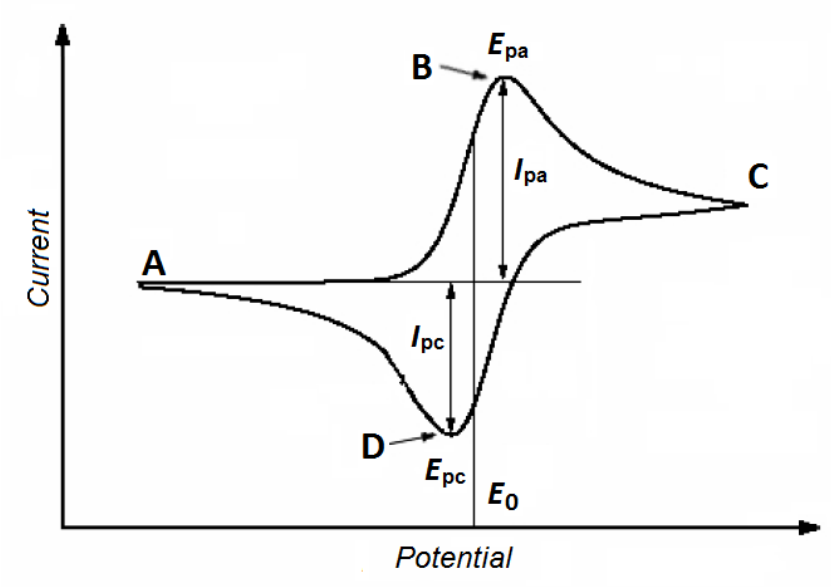

Scheme 2.3-4. The change of current as a function of potential of the working electrode in cyclic voltammetry[175] for a reversible red-ox couple. E_{pa} and E_{pc} stand for the anodic and cathodic peak potential, respectively, while I_{pa} and I_{pc} for anodic and cathodic peak current, respectively.

2.3.3 Differential pulse voltammetry (DPV)

As an experimental electroanalytical technique, DPV, with a small-amplitude pulse was developed for substantial elimination of the background capacitive currents, thus increasing sensitivity of determination of red-ox species. Typical DPV potential program is shown in Scheme 2.3-5. The pulse height is 10 to 100 mV and it is maintained constant with respect to the base potential.[176, 177]

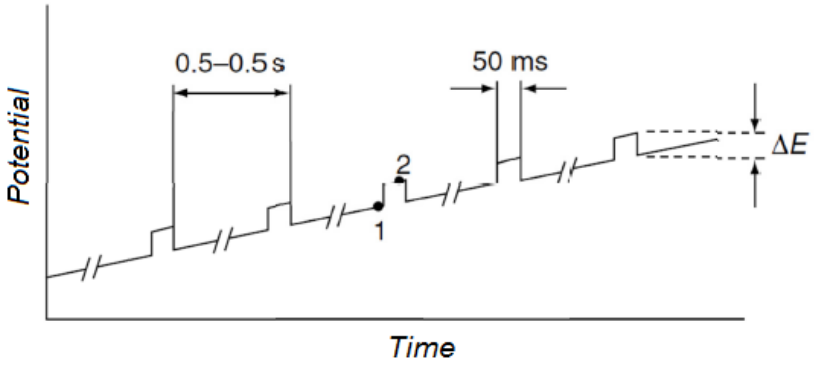

Scheme 2.3-5. The potential-time program in DPV. ΔE and t_P is the pulse amplitude, and duration, respectively, *1* and *2* is the time before pulse application and at the end of the pulse, respectively, at which time the currents are sampled [177].

The current difference, $\delta I = I(t_1) - I(t_2)$, is recorded versus the base potential ramp, where t_1 and t_2 is the time before pulse application and at the end of the pulse, respectively, at which current is recorded. The pulse duration, t_P, is selected from the range of 5 to 100 ms. The peak current is directly related to the analyte concentration,

$$i_{\mathrm{p}} = \frac{nFAD^{1/2}c}{\sqrt{\pi t_{\mathrm{m}}}}\left(\frac{1-\sigma}{1+\sigma}\right) \qquad \text{(Equation 2.3-4)}$$

where t_m is the time at which the time is measured from the moment of application of the pulse and

$$\sigma = exp\left[\left(\frac{nF}{RT}\right)\left(\frac{\Delta E}{2}\right)\right] \qquad \text{(Equation 2.3-5)}$$

and ΔE is the pulse amplitude. The peak potential can be identified by

$$E_{\mathrm{p}} = E_{\mathrm{p}/2} - \frac{\Delta E}{2} \qquad \text{(Equation 2.3-6)}$$

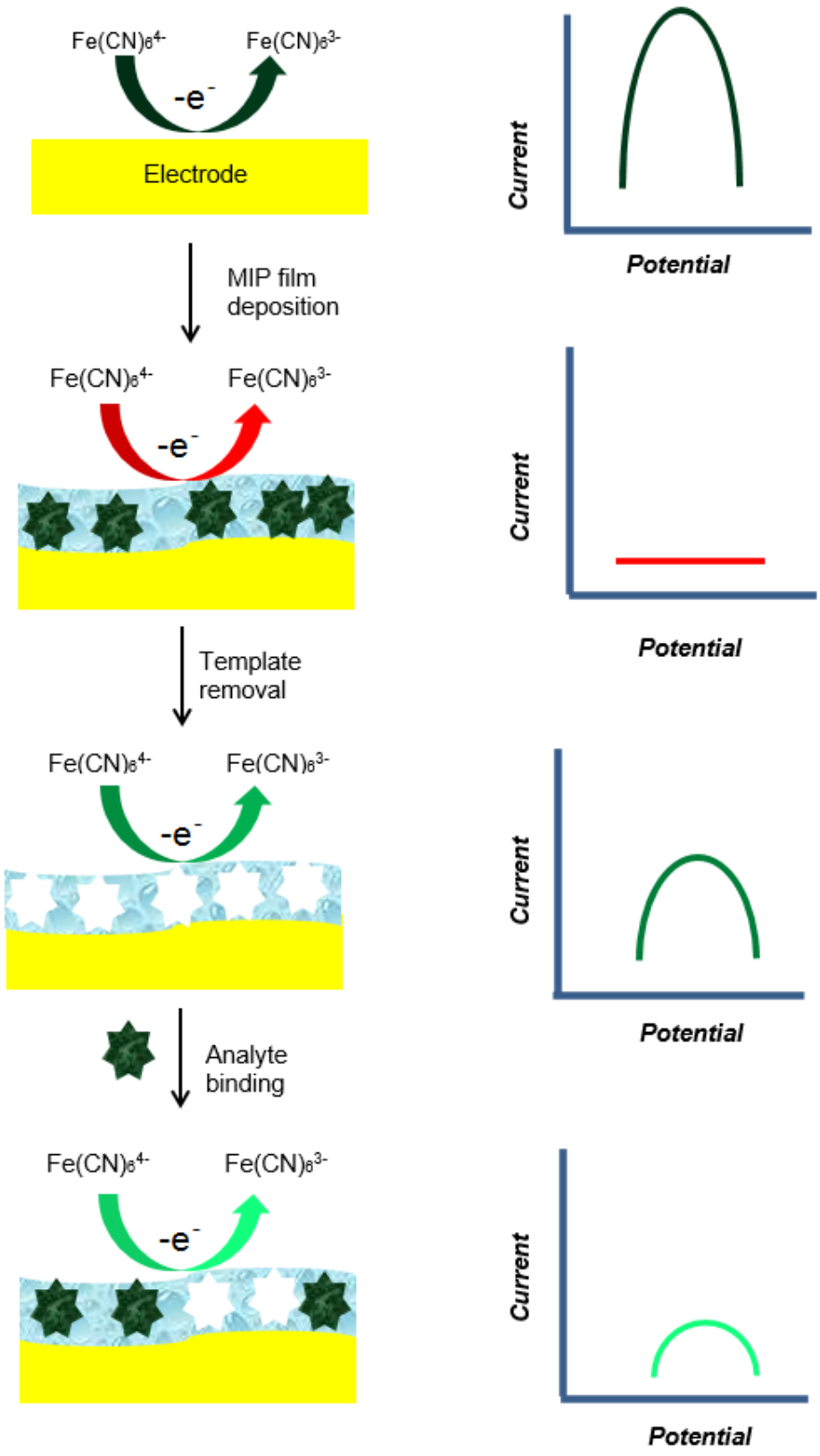

Scheme 2.3-6. Indirect electrochemical determination of an analyte at the MIP film coated electrodes using the "gate effect" and the corresponding DPV current-potential responses.[44]

Due to high sensitivity, DPV allows for analyte determination at concentrations as low as 10^{-8} M. Herein, DPV was used as the indirect proof of template removal from MIP molecular cavities by the so-called "gate effect" (Scheme 2.3-6) using an electrochemical setup shown in Scheme 2.2-2. The 1-mm diameter Pt disk electrode, coated with an MIP film, was immersed in the 0.1 M $K_4[Fe(CN)_6]$ red-ox probe, in 0.1 M KCl.

2.3.4 Piezoelectric microgravimetry (PM)

Piezoelectric microgravimetry is a technique that is based on a converse piezoelectric effect. Piezoelectric effect is a physical phenomenon of electric charge generation while mechanical stress is applied to the piezoelectric material. Piezoelectricity occurs in crystals with no symmetry centers. The converse effect is observed when alternating voltage is applied to the electrical contacts mounted to the sides of such a crystal. Then, the crystal mechanically oscillates at the natural resonance frequency proportional to its thickness.[178] When mass is deposited on an AT-cut QCR surface, a drop in oscillation frequency is observed. The frequency change is correlated with the mass change by the Sauerbrey relation (Equation 2.3-7),[179]

$$\Delta f_{\mathrm{mass}} = -\frac{2f_0^2 \Delta m}{A_{\mathrm{acoust}}(\mu_{\mathrm{q}}\rho_{\mathrm{q}})^{1/2}} \qquad \text{(Equation 2.3-7)}$$

where f_0 is the fundamental frequency of the resonator (here 10 MHz), A_{acoust} is the acoustically active area of the resonator (here 0.1963 cm^2), μ_{q} is the shear modulus of quartz (2.947×10^{11} g s^{-2} cm^{-1}), and ρ_{q} is the quartz density (2.648 g cm^{-3}).

The Sauerbrey equation holds if several assumptions are fulfilled. An important one requires that the film deposited on a resonator was perfectly elastic, i.e., as rigid as the resonator material itself. If the resonator is contacted with a liquid, then the frequency change is described by Equation 2.3-8,[178]

$$\Delta f_{\mathrm{mass}} = -\left[\frac{2f_0^2}{(\mu_{\mathrm{q}}\rho_{\mathrm{q}})^{1/2}}\right]\left[\left(\frac{\Delta m}{A}\right) + \left(\frac{\mu_{\mathrm{L}}\rho_{\mathrm{L}}}{4\pi f_0}\right)^{1/2}\right] \qquad \text{(Equation 2.3-8)}$$

where μ_{L} and ρ_{L} are the shear modulus and density of the contacting liquid, respectively. This formalism has been extended to resonators coated with viscous films. In this case,

contribution of the frequency change because of the change of film viscosity is given by Equation 2.3-9,[178]

$$\Delta f = -\Delta f_0^{3/2} \left(\frac{\mu_\mathrm{L} \rho_\mathrm{L}}{\pi \mu_\mathrm{q} \rho_\mathrm{q}} \right)^{1/2} \qquad \text{(Equation 2.3-9)}$$

This change can indirectly be measured by the dynamic resistance, R_D, described by Equation 2.3-10

$$R_\mathrm{D} = \frac{A}{k_\mathrm{QCR}^2} (2\pi f_0 \mu_\mathrm{L} \rho_\mathrm{L})^{1/2} \qquad \text{(Equation 2.3-10)}$$

Where $k_\mathrm{QCR}^2 = 7.47 \times 10^{-3} A^2 s\, m^{-2}$ is the electromechanical coupling factor of QCR. From the last two equations, a relation (Equation 2.3-11) between the resonant frequency change and R_D can be derived as

$$\Delta f = \frac{k^2 R_D f_0}{\pi A (2\mu_q \rho_q)^{1/2}} \qquad \text{(Equation 2.3-11)}$$

Therefore, the mass change can be determined from a simultaneously recorded resonant frequency and dynamic resistance change (Scheme 2.3-7).

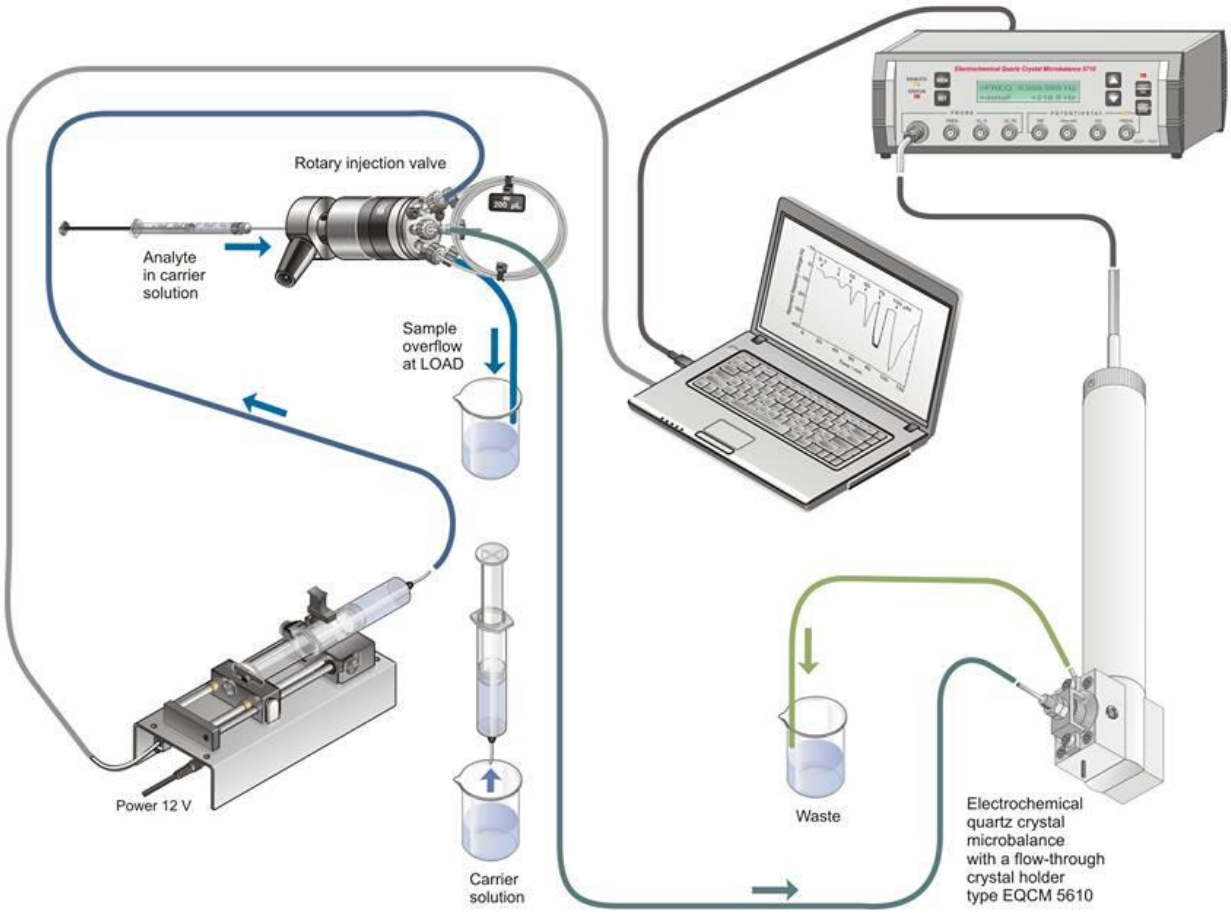

Scheme 2.3-7. Sketch of the setup used herein for measurement under flow-injection analysis (FIA) on the MIP-extracted (or NIP) film coated 10-MHz AT-cut quartz crystal resonator (QCR). Such setup provide simultaneous record of resonant frequency together with dynamic resistance changes.

2.3.5 Ultraviolet-visible (UV-vis) spectroscopy

Ultraviolet-visible (UV-vis) spectroscopy is a routinely used spectroscopic technique for quantitative determination of analytes, such as organic compounds or biological macromolecular compounds.

When light passes through or is reflected from a sample, the amount of light absorbed is the difference between the incident and the transmitted radiation (Scheme 2.3-8).

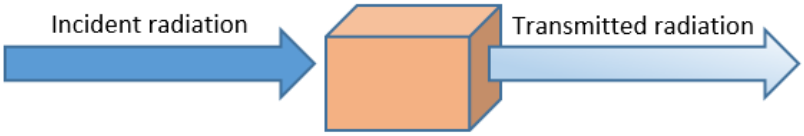

Scheme 2.3-8. Sketch illustrating light absorption.

The amount of light absorbed is expressed as transmittance (Equation 2.3-12) or absorbance (Equation 2.3-13). The relation between absorbance and concentration of an analyte is expressed by the law of Lambert-Beer (Equation 2.3-14)

$$Transmittance = \frac{Intensity\ of\ transmitted\ radiation}{Intensity\ of\ incident\ radiation} \qquad \text{(Equation 2.3-12)}$$

$$Absorbance = -\log(Transmittance) \qquad \text{(Equation 2.3-13)}$$

$$Absorbance = \varepsilon cL \qquad \text{(Equation 2.3-14)}$$

where ε is the molar absorptivity coefficient (M^{-1} cm^{-1}), c is concentration and L is the path length of the beam of light through the material sample (cm).

Most of organic compounds absorb the UV light. This is why the UV-vis spectroscopy is frequently used as a technique for determination of these compounds. The UV-vis spectrum is an effect of the energy transitions of electrons resulting from absorption of radiation between 200 and 380 nm. It is presented as the relation between absorbance (or transmittance) and wavelength. The presence of different groups results in appearance of absorption bands in different spectral ranges (Scheme 2.3-9).

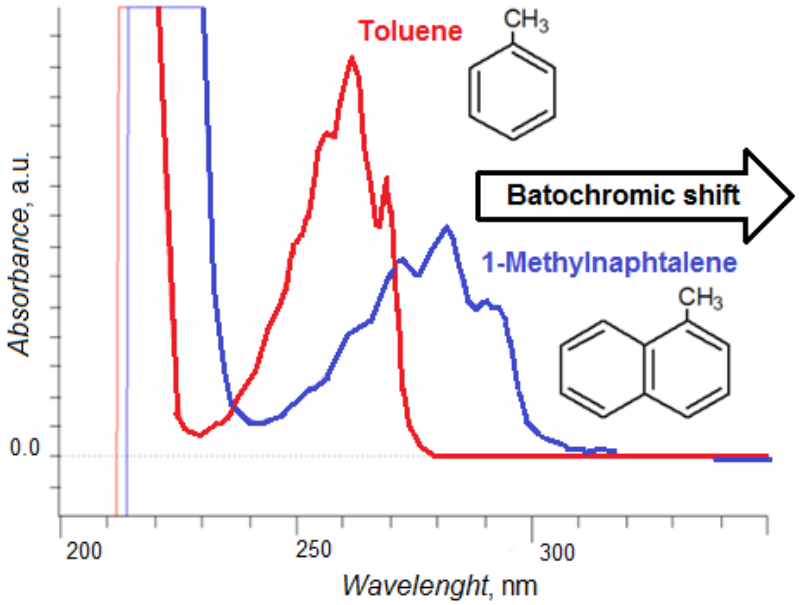

Scheme 2.3-9. UV-vis spectra of toluene and 1-methylnaphtalene, illustrating the bathochromic shift.[180]

Bathochromic or hypsochromic shift is a change of spectral band position in the spectrum of a molecule to longer or shorter wavelength, respectively. This shift can occur because of a change in environmental conditions, e.g., in solvent polarity. Moreover, this shift is observed in a series of structurally related compounds with different substituents.

Herein, the UV-vis spectroscopy was used to determine removal of the inosine template from molecular cavities of the MIP before determination of the sensor performance.

2.3.6 Polarization-modulation infrared reflection-absorption spectroscopy (PM-IRRAS)

Polarization-modulation infrared reflection-absorption spectroscopy (PM-IRRAS) is used for characterization of orientation of molecules in thin films or monolayers deposited on metal substrates (Scheme 2.3-10). It has an advantage of high surface sensitivity. Moreover, the advantage over the conventional IRRAS mode is that modulated reflectivity is independent of the isotopic absorption from gas or bulk water. Consequently, the interfering effect of water vapor and carbon dioxide is eliminated.

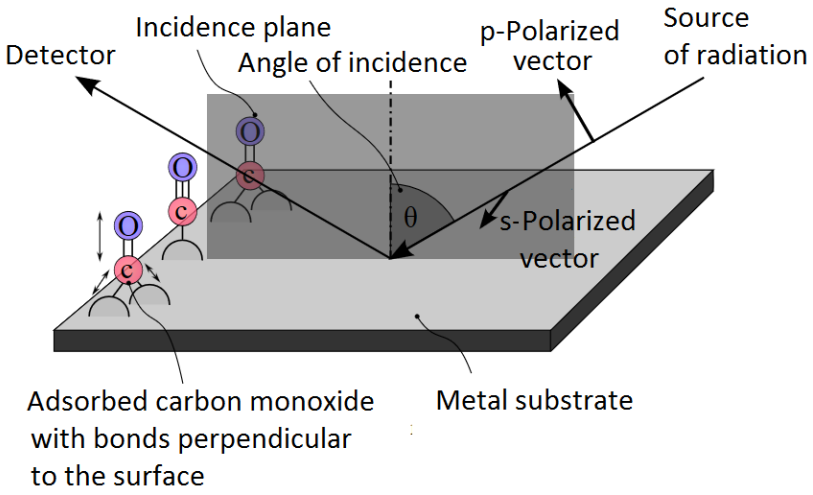

Scheme 2.3-10. Principle of polarization-modulation infrared reflection-absorption spectroscopy (PM-IRRAS) using the example of carbon monoxide adsorbed on a metal surface. The CO group, vibrating perpendicularly to the substrate surface, can interact only with p-polarized radiation.[181]

An infrared beam can be split into s- and p- polarized components, in which the electric vector oscillation is parallel (for p-polarized component) and perpendicular (for s-polarized component) to the plane of incidence. When one of s- or p- component is incident on a metal surface, a stationary wave is resulting from the interference between incident and reflected beams. The amplitude of electric field is maximized at high angles of incidence. Signals can be obtained due to the surface species by grazing incidence of p-polarized light.

Herein, the PM-IRRAS technique was used to compare thin MIP films before and after template extraction as well as for composition determination of MIP and NIP films.

2.3.7 Atomic force microscopy (AFM)

AFM is a technique of high-resolution imaging of materials surfaces. In AFM, the tip of a vertically vibrating flexible cantilever is brought very close to the sample surface to allow for interactions between them. The measurement of the force generated enables sample imagining.[182] This force can be measured as the cantilever deflection. This deflection can be measured by shining a laser beam on the cantilever top and determining position of the reflected beam (Scheme 2.3-11).

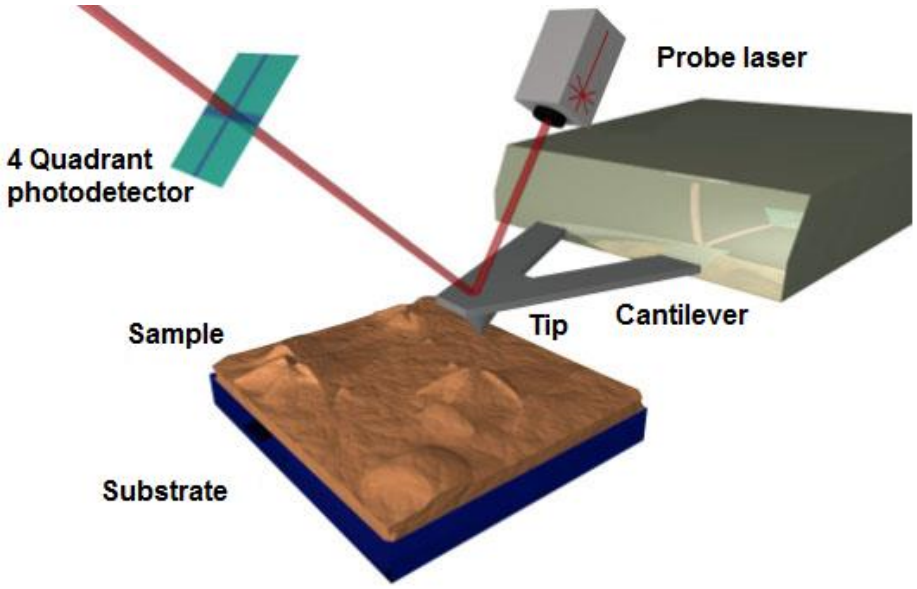

Scheme 2.3-11. A sketch of the AFM setup showing the tip interacting with the sample surface.[183]

There are at least three modes of AFM operation, namely, the contact, semi-contact, and non-contact mode.[184] In the contact mode, the force between the AFM tip and the sample is kept constant using a feedback signal to keep the cantilever deflection constant. In the semi-contact mode, the AFM tip oscillates with its resonance frequency. The oscillation is affected by tip interaction with the sample. The instrument adjusts the tip position, so that the oscillation frequency of the AFM tip stays constant. In the non-contact mode, AFM tip is moved close (in the order of Angstroms) to the sample.

Herein, AFM was used to determine the MIP and NIP topography and morphology as well as film thickness.

2.3.8 Scanning electron microscopy (SEM)

In scanning electron microscopy (SEM), electrons scattered back from a small irradiated area of the sample are detected and the electrical signal is sent to a video screen. An image of the surface is then obtained by scanning an electron beam across the sample. The electrons interact with atoms in the sample producing signals that contain information about both the sample surface topography and composition.

A scanning electron microscope is a type of electron microscope that produces images of a sample by scanning it with a focused beam of electrons. The microscope consists of an electron optical column, a vacuum system, electronic circuit, and software. The electron gun at the top of the column produces an electron beam that is focused into a 1 nm diameter spot on the sample surface. The beam, whose typical energy ranges from 0.2 to 40 keV, passes through pairs of scanning coils or pairs of deflector plates in the electron column, typically in the final lens. This lens deflects the beam so that it scans in a raster fashion over a rectangular area of the sample surface. Various signals created by interactions between the beam and the sample are measured. The stored values are then mapped as variations in brightness on the image display.[185]

The types of signals produced by a scanning electron microscope include secondary electrons, reflected or back-scattered electrons, photons of characteristic X-rays and light (cathodoluminescence), absorbed current (specimen current) and transmitted electrons. The secondary electrons signal is the signal most frequently used. It varies with the topography of the sample surface much like an aerial photograph – edges are bright, recesses are dark (Figure 2.3-1). The ratio of the size of the displayed image to the size of the area scanned on the specimen gives the magnification.[186]

Magnification in SEM can be controlled over a range of about 6 orders of magnitude, namely from 10 to 3,000,000 times. Requirement of each technique of electron microscopy is a high vacuum of at least 10^{-4} Pa.[187] Figure 2.3-1 shows the photography recorded with Nova NanoSEM 450 operating in IPC PAS. The images show a MOF magnified 1,500 times (Figure 2.3-1a) and 10,000 times (Figure 2.3-1b).

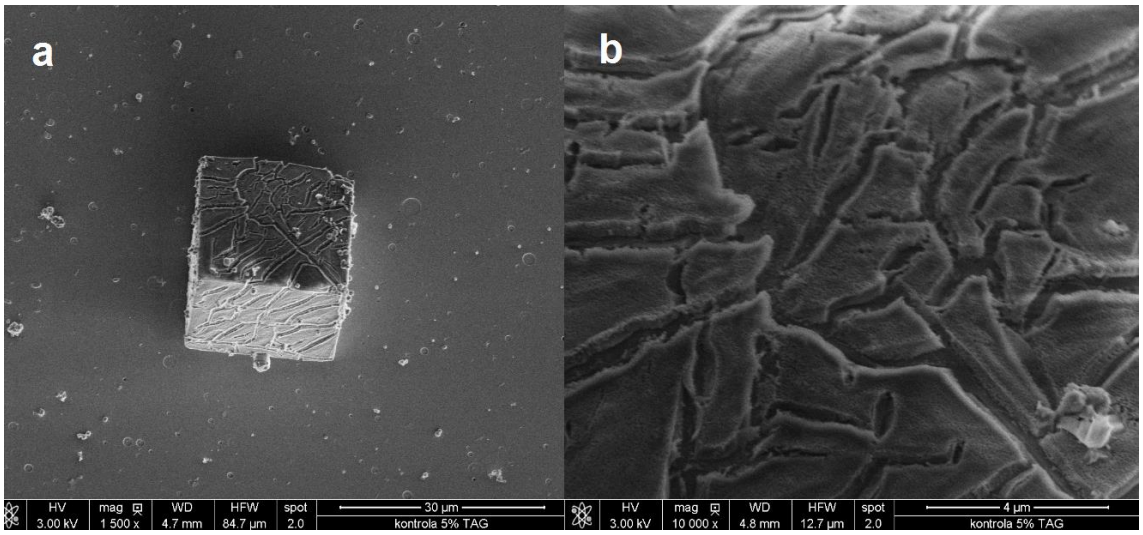

Figure 2.3-1. SEM images of the metal-organic framework (MOF), IRMOF-1,[154] with magnification of (a) 1,500 times, and (b) 10,000 times.

2.3.9 Powder X-ray diffraction (PXRD)

Powder X-ray diffraction (PXRD) is a technique using X-ray diffraction on powder or microcrystalline samples for structural characterization of materials.[188] An instrument dedicated to perform such powder measurements is called a powder X-ray diffractometer. In contrast to single-crystal diffraction techniques working best with a single well-ordered crystal, the powder diffraction technique uses a powdered sample and monochromatic X-ray radiation. When a crystal is powdered, at least some of the crystallites are oriented so as to give rise to diffraction. In present powder XRD diffractometers, the intensity of reflections are monitored electronically as the detector is rotated around the sample in a plane containing the incident ray. The PXRD technique is used to identify a sample of a solid substance by comparison of the positions of the diffraction lines and their intensities with theoretical diffraction patterns. PXRD data are also used to determine phase diagrams. For different crystalline phases different diffraction patterns are obtained. Therefore, determination of relative amounts of each phase present in a mixture is possible. This technique is also used for the initial determination of the dimensions and symmetry of a unit cell.

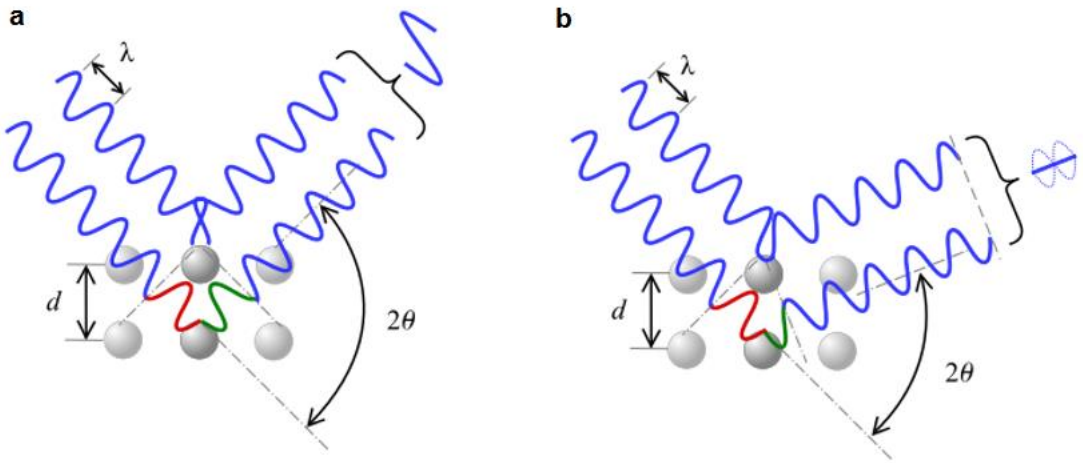

Scheme 2.3-12. According to the 2 *Θ* deviation, the phase shift causes (a) constructive or (b) destructive interferences.[189]

Principle of this experimental technique is based on the Bragg's law

$$n\lambda = 2d\sin\Theta \qquad \text{(Equation 2.3-15)}$$

where *n* is a positive integer, λ is wavelength, *d* is distance between two planes in a crystal, *Θ* is the glancing angle or the scattering angle. For many glancing angles the path-length difference is not an integer number of wavelengths, and the waves interfere destructively (Scheme 2.3-12b). However, when the path-length difference is an integer number of wavelengths, the reflected waves are in phase and interfere constructively (Scheme 2.3-12a). Apparently, a reflection should be observed when the glancing angle satisfies the Bragg's law (Equation 2.3-15).

Chapter 3

Results and discussion

3. 1 Chemical sensor for inosine

3.1.1 Quantum-chemical modeling of the pre-polymerization complex

Structure of the pre-polymerization complex (Scheme 3.1-1a) of the inosine template with chosen functional monomers was optimized using the density functional theory (DFT) with the B3LYP functional and the 6-31G* basis set (Scheme 3.1-1b). Moreover, selected thermodynamic parameters were calculated.

Calculation results proved that the stability of the complex of the 1 : 1 : 1 molar ratio of **1** : **5** : **6** was the highest. The ΔG value (–135.6 kJ·mol^{-1}) calculated indicated the formation of a stable pre-polymerization complex. Our attempts to optimize complex structure with the stoichiometry of 1 : 2 : 1 led to a less stable complex (lower value of ΔG = –126.1 kJ·mol^{-1}). Therefore, the former stoichiometry was selected for MIP preparation. Interactions between inosine and **6** was stronger than those for inosine and **5**. The ΔG values, calculated separately for complexes of **1** and **5**, as well as **1** and **6**, were –54.3 kJ·mol^{-1} and –87.7 kJ·mol^{-1}, respectively. Furthermore, molecular modeling proved multi-point interactions in the complex. Besides, the calculation results showed the formation of hydrogen bonds between vicinal diols of the ribose moiety of inosine (atoms O1 and O2) and oxygen atoms of boronic acid moiety of **5** (atoms O3 and O4). Moreover, the cytosine moiety of **6** formed another pair of hydrogen bonds between the N1 atom of the –NH_2 group and the N2 atom of the heteroaromatic ring of cytosine and the O5 oxygen atom and the N3 nitrogen atom of inosine. These interactions decided on selectivity of the molecular cavities of the MIP recognition unit prepared.

a

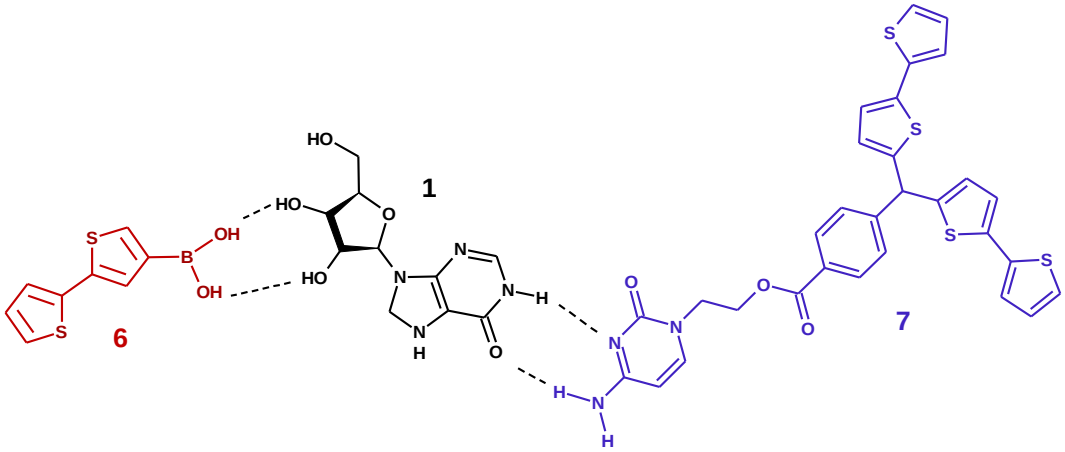

b

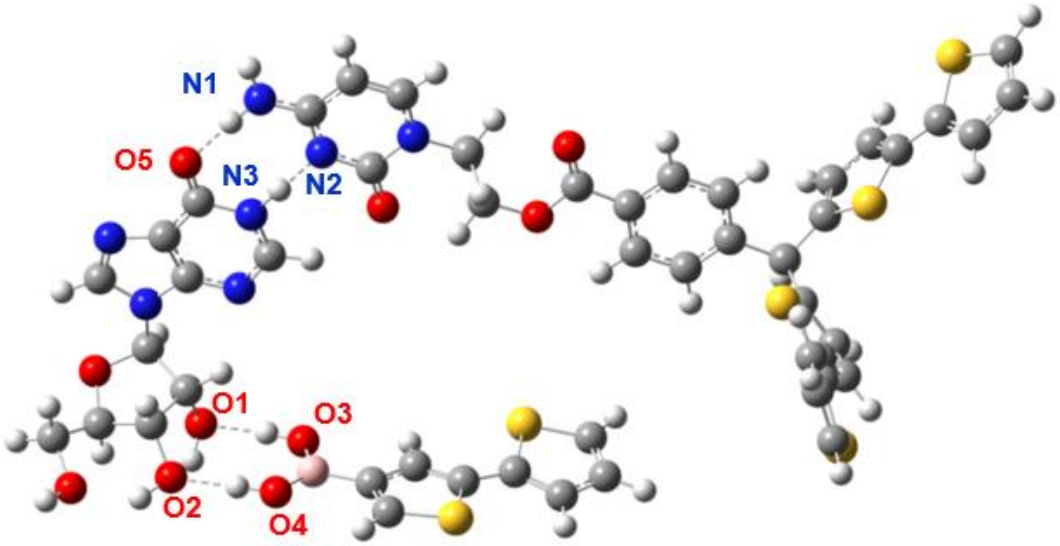

Scheme 3.1-1. (a) Structural formula of the pre-polymerization complex of inosine **1** with functional monomers **5** and **6** and (b) the B3LYP/6-31G* optimized structure of the pre-polymerized complex of **1** with functional monomers **5** and **6**.

3.1.2 Preparation of the thin MIP-inosine film

The growth of the MIP-inosine (MIP-**1**) film on the Au-QCR was followed by the simultaneously recorded current, *I*, (Figure 3.1-1a), resonant frequency, Δf, (Figure 3.1-1b), and the dynamic resistance change, ΔR_D (Figure 3.1-1c) with the potential scanned. The anodic peak at ~1.30 V (Figure 3.1-1a) indicated electro-polymerization and growth of the polymer film, as evidenced by the Δf decrease (Figure 3.1-1b). In the subsequent cycle, decrease at ~1.0 V, followed by the increase in ΔR_D with the anodic potential increase (Figure 3.1-1c) at around 1.20 V, are probably due to the egress of cations and ingress of anions of the supporting electrolyte, substantiating the rigidity variations of the MIP film. Interestingly, growth in current was observed with each potentiodynamic cycle (Figure 3.1-1a), which indicates that the growing polymer is conducting.

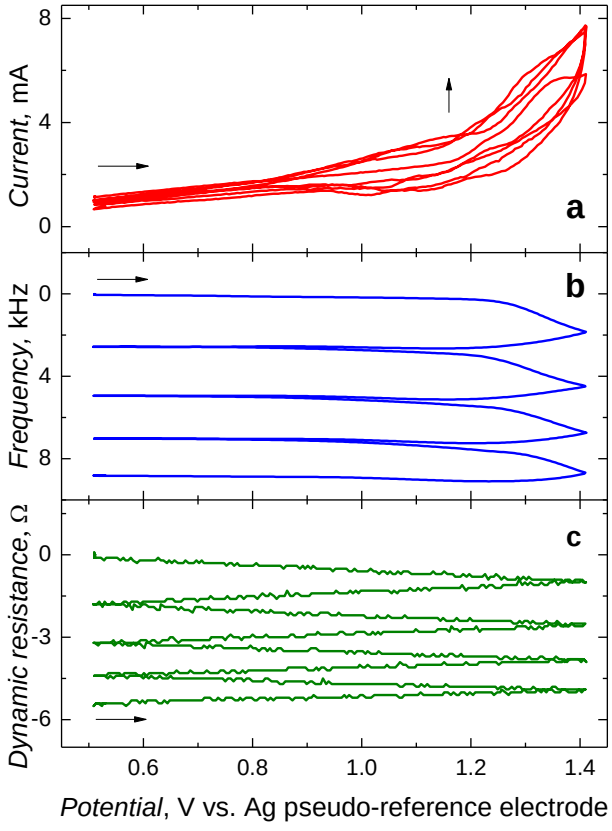

Figure 3.1-1. Curves of the potential dependence of (a) current, as well as changes of (b) resonant frequency, and (c) dynamic resistance simultaneously recorded for thin MIP-**1** film deposition by potentiodynamic electropolymerization on the 5-mm diameter electrode of the 10-MHz Au-QCR. The electropolymerization was carried using ACN solution of 0.1 mM inosine **1**, 0.1 mM **5**, 0.1 mM **6**, 0.4 mM **10**, and 0.1 M $(TBA)ClO_4$. The potential scan rate was 50 mV s^{-1}.

The total frequency changes for MIP and NIP after four deposition cycles were nearly the same reaching 8.8 and 8.9 kHz for MIP and NIP, respectively. Because, changes of R_D were negligible, the total mass of the polymer deposited on the electrode could be calculated using the Saurebrey equation.[190] The MIP and NIP mass was 11.3 and 11.5 μg, respectively. Taking into account the estimated polythiophene density of 1.3 g·cm^{-3}, thickness of the deposited MIP and NIP films can be assessed to be 444 and 449 nm, respectively.

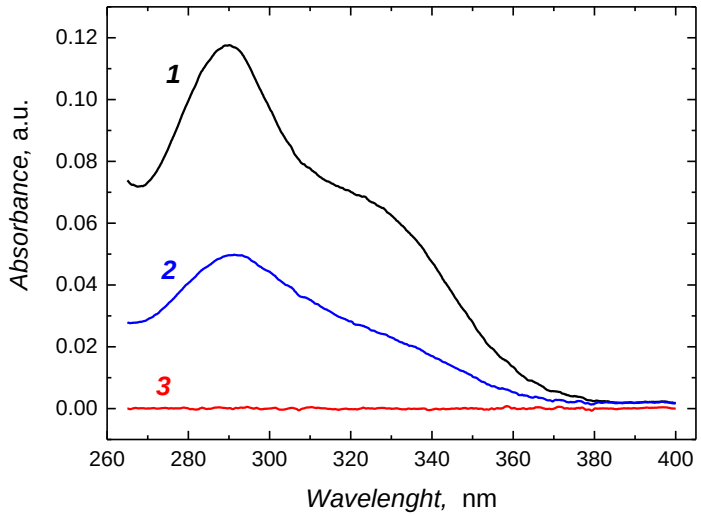

Figure 3.1-2. The UV-vis spectra of the 0.1 M HCl extracts after removal of inosine from the inosine-templated MIP film. The extraction was carried out at 35 °C for (*1*) 3 h, (*2*) 6 h, and (*3*) 16 h.

The inosine template was then extracted from the MIP-**1** film before determination of the inosine analyte. For that, liquid-solid extraction with 0.1 M HCl at 35°C was performed. The completeness of the extraction was confirmed by the UV-vis spectroscopy measurement (Figure 3.1-2). Repeated inosine extraction from MIP with 0.1 M HCl resulted in disappearance of the inosine absorption band at ~290 nm, confirming its complete removal from the MIP.

Moreover, this removal was supported by PM-IRRAS spectra of the MIP-**1** before extraction, MIP-**1** after extraction and NIP (Figure 3.1-3). The band characteristic of the C-O- vibration of ribose was observed at 1150 cm^{-1}. This band substantially decreased after inosine extraction from the MIP and was absent in the NIP spectrum.

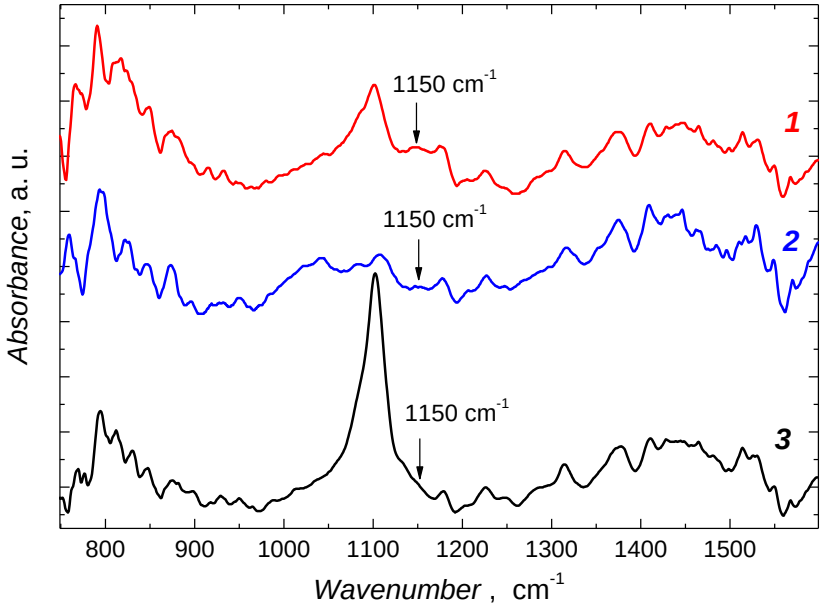

Figure 3.1-3. PM-IRRAS spectra of the MIP-**1** film (*1*) before and (*2*) after inosine extraction, from the MIP-**1** film with 0.1 M HCl at 35 °C, as well as (*3*) of the NIP film deposited by potentiodynamic electropolymerization on Au-glass slides.

3.1.3 Characterization of the MIP-inosine film

For characterization of the MIP-**1** film, its surface was imaged with AFM (Figure 3.1-4). Apparently, the film was relatively rough, and appeared to be composed of small, 20-60 nm in diameter, grains. The film thickness and roughness was 209 ± 5 and 2 nm, respectively.

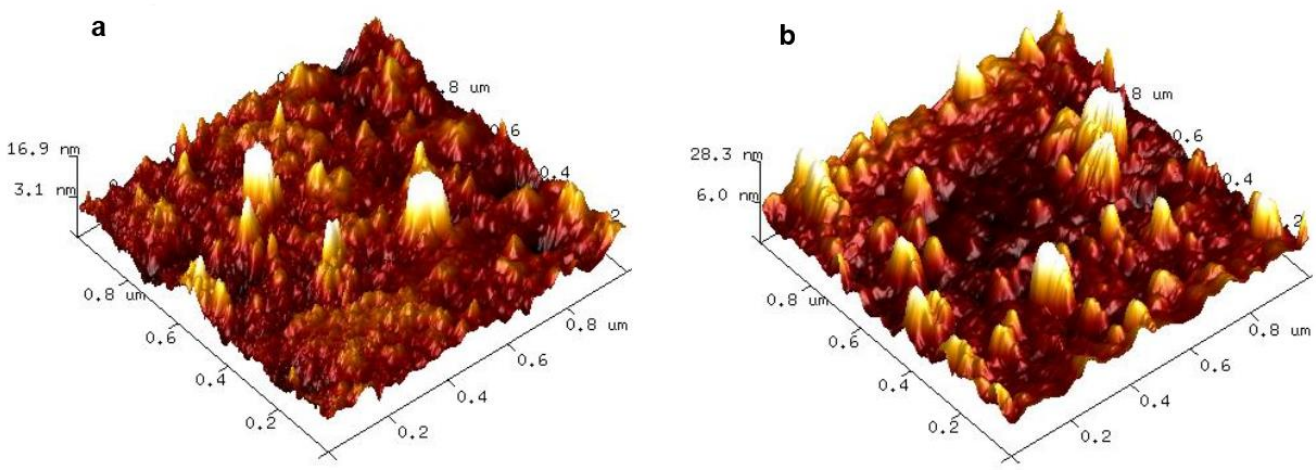

Figure 3.1-4. The 1×1 μm^2 area AFM images of (a) MIP and (b) NIP films.

For comparison, the NIP film was also AFM imaged. Apparently, thickness and roughness of this film was 334 ± 7 and 3 nm, respectively. The NIP film was thicker and rougher than the MIP film. The measured MIP and NIP film thickness was lower than that estimated from the PM measurements. This discrepancy indicates that electrochemically deposited films might be denser than expected on the basis of the density of non-derivatized polythiophene, presumably because of the supporting electrolyte presence.

3.1.4 Analytical performance of the EG-FET chemosensor for inosine

The extended-gate field-effect transistor (EG-FET) sensing system was composed of two parts. The sensing part was made of a thin MIP-**1** film with surface area of 21 mm^2, deposited on the Au-glass slide. This part was electrically connected to the gate of a commercial MOSFET device (Scheme 2.2-5).

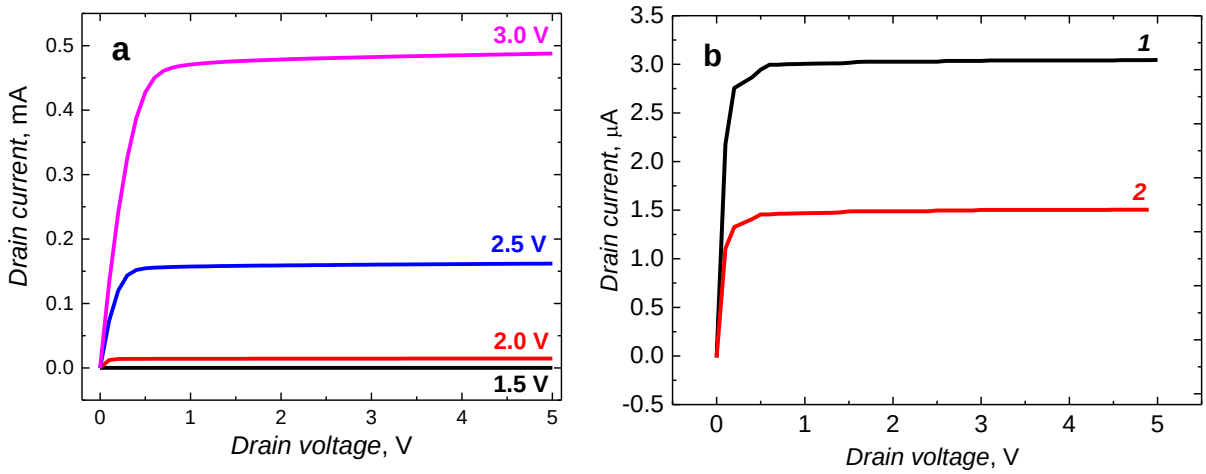

Figure 3.1-5. (a) The drain current, I_D, dependence on drain voltage, V_D, for the MIP-**1** EG-FET chemosensor for different gate voltages, V_G, applied as well as (b) (*1*) before and (*2*) after addition of 50 µM inosine at the constant V_G of 1.50 V applied.

Figure 3.1-5 shows the drain current, I_D, vs. drain voltage, V_D, characteristics of the EG-FET devised. The current saturation region can be expressed by Equation 3.1-1

$$I_D = \frac{\mu_0 C_{ox}}{2} \times \frac{W}{L} \times (V_{ref} - V_T)^2 (1 + \lambda V_D) \qquad \text{(Equation 3.1-1)}$$

As expected, the current measured was higher the higher was V_G applied to the reference electrode in the range of 1.5 – 3.0 V (Figure 3.1-5a). Importantly, addition of inosine to the solution at constant V_G led to a pronounced decrease of I_D (Figure 3.1-5b). Apparently, inosine binding to imprinted molecular cavities caused a surface potential change of the recognition MIP-**1** film. This change resulted in the decrease of the effective voltage applied to the gate. In effect, the current flowing through the channel decreased because of the decrease of the electron density in the gate region at the enhancement-mode n-MOSFET. This measured change in I_D was used as the analytical signal for inosine determination.

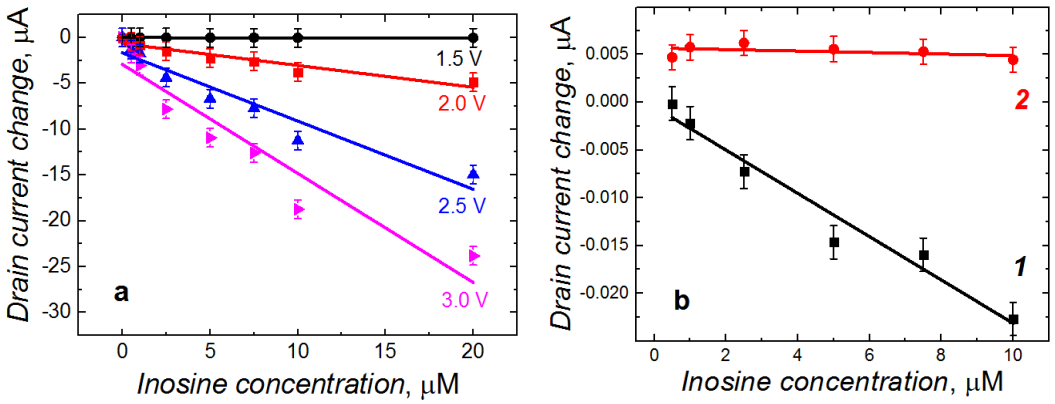

Figure 3.1-6. (a) Calibration plots for the MIP-**1** EG-FET chemosensor drain current response to inosine of different concentrations for different values of V_G and (b) comparison of the calibration plots for (*1*) the MIP-**1** and (*2*) the respective NIP film, for V_G = 1.5 V (b).

For optimizing V_G at which the I_D was the highest for a given inosine concentration, different V_G values were tested (Figure 3.1-6a). As expected, higher V_G resulted in higher I_D. Moreover, sensitivity of the chemosensor was higher, the higher was V_G (Table 3.1-1). However, apparent imprinting factor (AIF), which is the primary imprinting criterion, was drastically higher the lower was V_G (Table 3.1-1). Apparently, higher V_G promoted non-specific binding of the analyte in the polymer film. Furthermore, LOD of the EG-FET chemosensor increased at V_G exceeding 2.50 V indicating a noise increase. Therefore, relatively low V_G of 1.50 V was selected as the optimum gate voltage for further inosine determination.

Figure 3.1-7 presents the time dependence of the maximal I_D for different inosine concentrations determined with the use of the MIP-**1** film or the NIP film based EG-FET chemosensors under stagnant-solution conditions. Both chemosensors exhibited a decrease of the I_D after inosine addition. However, the response of the (NIP film)-coated chemosensor was significantly lower. As expected, sensitivity of the MIP-film coated EG-FET was much higher (Table 3.1-1) than that of the NIP film to inosine because of selective pre-concentration of inosine in the imprinted molecular cavities. The performance of the MIP chemosensor was examined over a concentration range of 0.5 to 50 μM with detectability and sensitivity sufficient for inosine determinations in body fluids (Table 3.1-1).[9]

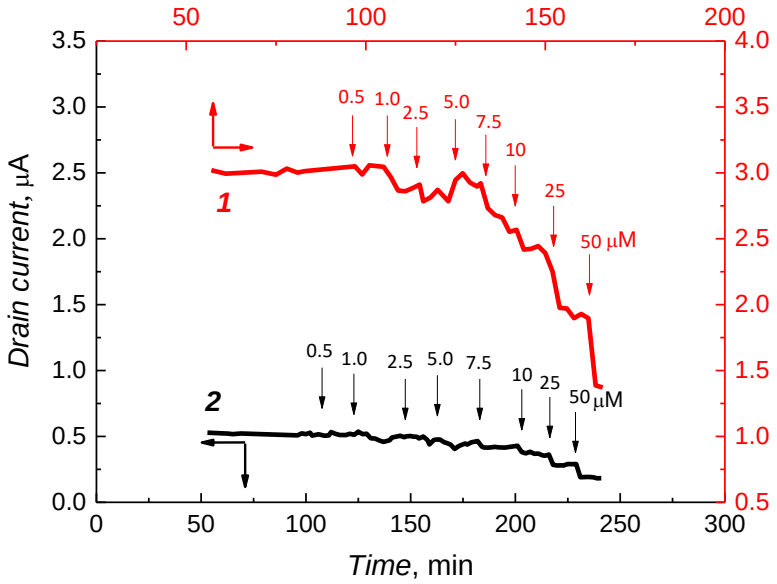

Figure 3.1-7. The change of drain current, I_D, with time for the EG-FET chemosensor with the gate area coated with (*1*) the MIP-**1** and (*2*) NIP thin film deposited by electropolymerization under potentiodynamic conditions on the Au-glass slides. The final inosine concentrations are indicated with vertical arrows. The extended gate surface area was 21 mm^2. The applied V_G was 1.50 V.

The physiological levels of inosine are in the range of 0 to 2.9 μM in patients with diagnosed diabetic nephropathy, gout, or hyperuricemia, and up to 25 μM in people after intensive physical exercises.

The developed chemosensor was highly selective with respect to inosine (Figure 3.1-8). Sensitivity to inosine was ~90 times that to glucose, and over 100 times that to

thymine, guanosine, or adenosine. Worth mentioning, the adenosine and guanosine functionalities are very similar to that of inosine, while glucose is a common interference present in body fluid samples. This high selectivity confirmed formation of selective molecular cavities in the MIP film. These results proved suitability of the devised chemosensor for selective determination of inosine.

Table 3.1-1. Analytical parameters of the EG-FET MIP-**1** chemosensor for different V_G values.

Analytical parameters	Gate voltage, V			
	1.50	2.00	2.50	3.00
LOD, (μM) at S/N = 3	(0.62±0.01)	(0.11±0.04)	(1.85±0.17)	(3.44±0.10)
Sensitivity, MIP (μA μM^{-1})	(2.3±0.2) × 10^{-3}	(0.32±0.03)	(0.99±0.08)	(1.64±0.15)
Sensitivity, NIP (μA μM^{-1})	(8.0±1.2) × 10^{-5}	(0.060±0.006)	(0.261±0.026)	(0.512±0.051)
Apparent imprinting factor (AIF)	(29.0±1.8)	(5.35±0.04)	(3.80±0.07)	(3.20±0.03)

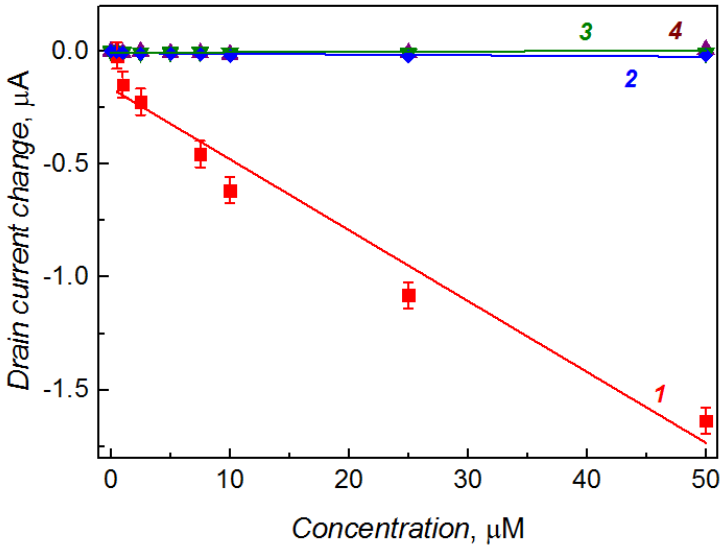

Figure 3.1-8. Calibration plots for the MIP-**1** EG-FET chemosensor of I_D change for different concentrations of (*1*) inosine, (*2*) adenosine, (*3*) glucose, and (*4*) thymine.

3.1.5 Analytical performance of the PM chemosensor for inosine

The above results confirmed that the MIP-**1** film coated EG-FET can be applied as an analytical tool to monitor concentration of the inosine analyte. In order to get deeper insight into the binding of the MIP-**1** film, the EG-FET chemosensor results were compared with those obtained with an alternative piezomicrogravimetric (PM) transduction.

For preparation of the recognition film for the PM chemosensor, the same electropolymerization conditions were used as those for the MIP and NIP film deposition on the extended gate of the EG-FET system. To this end, Au-QCR was used as the working electrode. The experiments of inosine determination were carried out under FIA conditions. After injection of inosine to the carrier solution, the Δf decreased. This behavior confirmed inosine binding by MIP-**1**. The Δf nearly returned to its original value as the carrier solution eluted the inosine analyte from the MIP film. It means that the analyte was bound reversibly. The calibration curves for inosine was constructed by injecting the analyte solutions of different concentrations (Figure 3.1-9). The frequency decrease was linear with the analyte concentration up to at least 50 mM and its sensitivity was –1.06 ± 0.04 Hz mM^{-1} (Figure 3.1-9).

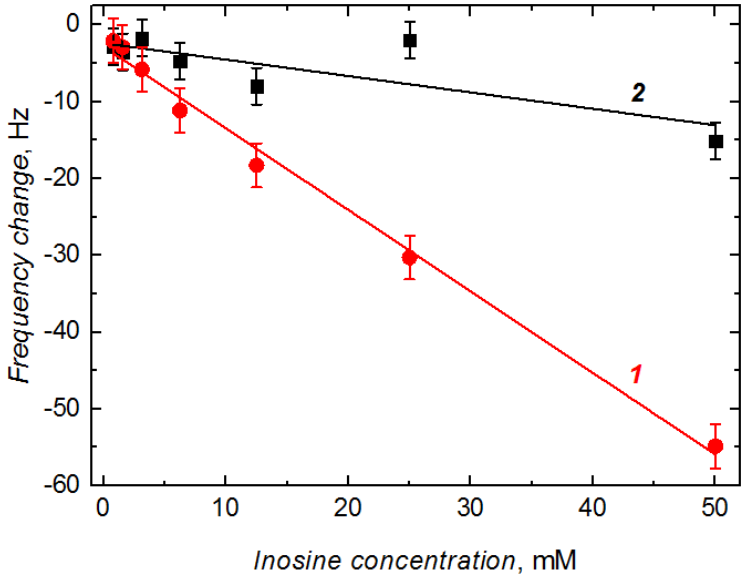

Figure 3.1-9. Calibration plots for inosine recorded (*1*) at the inosine extracted MIP film and (*2*) the NIP film coated 10-MHz Au-QCRs under flow-injection analysis (FIA) conditions. The carrier solution flow rate was 35 µL min^{-1} and the injected sample volume was 200 µL.

Similarly, Δf, due to the analyte binding by the NIP under the FIA conditions, were also used to construct the calibration plots. From the slope (–0.21 ± 0.07 Hz mM^{-1}) of the plot, the sensitivity to inosine for the NIP film was determined. From the ratio of the MIP-**1** sensitivity (curve *1* in Figure 3.1-9) and that of NIP (curve *2* in Figure 3.1-9) to inosine, the imprinting factor was determined as, IF = 4.9 ± 0.5.

Importantly, the Δ*f* values measured are directly proportional to mass changes related to the analyte binding, while EG-FET measurements are affected also by the charge of sorbed species.

Integration of the MIP-**1** film with the PM transducer for determination of inosine proved suitability of the devised MIP for integration with different transduction platforms. However, higher detectability was obtained for the EG-FET (0.62 ± 0.01 μM) than that for the PM chemosensor (0.85 ± 0.15 mM). The higher detectability of the EG-FET chemosensor may originate from its sensitivity to charge changes rather than to the mass changes. Furthermore, the EG-FET sensor allows for signal amplification via the V_G adjustment. The higher detectability of the EG-FET chemosensor and its ease of use lead to conclusion that the EG-FET chemosensor is better suited for practical purposes.

3. 2 Chemical sensor for human lipocalin-2 (NGAL)

3.2.1 Ligand-to-protein docking

For designing a selective molecular cavity, *bis*(bithiophene) derivatized with catechol **8** was used as the functional monomer. The choice of this monomer was based on known interaction between catechol and NGAL **2**.[191] Series of simulations were performed for further determination of the most probable interaction sites on NGAL for **8**. Firstly, possible binding pockets of **2** and its druggability, i.e., ability to bind drug-like molecules with high affinity, was determined. The analysis of the crystal structure of NGAL complexed with 4-methylcatechol native ligand (PDB: 3FW5, chain A) with the DoGSite server[167] indicated seven possible binding pockets (P0-P6) on the protein surface. The pocket with the highest volume, depth, and the best drug score was P0. Other pockets (P1-P6) were smaller and had lower drug score than that of P0. These results showed the preference of NGAL to accommodate small molecule ligands in the P0 pocket, i.e., that binds the native ligand.

Table 3.2-1. Binding pockets of NGAL **2** with their volumes, depths, drug scores, and docking scores determined by examination of docking **8** in these pockets.[167]

Pocket symbol	Volume [nm³]	Depth [nm]	Drug score	Docking score [kJ/mol]
P0	0.393	1.382	0.65	-28.9
P1	0.315	1.060	0.51	-25.9
P2	0.218	1.090	0.43	-21.8
P3	0.164	1.029	0.35	-22.6
P4	0.134	0.972	0.32	-5.0
P5	0.130	0.845	0.28	7.1
P6	0.120	0.819	0.25	7.9

In the next step, functional monomer **8** was independently docked to each of the seven binding sites of the protein. This simulation was conducted using Autodock Vina (version 1.1.2).[192] The best docking score, –28.9 kJ/mol, was reached for the main binding pocket (P0, Table 3.2-1). Examination of the docking orientations of **8** reveals that its dihydroxybenezene moiety most likely mimicked the orientation of the native 4-methylcatechol molecule docked into this pocket (Figure 3.2-1a). Moreover, both bithiophene side chains of **8** were directed outside of this pocket for easy cross-linking

and growth of the bithiophene polymer chain. For the second best binding pocket (P1), the docking score was slightly lower, equaling −25.9 kJ/mol. However, examination of docking orientations of **8** showed that one of the bithiophene side chain was buried in the P1 subpocket, thus forming the cross-linked polymer chain was less favorable (Figure 3.2-1b). For the other binding pockets (P2−P6), both the pocket drug scores and scores determined from docking were significantly lower. However, these pockets also were able to contribute to interactions with **8** but to a much lesser extent. The simulation results clearly indicated the possibility of generation of recognition sites in MIP.

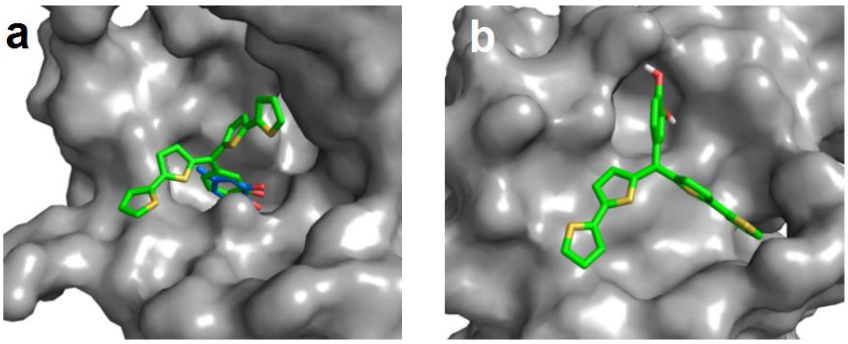

Figure 3.2-1. Predicted orientation of functional monomer **8** in possible binding pockets of the NGAL protein (PDB code: 3FW5). (a) The main binding pocket, P0, with the native ligand, 4-methyl catechol. (b) The second highest ranked pocket, P1.

3.2.2 Electrode modification with MOF

Imprinting of macromolecular compounds, such as proteins, is difficult and usually not straightforward.[84] This is mainly because of molecular structure, size, that is incomparably bigger than the molecules of functional monomers, and instability in organic solvents of their pre-polymerization complexes. Molecular cavities left after protein template removal are also big and, moreover, a protein molecule does not always react with synthetic functional monomers. Therefore, there are not many molecular cavities on the surface of an MIP after template removal. This effect influences the chemosensor response. Thus, developing artificial recognition device for protein detection and determination is challenging. To overcome this problem, one idea is to expand the working surface area of an MIP, thus improving the response of the chemosensor. One of ideas of enhancing working surface of the MIP is to use a sacrificial underlayer. After MIP synthesis, this underlayer is removed together with the template. For this underlayer, MOF was herein chosen because of well-known and fast synthesis

and its subsequent easy dissolution. Furthermore, the same extraction solvent may simultaneously remove the protein template and MOF, thus leaving the resulting MIP in the shape of a structured net (Scheme 3.2-1a) and with empty molecular cavities. As a support material to grow the MOF structure, Au-glass slides derivatized with carboxyl moieties were used. A detailed procedure is described in Chapter 2.2.3.

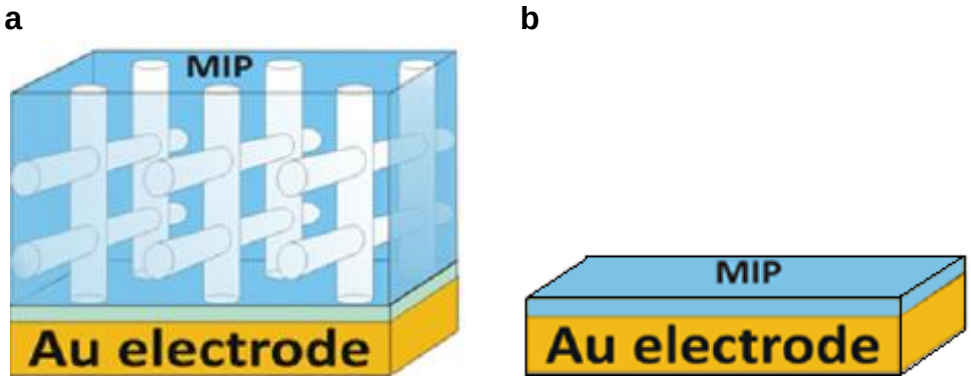

Scheme 3.2-1. Schematic representation of (a) MIP-**2** film deposited on the MOF-modified and (b) non-modified gold electrode.

Crystallinity and homogeneity of the MOF-5 phase was verified by PXRD analysis (Figure 3.2-2a). The pattern obtained for MOF-5 crystalline peaks matched the PXRD pattern simulated for the single-crystal X-ray structure of MOF-5. However, peaks at 12, 14, and 21° corresponding to (222), (004), and (006) planes, could also be observed. These peaks are more pronounced because of growth of the MOF crystallites with preferential orientation.[193] In the studied diffraction angle range there were no peaks for the Au substrate and poly(2,2'-bithiophene-5-carboxylic acid) film, as shown in Figure 3.2-2b.

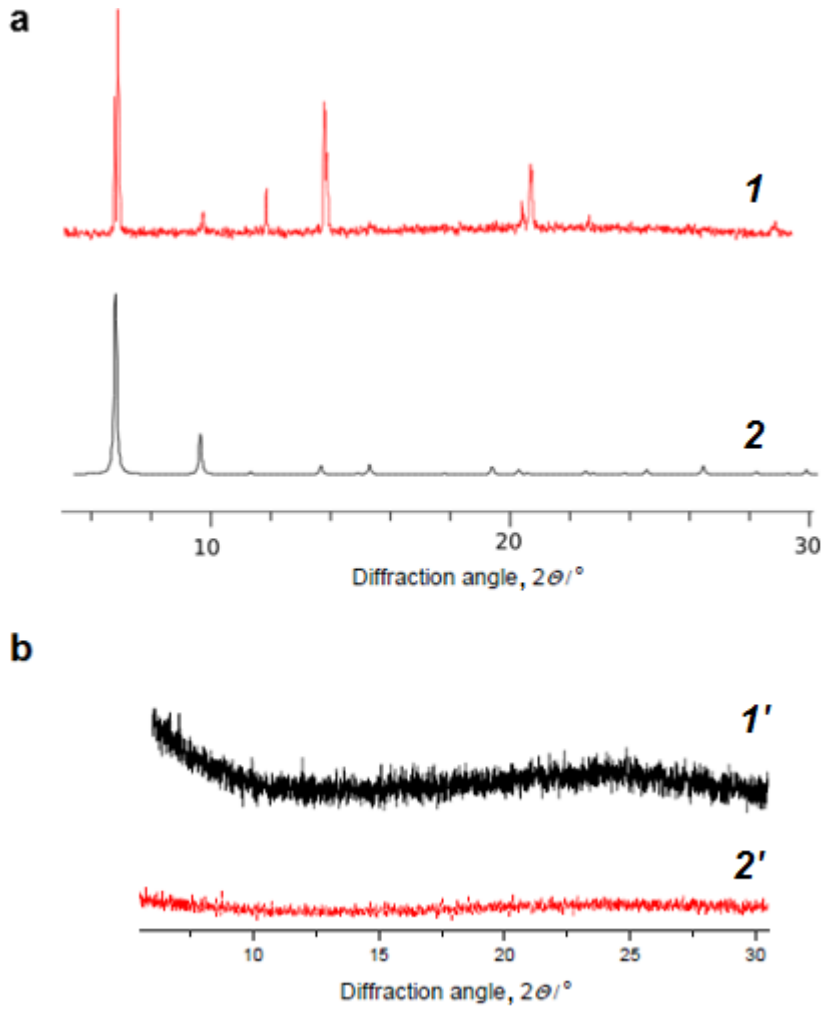

Figure 3.2-2. (a) Comparison of powder X-ray diffraction (PXRD) patterns for (*1*) a polycrystalline MOF-5 film deposited on an Au-glass slide and (*2*) simulated for MOF-5. (b) Comparison of PXRD patterns for (*1'*) bare Au-coated glass slide and (*2'*) poly(2,2'-bithiophene-5-carboxylic acid) supporting layer deposited on Au-coated glass slide.

3.2.3 Preparation of MIP films on MOF modified and non-modified Au electrodes

To demonstrate the effect of the MIP surface development in the presence of MOF, the MIP film was directly deposited on the Au-glass slide in the absence of any sacrificial MOF (Scheme 3.2-1b). Figure 3.2-3 shows potentiodynamic curves of deposition of an MIP film on the MOF-modified (Figure 3.2-3a) and non-modified (Figure 3.2-3b) electrode. The anodic peak at the MOF-coated Au electrode was relatively higher than that at the bare Au electrode. Apparently, the MOF presence on the Au surface resulted in the increase of this peak. Moreover, this peak was positively shifted. To confirm the imprinting, NIP film was also deposited in the presence of MOF but in the absence of **2**.

Several reports described adsorption of proteins and enzymes on the MOF surface.[194, 195] Therefore, it can be postulated that **2** assembled on the external surface of MOF. Moreover, molecules of functional monomer **8** were then assembled over the **2** protein via hydrogen bonding, thus improving the recognition properties of the MIP by generating homogeneous molecular cavities. The presence of cross-linking monomer **11** at high concentration rendered stability of the generated molecular structure after the electropolymerization.

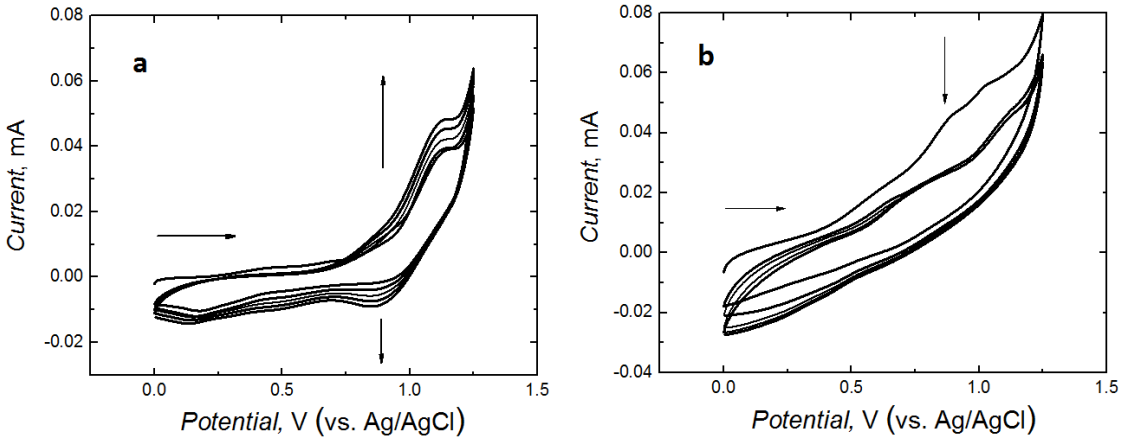

Figure 3.2-3. Deposition of the MIP-**2** film by electropolymerization under potentiodynamic conditions on (a) the MOF-modified and (b) non-modified Au electrode in the TL and ACN (7 : 3, *v* : *v*) mixed solvent solution of the T : FM : CM molar ratio of 1 : 100 : 400. The potential scan rate was 50 mV s^{-1}.

3.2.4 Characterization of MIP-NGAL films

Both non-structured and surface developed MIP films were SEM imaged to investigate their morphology (Figure 3.2-4). This imaging revealed that, as expected, the SEM image of a non-structured MIP film was relatively smooth (Figure 3.2-4a). However, a rough film was grown in the presence of MOF structures (Figure 3.2-4b).

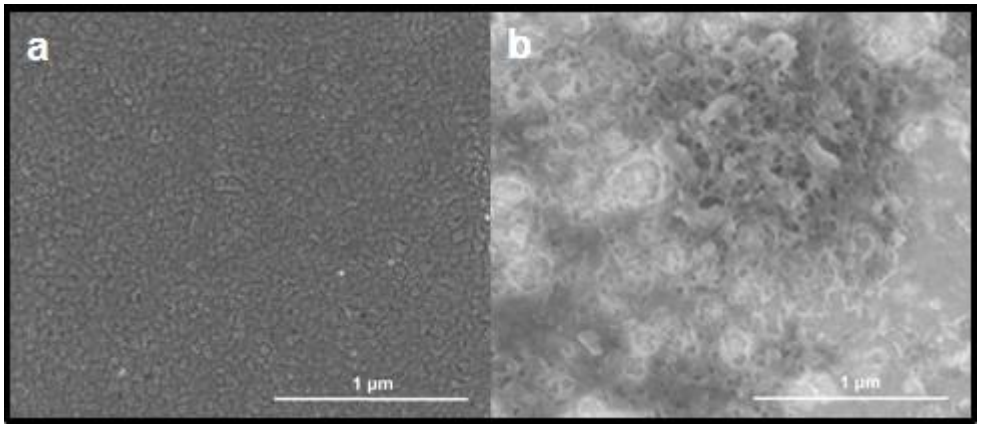

Figure 3.2-4. SEM images of (a) thin MIP film prepared without sacrificial MOF and (b) MIP film prepared in the presence of the MOF on the Au-glass slide electrode after removal of MOF and template.

The MIP films prepared both in the presence and in the absence of the MOF were further characterized by IR spectroscopic measurements. Results of the studies are shown in Figure 3.2-5. The non-structured MIP and NIP films were studied using PM-IRRAS. However, the MIP and NIP films deposited on the MOF scattered the infrared beam to such an extent that it was impossible to record spectra with this technique. Therefore, we have used diffuse reflectance FTIR for that purpose. Spectra recorded for non-structured polymer films showed the presence of bands characteristics of the thiophene polymer. Moreover, MIP-**2** spectrum (curve *1* in Figure 3.2-5a) showed bands at 1668 cm^{-1} characteristic of Amide I band of peptides.[196] This band disappeared after template extraction (curve *2* in Figure 3.2-5a), thus indicating removal of **2**. A similar result was obtained for the structured MIP film (Figure 3.2-5b). In this case, however, the bands at 1593, 1382, and 660 cm^{-1} were absent. These bands are attributed to MOF-5 characteristic vibrations.[197] Apparently, both NGAL and MOF-5 was completely removed from the films.

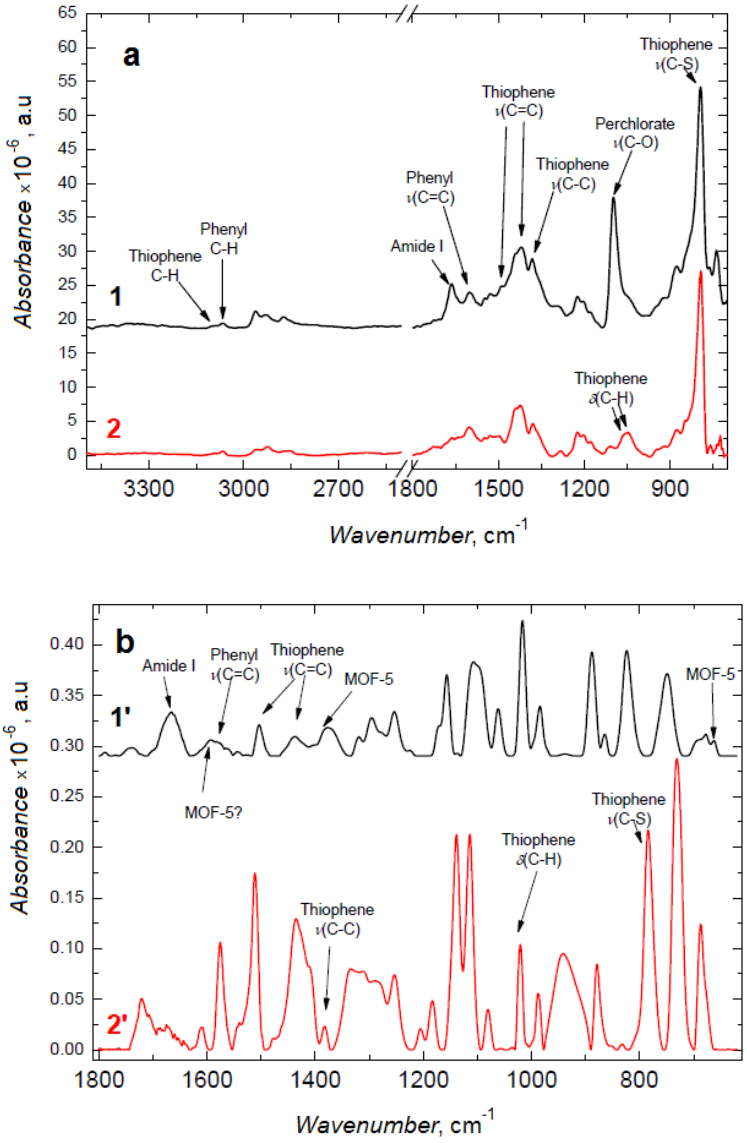

Figure 3.2-5. PM-IRRAS spectra of (a) (*1*) the non-structured NGAL-templated MIP and (*2*) NGAL-extracted MIP films, deposited on Au-coated glass slides by potentiodynamic polymerization, recorded at 83° incidence angle. (b) Diffuse reflectance FTIR spectra of surface-enhanced (*1'*) NGAL-templated MIP and (*2'*) NGAL-extracted MIP films deposited on the MOF-5 films grown on Au-coated glass slides.

3.2.5 Analytical performance of the EG-FET MIP-NGAL chemosensors with and without MOF supports

NGAL **2** analyte was determined using the EG-FET sensing system (Scheme 2.1-3). The recognition unit was made of a non-structured MIP-**2** or surface developed MIP on MOF film deposited on an Au-glass slide. Similarly as in the case of the EG-FET chemical sensor for inosine, this MIP recognition unit was integrated with the transduction unit, i.e., the extended gate of a commercial MOSFET.

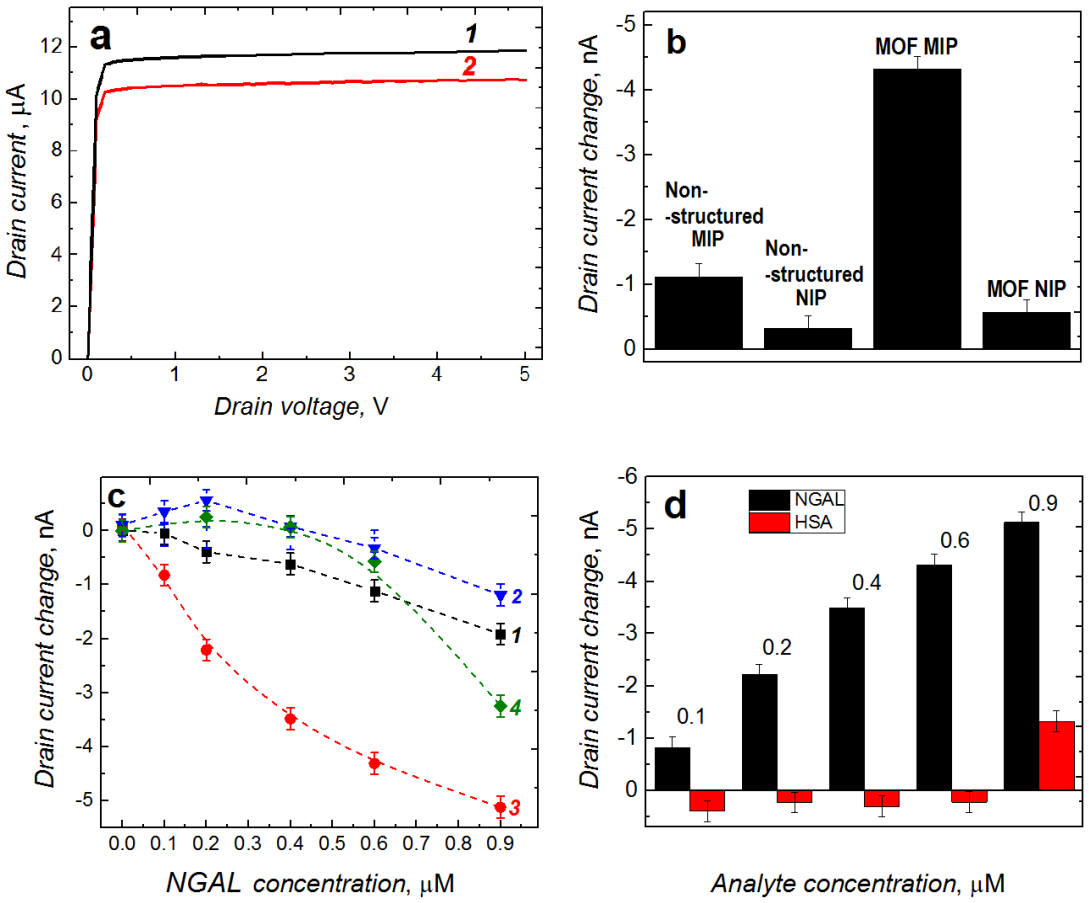

Figure 3.2-6. (a) The drain current (I_D) vs. drain voltage (V_D) characteristics of the MOF-structured MIP-**2** film chemosensor at the gate voltage (V_G) of 2.0 V (*1*) in the absence and (*2*) in the presence of 0.6 μM NGAL. (b) The histogram of the I_D change of the EG-FET corresponding to the NGAL analyte binding by the non-structured and surface developed MIP and NIP film. Concentration of the NGAL analyte was 0.6 μM. (c) Calibration plots for NGAL, constructed for V_G = 1.50 V, at (*1*) the NGAL-extracted non-structured MIP film, (*2*) NIP non-structured film, (*3*) NGAL-extracted MOF-MIP film, and (*4*) MOF-NIP film, deposited on Au-glass slides. (d) Selectivity test of the MOF-MIP chemosensor based on the EG-FET. HSA – human serum albumin **16**. V_G was 1.50 V.

As shown in Figure 3.2-6, the drain current at the MIP film coated electrode decreased with the increase of the NGAL analyte in solution. This decrease was caused by the NGAL molecules binding to the imprinted cavities of the MIP. This binding resulted in the decrease of the electron density in the gate region at the enhancement-mode n-MOSFET. In effect, the current flowing through the gate channel decreased. This change in I_D was different for the same concentration of NGAL protein for differently prepared electrodes (Figure 3.2-6b). Interestingly, the change in I_D at the MIP film deposited on the MOF scaffold was significantly higher than that for this film prepared in the absence of MOF. The change in I_D for the control NIP film prepared in the MOF presence was not so pronounced (Figure 3.2-6b). This change in I_D was then used as the analytical signal for NGAL determination (Figure 3.2-6c).

For determination of sensitivity and the linear dynamic concentration range of NGAL, calibration plots were constructed by averaging the change in the drain currents for each concentration of **2**. Figure 3.2-6c presents these plots for the MIP-**2** non-structured film (curve *1*), the MIP-**2** film on the MOF (curve *3*), and the respective NIP films (curves *2* and *4*) based on EG-FET chemosensors response under stagnant-solution conditions. As expected, with each addition of the NGAL solution sample, I_D decreased. Moreover, sensitivity to the NGAL analyte of the MIP-film coated EG-FET was markedly higher (Table 3.2-2) than that of the NIP film because of selective preconcentration of NGAL molecules in the imprinted molecular cavities. Interestingly, the response of the NIP film on the MOF is only slightly dependent upon the NGAL concentration up to 0.6 μM. Above this value, the recorded I_D values started to decrease, suggesting nonspecific adsorption of the NGAL on the MOF-NIP film at higher concentrations. Importantly, sensitivity of the surface developed MOF-MIP film was ~2.3 times that of the non-structured MIP film (Table 3.2-2). Therefore, performance of the MOF-MIP chemosensor was appreciable in the concentration range of at least 0.1 to 0.9 μM with LOD of 120 nM and sensitivity of 5.10 nA μM^{-1}. The LOD determined from this experiment was comparable to that reported for the chemosensor for NGAL.[25] Worth mentioning, the basic parameter of a FET-based chemosensor is V_G. The appropriate V_G generates the charge in the film, which modulates electron mobility in the gate channel. Therefore, two different gate voltages (1.50 and 2.00 V) were herein applied and their effect on sensitivity of the chemosensor was evaluated. Table 3.2-2 summarizes

the analytical parameters determined for EG-FET based MIP-2 chemosensor. Clearly, sensitivity of the MOF-MIP chemosensor at the 1.50 V gate voltage is lower than that of the MOF-MIP at the voltage of 2.0 V.

Moreover, selectivity of the devised chemosensor with respect to an interfering protein was examined (Figure 3.2-6d). The chemosensor readily responded to the NGAL presence. However, the chemosensor response was rather negligible upon addition of human serum albumin (HSA) **16**, an interfering protein. Importantly, the chemosensor response was significant after subsequent NGAL additions. For 0.9 μM HSA, the chemosensor response was similar to that for 0.1 μM NGAL. Apparently, selectivity with respect to **16** of the devised chemosensor was appreciable.

Table 3.2-2. Analytical parameters of the EG-FET based MIP-**2** chemosensor for two different V_G values.

Analytical parameter	**Gate voltage**	
	1.50 V	2.00 V
Limit of detection (LOD) for non-structured MIP (at S/N = 3)	0.11 μM	0.15 μM
Limit of detection (LOD) for MOF-MIP (at S/N = 3)	0.27 μM	0.24 μM
Sensitivity, non-structured MIP	2.24 nA μM^{-1}	1.06 μA μM^{-1}
Sensitivity, MOF-MIP	5.10 nA μM^{-1}	2.33 μA μM^{-1}
Sensitivity, non-structured NIP	2.08 nA μM^{-1}	1.14 μA μM^{-1}
Sensitivity, MOF-NIP	2.29 nA μM^{-1}	1.04 μA μM^{-1}
Apparent imprinting factor (AIF) for non-structured MIP film	1.08	0.93
Apparent imprinting factor (AIF) for MOF-MIP film	2.22	2.23

3. 3 Chemical sensors for D- and L-phenylalanine

3.3.1 Quantum-chemistry modeling of pre-polymerization complexes

Structures of the pre-polymerization complex of L-phenylalanine **4** with the *p-bis*(2,2'-bithien-5-yl)methylbenzoic acid **9** functional monomer were computationally modeled using the DFT at the B3LYP level with the 3-21G* basis set, all implemented in the Gaussian 2009 software package. Several different functional monomers with different recognizing functionalities were tested to find the one most suitable. Table 3.3-1 summarizes ΔG values calculated for formation of the pre-polymerization complex with several of these monomers. With this preliminary screening step, the most stable complex-forming monomer **9** with carboxyl moiety was selected. Moreover, the stability of this complex increased after changing environment from vacuum (ΔG = -119.0 kJ mol^{-1}) to acetonitrile (ACN) (ΔG = -147.2 kJ mol^{-1}).

Moreover, stability of the phenylalanine dimer and **9** dimer was determined using the same quantum-chemical modeling (Table 3.3-2). Apparently, the complex of **4** with **9** (ΔG = -147.2 kJ·mol^{-1} in ACN) occurred to be more stable than those of the dimer of phenylalanine (ΔG = -6.1 kJ·mol^{-1} in ACN) and the dimer of **9** (ΔG = -130.0 kJ·mol^{-1} in ACN).

Scheme 3.3-1a shows the structural formula of the pre-polymerization complex revealing possible multiple-point interactions between two molecules of FM **9** and one molecule of **4** in vacuum. In the optimized complex (Scheme 3.3-1b), the hydrogen atom H39 of **9'** forms a hydrogen bond with the nitrogen atom N1 of **4**. Similarly, the hydrogen atom H16 of **9** interacts with the oxygen atom O3 of **4**. Moreover, the oxygen atom O2 of **9** forms a hydrogen bond with the hydrogen atom H27 of **4**.

Tables 3.3-1 and 3.3-2 summarize the ΔG values calculated for the formation of pre-polymerization complexes of **4** with functional monomers **7**, **8** and **9** and dimers of **4**, **7** and **9**, respectively. With this preliminary screening step, the most stable complex forming functional monomer **9** was selected.

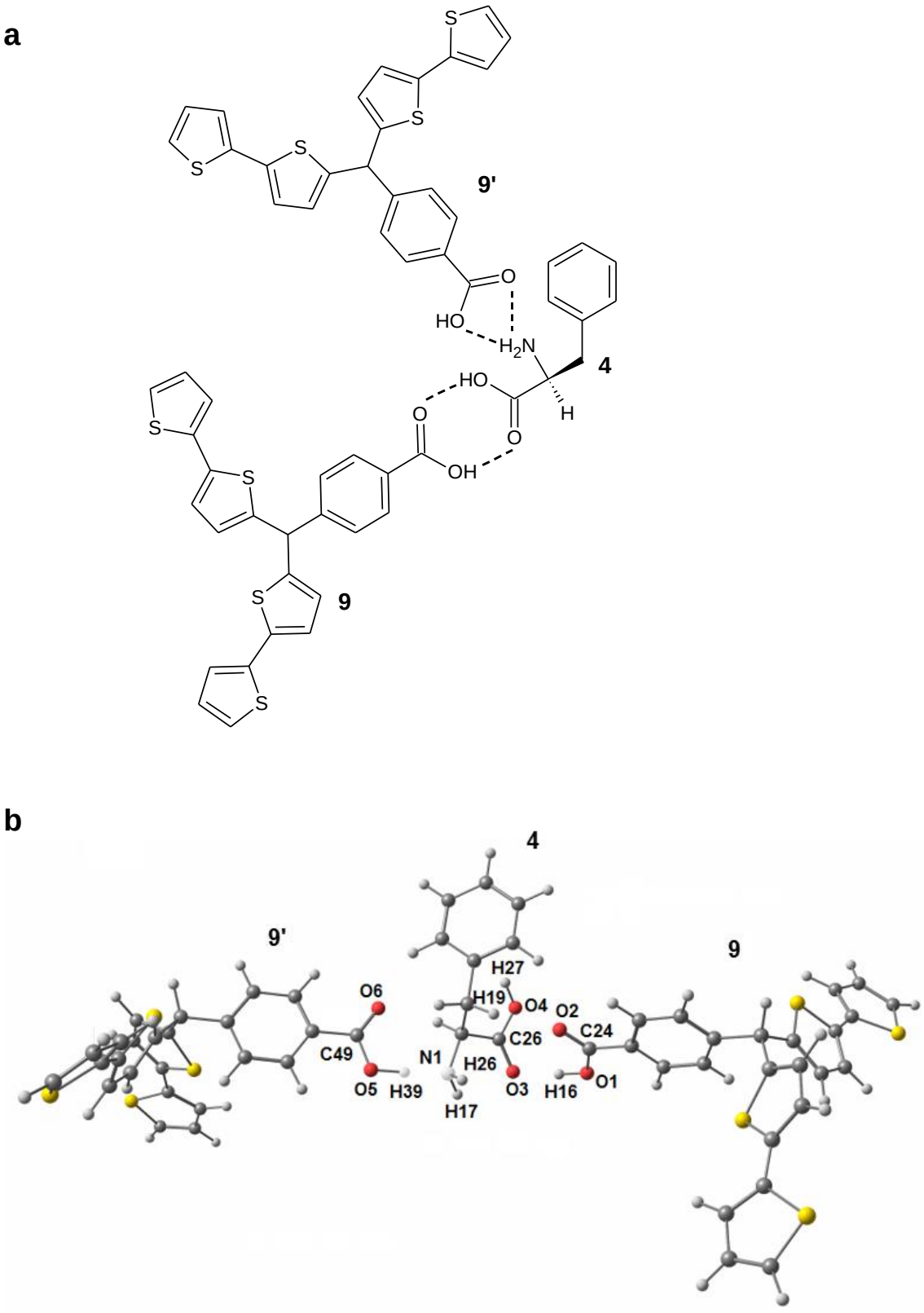

Scheme 3.3-1. (a) Structural formula and (b) the B3LYP/3-21G* optimized structure of the pre-polymerization complex of the molecule of **4** with two functional monomer **9** molecules (**9** and **9'**).

Table 3.3-1. The change of ΔG corresponding to formation of the pre-polymerization complex of **4** with different functional monomers, in vacuum and ACN, calculated using the DFT B3LYP/3-21G* method.

FM	Complex stoichiometry (4 : FM)	Δ*G* of complex formation in vacuum (kJ/mol)	Δ*G* of complex formation in ACN (kJ/mol)
7	1 : 1	-12.3	-
7	1 : 2	-58.9	-
8	1 : 1	-35.7	-19.2
9	1 : 1	-41.0	-
9	1 : 2	-119.0	-147.2

FM – functional monomer

Table 3.3-2. The change of ΔG corresponding to formation of the dimer of molecules calculated using the DFT B3LYP/3-21G* method.

Molecule	Δ*G* of complex formation in vacuum (kJ/mol)	Δ*G* of complex formation in ACN (kJ/mol)
4	-21.4	-6.1
7	-97.0	-78.6
9	-95.5	-130.3

3.3.2 Preparation of thin MIP-phenylalanine films on different electrodes

Figure 3.3-1 shows the current-potential curves of potentiodynamic electropolymerization of **3** (Figure 3.3-1a) and **4** (Figure 3.3-1b) resulting in deposition of respective MIP films on the Pt disk electrodes. In the first cycle, the anodic peak at ~1.0 V corresponds to irreversible electro-oxidation of the *bis*(bithiophene) moiety. During this electro-oxidation, a radical cation is formed.[198] This peak decreases in subsequent cycles indicating formation of a less conducting MIP film. Formation of such a film is most likely from the water presence in the system.

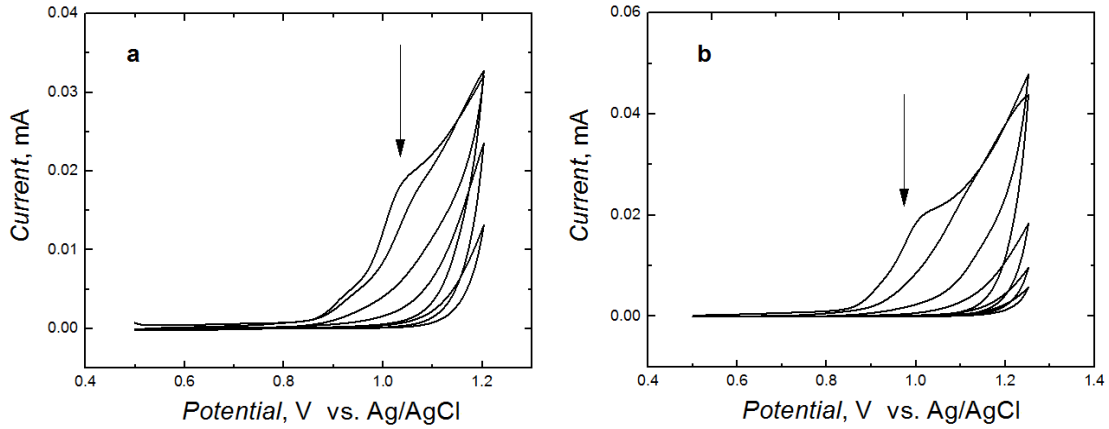

Figure 3.3-1. The current-potential curves for (a) the MIP-**3** and (b) the MIP-**4** film deposition by potentiodynamic electropolymerization on the 1-mm diameter Pt disk electrode in 0.1 mM solution of **3** or **4**, 0.2 mM **9**, 0.1 mM **10**, and 0.1 M $(TBA)ClO_4$ in the mixed solvent solution of the ACN-to-H_2O volume ratio of 9 : 1. The potential scan rate was 50 mV s^{-1}.

After rinsing with acetonitrile, **3** or **4** was extracted with 10 mM NaOH from the respective MIP film for application as the chemosensor recognition unit. To control the progress of extraction, the "gate effect" of the MIP film was examined (Figure 3.3-2). For that, electro-oxidation of the $K_4Fe(CN)_6$ red-ox probe was followed by differential pulse voltammetry (DPV) at the MIP film coated electrode for different time spans of template extraction. Apparently, removal of the template from the MIP molecular cavities resulted in the increase of the DPV peak current for the red-ox probe oxidation (Figure 3.3-2). Finally, it occurred that 90-min extraction with 10 mM NaOH allowed for complete removal of the template, as the DPV peak of red-ox probe was not increasing any more after this time (curve *5* in Figure 3.3-2).

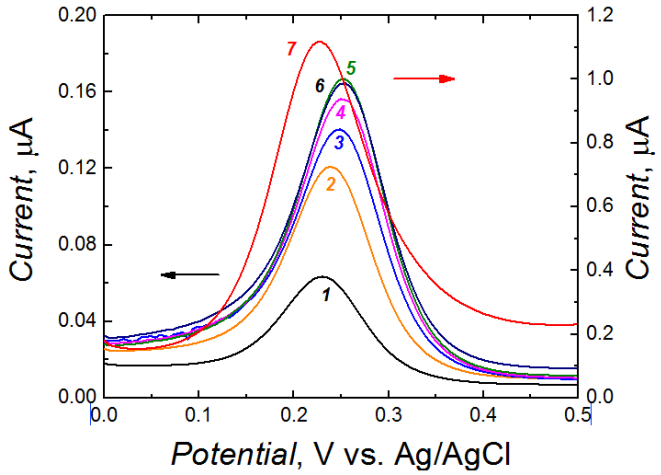

Figure 3.3-2. DPV curves for 0.1 M $K_4Fe(CN)_6$ in 0.1 M KNO_3 at the MIP-**3** film coated 1-mm diameter Pt disk electrode, (*1-black*) before extraction of **3**, after **3** extraction with 10 mM NaOH for (*2-orange*) 10, (*3-blue*) 45, (*4-magenta*) 60, (*5-green*) 90, (*6-brown*) 105 min, and (*7-red*) for the bare Pt electrode.

The extraction of **3** from the MIP film was confirmed with PM-IRRAS. Figure 3.3-3 presents experimental spectra recorded for MIP films before and after extraction as well as for the NIP film along with calculated and scaled theoretical frequencies of normal modes. The band assigned to perchlorate was removed before the band assignment to normal modes calculated for the MIP before and after extraction. Briefly, the **3**-templated MIP film showed (Figure 3.3-3a) the band at ~1666 cm^{-1} corresponding to N-H bending of the primary amine functionality of **3**. Vibration of carboxyl group of **3** resulted in the band at 1688 cm^{-1}. In the calculated spectrum, these peaks appeared at 1645 and 1678 cm^{-1} (Figure 3.3-3a). Importantly, these bands disappeared after the extraction of **3** from the MIP film (Figure 3.3-3b). The NIP film PM-IRRAS spectrum (Figure 3.3-3c) was similar to the spectrum of the MIP film after extraction of **3** (Figure 3.3-3b).

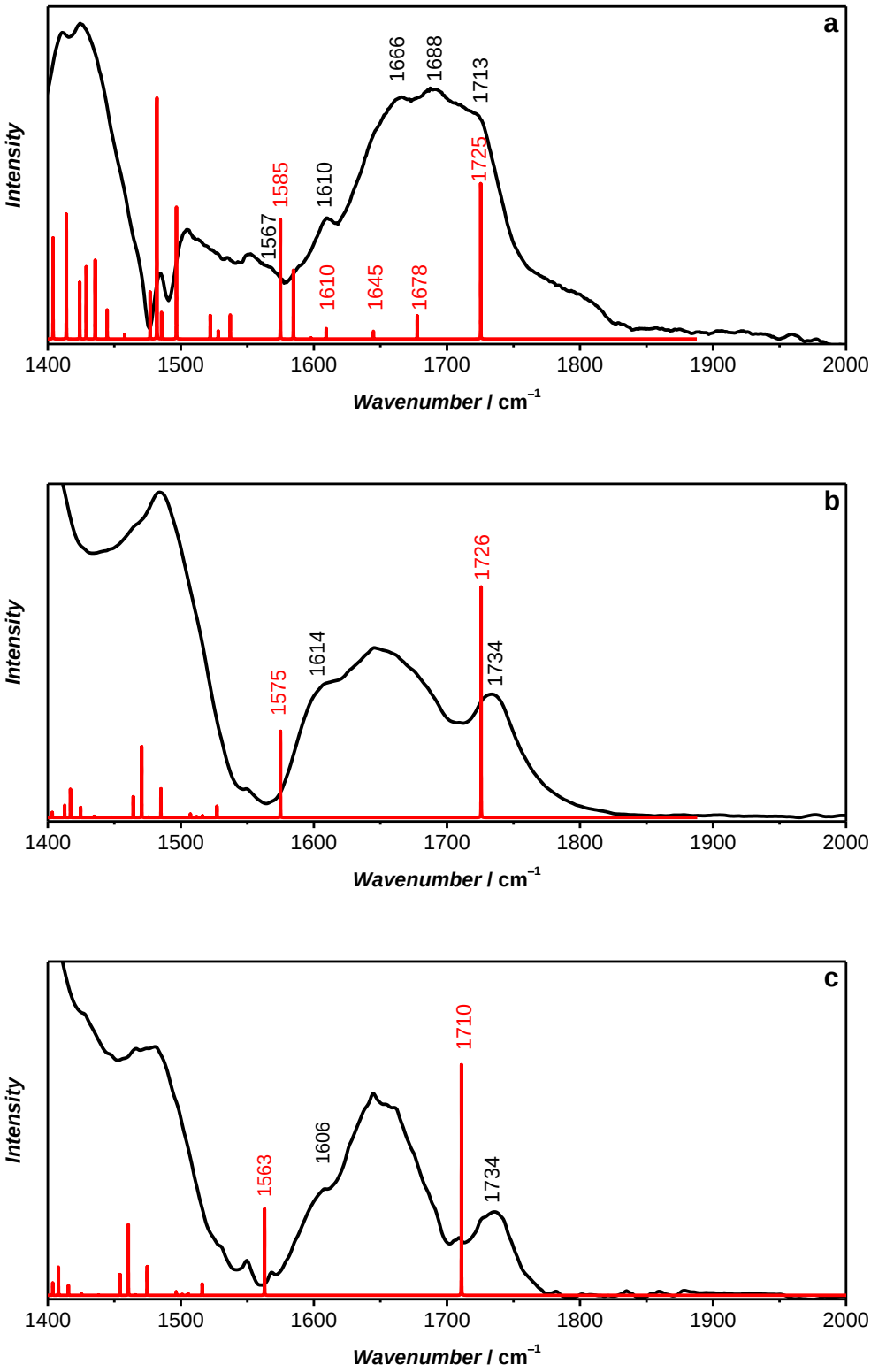

Figure 3.3-3. PM-IRRAS spectra (black, solid curves) measured for the **3**-templated MIP film (a) before and (b) after **3** extraction with 10 mM NaOH, and (c) NIP film along with calculated and scaled theoretical frequencies of normal modes (red, vertical segments).

3.3.3 Characterization of the MIP-phenylalanine films

A distinct surface morphological pattern was observed in AFM images of different MIP and NIP samples (Figure 3.3-4). Bright areas in the images correspond to bigger polymer grains. Interestingly, the **3**-templated MIP film was enriched with grains of a bigger size (Figure 3.3-4a). However, smaller grains appeared (Figure 3.3-4b) after extraction of the **3** template with 10 mM NaOH. Morphology of the NIP film was similar to that of the template-extracted MIP film (Figure 3.3-4c), i.e., it was composed of smaller grains. Moreover, thickness of the MIP film before extraction of **3** equaling 224 ± 14 nm decreased to 175 ± 51 nm after extraction. Presumably, this decrease resulted from removal of loose parts of the deposited MIP film. Thickness of the NIP film was 221 ± 24 nm.

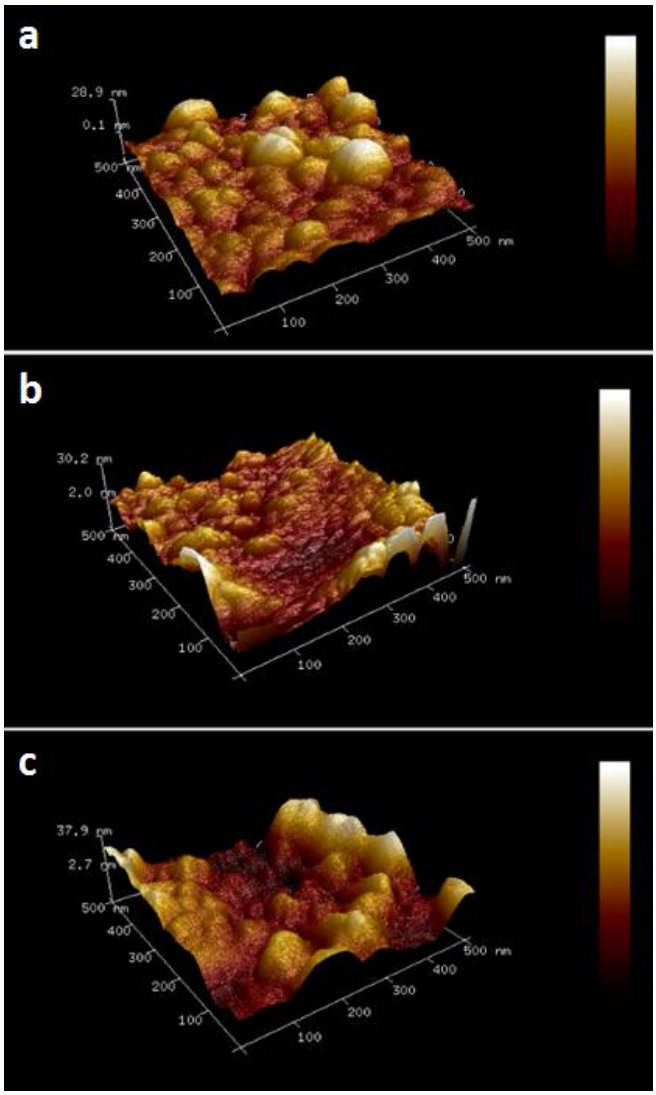

Figure 3.3-4. AFM images recorded using ScanAsyst Mode™ for the film of (a) **3**-templated MIP, (b) **3**-extracted MIP, (c) and NIP. Image dimensions are 0.5 × 0.5 μm^2.

3.3.4 Analytical performance of the EG-FET chemosensors

After the extraction of template, **3** or **4** analyte binding by the respective MIP was examined. For determination of this binding, electrical EG-FET transduction was used.

When a positive with respect to the source of the n-type channel MOSFET voltage is applied to the gate, electrons (which are major carriers in the substrate) are attracted to the surface of the gate and form a conducting channel between the source and drain. Fundamentals of this transduction method are described elsewhere.[45,116] Accordingly, characteristics of the transistor were measured at the constant gate voltage (V_G) of 1.50 V while drain voltage (V_D) was scanned from 0 to 5.0 V, and the change in the resulting drain current (I_D) was measured. This change, recorded for different analyte concentrations, was used to monitor analyte molecule binding to the MIP molecular cavity. The 10 mM NaH_2PO_4 was used as the working solution.

Figure 3.3-5 shows the dependence of the I_D change on the **3** or **4** concentration, as determined from the EG-FET characteristics. The recorded I_D changes are attributed to the interfacial potential shift at the EG-solution interface. The correlation between the I_D change and the analyte concentration in solution was linear up to 100 μM phenylalanine (both D- and L- enantiomer). Importantly, these chiral MIP films were cross-selective. To determine enantioselectivity in both cases, slopes of calibration plots for **3** and **4** at the MIP-**3** and vice versa were compared. It appeared that the MIP-**3** was highly sensitive to **3** (curve *1* in Figure 3.3-5a). However, advantageously, its response to **4** was appreciably low (curve *2* in Figure 3.3-5a). This led to the enantioselectivity factor ~2.3, determined as the ratio of these slopes. Similarly, the MIP-**4** was very sensitive to **4** and its sensitivity to **3** (curve *1'* and *2'*, respectively, in Figure 3.3-5b) was low, resulting in enantioselectivity factor of ~2.3. This enantioselectivity most likely arises from the presence of chiral cavities generated during respective imprinting. Table 3.3-3 summarizes analytical parameters of chemosensors devised.

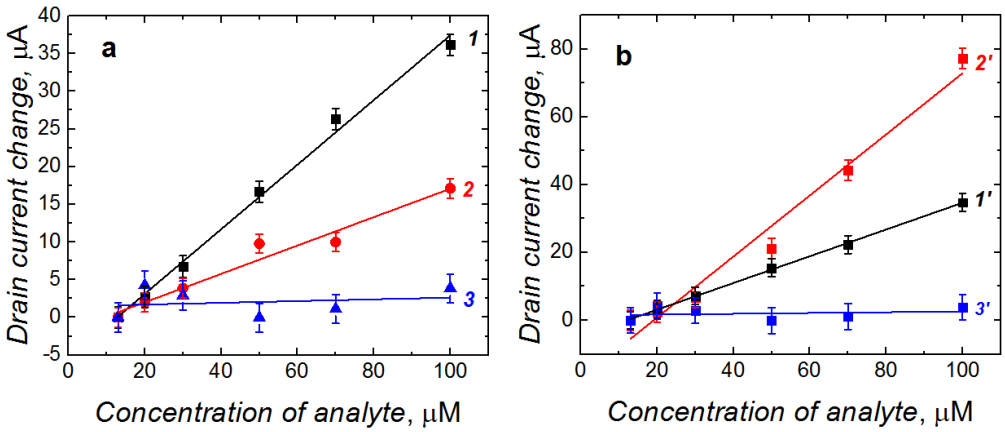

Figure 3.3-5. Calibration plots for **3**-templated MIP film for (*1*) **3**, (*2*) **4** (a), and the **4**-templated MIP film, for (*1'*) **3** (*2'*) **4** (b). These MIP films were deposited on the Au-glass slide extended gates of the EG-FET transducer. Curves (*3*) and (*3'*) are calibration plots for **3** and **4**, respectively, recorded for the NIP control film. V_G = 1.50 V.

In order to confirm the imprinting, an NIP control film, deposited on the Au-glass slide electrode, was assembled in the EG-FET system. Because of the absence of molecular cavities, binding of **3** to the NIP was low (curve *3* in Figure 5a). Therefore, sensitivity of the NIP electrode towards **3** was much lower than that of the MIP electrode (Table 3.3-3). The chemosensor for **4** behaved similarly (curve *3'* in Figure 5b). Evidently, NIP film low sensitivity to both enantiomers confirmed importance of the presence of molecular cavities in the MIP films. From the ratio of the sensitivity of the MIP-**3** chemosensor to **3** (curve *1* in Figure 5a) and that to NIP (curve *3* in Figure 5a) the AIF value was determined to be as high as 36.

Then, selectivity of both MIP films with respect to functionally and structurally similar interferences including D-alanine, D-proline, and D-tyrosine was determined (Figure 3.3-6). Results of selectivity studies are summarized in Table 3.3-3. The MIP-**3** chemosensor sensitivity to **3** was ~7 times that to D-tyrosine as well as over twice that to D-alanine and D-proline. Similarly, the MIP-**4** chemosensor sensitivity to **4** was nearly twice that to D-alanine, D-proline, and D-tyrosine. Remarkably, the charge of phenylalanine and most of its interferences was similarly positive under the measurement conditions (pH = 3.0). Therefore, the change in I_D corresponded to the extent of selective binding of the analyte by its MIP molecular cavities.

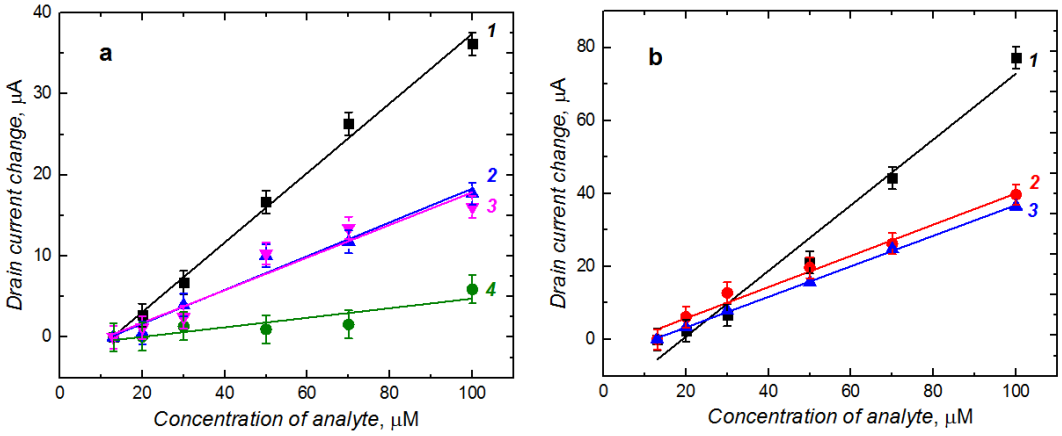

Figure 3.3-6. Calibration plots (a) for (*1*) **3**, (*2*) D-proline, (*3*) D-alanine, and (*4*) D-tyrosine at the **3**-templated MIP film and (b) for (*1'*) **4**, (*2'*) D-tyrosine, and (*3'*) D-alanine at the **4**-templated MIP film deposited on the Au-glass slide gates (WE) of the EG-FETs. V_G = 1.50 V.

3.3.5 Analytical performance of the PM chemosensors – determination of IF

In the field of molecular imprinting, the imprinting factor (IF) value is the measure of the concentration of selective molecular cavities imprinted in the MIP network. Analytical signal response of the MIP is compared with that of NIP to determine IF. The strength of multiple interactions of the analyte molecules with matching molecular cavities determines this value. In the present study, a high value of AIF was determined from the ratio of slopes of calibration curves for the MIP and NIP EG-FET chemosensors. However, this approach does not provide the true IF values. This is because several factors other than the presence of the analyte in MIP, such as charge or dipol moment of the analyte, may govern the I_D change measured. Therefore, PM transduction was herein used to determine the true amount of the analyte bound to the MIP and NIP film.

For that, the MIP-**3** thin film was deposited on an Au-QCR mounted in the FIA holder.[170] 100-μL samples of solutions of increasing concentrations of **3** were injected under FIA conditions in order to construct calibration plots. The change in Δf is opposite to the change in mass of the Au-QCR coated with the deposited MIP or NIP film, as the Sauerbrey equation predicts.[179] Each consecutive injection of **3** of different concentration resulted in different decrease in Δf, thus confirming **3** binding by molecular cavities (Figure 3.3-7a). Importantly, a similar change for the NIP film coated Au-QCR was much lower.

The measured frequency decrease for the **3**-templated MIP film obeyed the linear regression equation of Δf (Hz) = -7.04 (Hz mM^{-1}) c (mM) - 2.02 (Hz) for the analyte concentration up to 20 mM with the sensitivity of -7.04 ± 0.97 Hz mM^{-1} and correlation on coefficient of 0.9285 (curve *1* in Figure 3.3-7b). Similarly, Δf changes corresponding to analyte binding by the NIP film were measured to construct the calibration plot (curve *2* in Figure 3.3-7b). Sensitivity of the NIP film to **3** (-0.57±0.16 Hz mM^{-1}) was determined from the slope of a similar FIA calibration plot described by the following equation. Δf (Hz) = -0.57 (Hz mM^{-1}) c (mM^{-1}) - 6.65 (Hz). From the ratio of sensitivity to **3** of the MIP-**3** and that of the NIP, the IF value was determined as 12. This relatively high IF confirms high concentration of molecular cavities in the MIP.

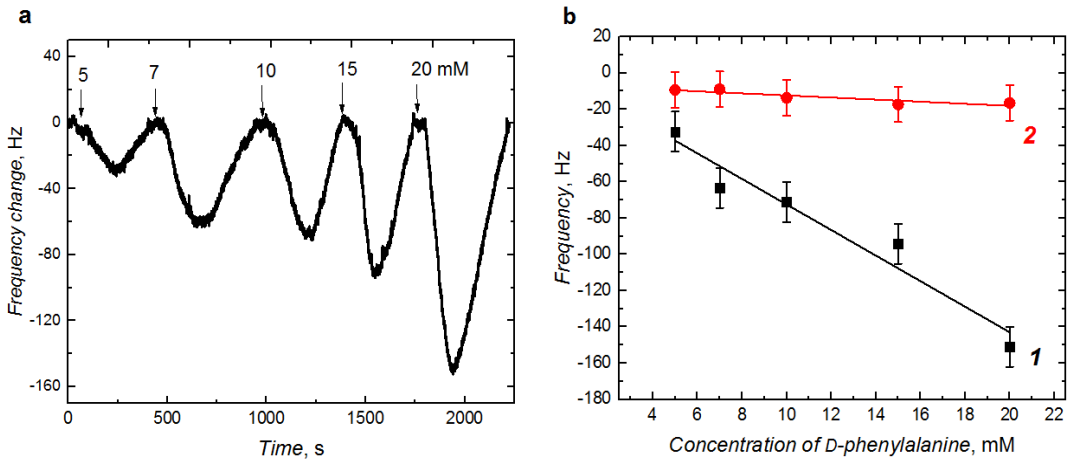

Figure 3.3-7. The Δf change with time after injection of 100-µL samples of **3** of different concentrations, indicated at the foot of each peak, under FIA conditions for (a) the **3**-templated MIP film, and (b) calibration plots for **3** on the Au-QCR coated with either the (*1*) MIP or (*2*) NIP film. A 10-mM NaH_2PO_4 served as the carrier solution.

Table 3.3-3. Analytical parameters of the devised MIP based EG-FET chemosensors for determination of **3** and **4**.

MIP	Analytical parameter	Interference	Value ± st.dev.
D-Phenylalanine templated MIP	Sensitivity to D-phenylalanine, μA mM^{-1}		0.43 ± 0.02
	Linear dynamic concentration range, μM		13 – 100
	Limit of detection at 3σ, μM		13
	Sensitivity to interferences, μA mM^{-1}	L-Phenylalanine	0.19 ± 0.02
		D-Alanine	0.20 ± 0.02
		D-Tyrosine	0.06 ± 0.01
		D-Proline	0.20 ± 0.02
L-Phenylalanine templated MIP	Sensitivity to L-phenylalanine, μA mM^{-1}		0.90 ± 0.07
	Linear dynamic concentration range, μM		13 – 100
	Limit of detection at 3σ, μM		13
	Sensitivity to interferences, μA mM^{-1}	D-Phenylalanine	0.39 ± 0.01
		D-Alanine	0.42 ± 0.03
		D-Tyrosine	0.43 ± 0.01
NIP	Sensitivity to D-phenylalanine, μA mM^{-1}		0.012 ± 0.03

Chapter 4

Conclusions

A series of four EG-FET chemosensors was successfully devised, fabricated, and tested. These chemosensors were prepared for selective determination of such compounds of health importance as inosine, human lipocalin-2 (NGAL), as well as D- and L-phenylalanine. All the molecularly imprinted polymer-based recognition films were prepared by potentiodynamic electropolymerization on the extended gates of FETs. For designing molecular cavities, composition of the most stable pre-polymerization complexes was determined using quantum-chemical calculations. Well-adhering, rigid films of MIPs and NIPs were deposited on the EG-FETs and PM signal transducing units, Au-QCRs. Moreover, the suitability of different transducers was critically examined. High values of AIFs confirmed formation of selective molecular cavities in the imprinted polymers.

The detectability of the inosine EG-FET chemosensor was higher than that of its PM chemosensor. The LOD for the EG-FET chemosensor reached 0.62 ± 0.01 μM, which is suitable for studies of biological samples, where the inosine level is reported to be ranged from 0 to 2.9 μM in patients with diagnosed diabetic nephropathy,[2] gout, or hyperuricemia,[3] and 25 μM in humans after intensive physical exercises.[9] Furthermore, the MIP film-coated EG-FET chemosensor allowed for advantageous flexibility during measurements through V_G adjustments. This procedure enabled for obtaining either increased detectability or selectivity, depending on requirements. Importantly, selectivity of the developed MIP film-coated EG-FET chemosensor was very high with respect to inosine structural analogs and interferences, including thymine, adenosine, guanosine and glucose.

The combination of electrical EG-FET transduction with surface-enhanced MIP recognition allowed fabricating a highly sensitive chemosensor for determination of the NGAL biomarker. The required surface enhancement and porosity was reached because of retaining sufficient mechanical strength incurred by the MOF inorganic-organic microporous materials. Additionally, removal of the MOF helped to remove the NGAL protein from the imprinted polymer. The chemosensor devised that way exhibited appreciable sensitivity (5.1 nA μM^{-1}), a low LOD (0.12 µM NGAL), and a reasonable linear dynamic concentration range (0.1 to 0.9 µM NGAL). Moreover, the chemosensor was selective with respect to a common interfering protein, HSA.

The EG-FET chemosensors for enantioselective determination of D- and L-phenylalanine successfully discriminated between these two enantiomers. Determination was possible in the concentration range of 13 to 100 µM with the LOD of 13 µM. The highest enantioselectivity factor ever reported for MIP (∼2.3) was obtained. Both chemosensors were selective with respect to the interferences of common amino acids including D-proline, D-alanine, and D-tyrosine. Moreover, the D-phenylalanine EG-FET chemosensor was able to determine the D-phenylalanine analyte concentration in a mixture of interfering amino acids.

Chapter 5

Further research

Plans of the future research emerged from unusually tempting results involving a chemosensor capable of the gluten epitope detection.[199] This chemosensor is based on the recognition unit involving MIPs as a nature-mimicking system.

Gluten is the allergen that triggers autoimmune reactions in humans suffering of celiac sprue (CS). CS, also known as gluten enteropathy or celiac disease, is, after hypolactasia, the second most common food intolerance. It is estimated that CS affects the 1-2% of the European population with direct costs on the healthcare estimated at ~3 billion € per year.[200] This autoimmune disease of a small intestine is caused by the ingestion of gluten proteins from a wide and ubiquitous food sources, such as wheat, rye, and barley. Exposure to gluten induces an inflammatory response leading to destruction of the villous structure of the intestine. Very often CS appears in the early childhood with severe symptoms including chronic diarrhea, abdominal distention, and failure to thrive. In many cases, symptoms may develop solely later in life, that is when the disease symptoms include fatigue, diarrhea, and weight loss due to malabsorption, anemia, and neurological symptoms.[201] CS is more often diagnosed in women than in men[202] and is a life-long disease. If it remains untreated, CS is associated with increased morbidity and mortality. Despite its high prevalence in most population groups and serious manifestations, the only effective therapy is strict dietary abstinence from gluten. Even a slight contamination of food with gluten can cause serious adverse reactions from digestive system. Food should contain less than 20 mg/kg gluten in order to be considered as "gluten-free" and to be eaten safely. This is why devising small, portable gluten detection tool, is very important. Such a device would make the daily routine of CS sick people significantly easier.

Hence, the main goal of my future research is to devise a chemical sensor, with MIPs as the recognition unit, capable of gluten detection and determination in food.

Gluten is a mixture of proteins.[203,204] From the molecular point of view the structure of gluten is very complex. Although fabrication of an MIP against small molecules or peptides is now relatively easy and straightforward, imprinting of large molecular structures is challenging.[84] The major problem associated to the imprinting of proteins consists in their restricted mobility within highly cross-linked polymer networks and, in consequence, poor efficiency of release and binding. Moreover, the molecular size, conformational flexibility, and sensitivity to denaturation makes them difficult for imprinting. To circumvent these problems, several strategies including surface imprinting and epitope imprinting[91,90] have been developed. Chapter 3.2 describes successful imprinting of NGAL protein through surface imprinting. However, to imprint gluten proteins the latter approach will be utilized.

Epitope imprinting is successfully used to imprint proteins.[90] In this approach, a surface exposed peptide fragment of the protein (an epitope), is used as the template (Scheme 5-1). The resulting MIP recognizes therefore not only the template but also the whole macromolecule. For example, the epitope peptides of cytochrome *c* and BSA were used as templates for fabrication of macromolecular receptors for proteins.[205] Moreover, an MIP-film coated Au-QCR sensor for the dengue virus NS1 protein using epitope-mediated imprinting was devised.[206] Compared with traditional protein imprinting approaches, the epitope imprinting has several advantages. Firstly, more selective and stronger interactions with a fragment or a small part of the macromolecule can lower the non-specific binding and improve the affinity. Secondly, the polymer can not only recognize the template but also the entire protein and, therefore, the operation procedures are easier. Thirdly, short peptides to be used as the epitopes for imprinting are less expensive than full proteins.

Thus, the final objective of my future research is to devise chemosensors featuring transduction units integrated with MIP recognition units, for determination of immunogenic gluten components.

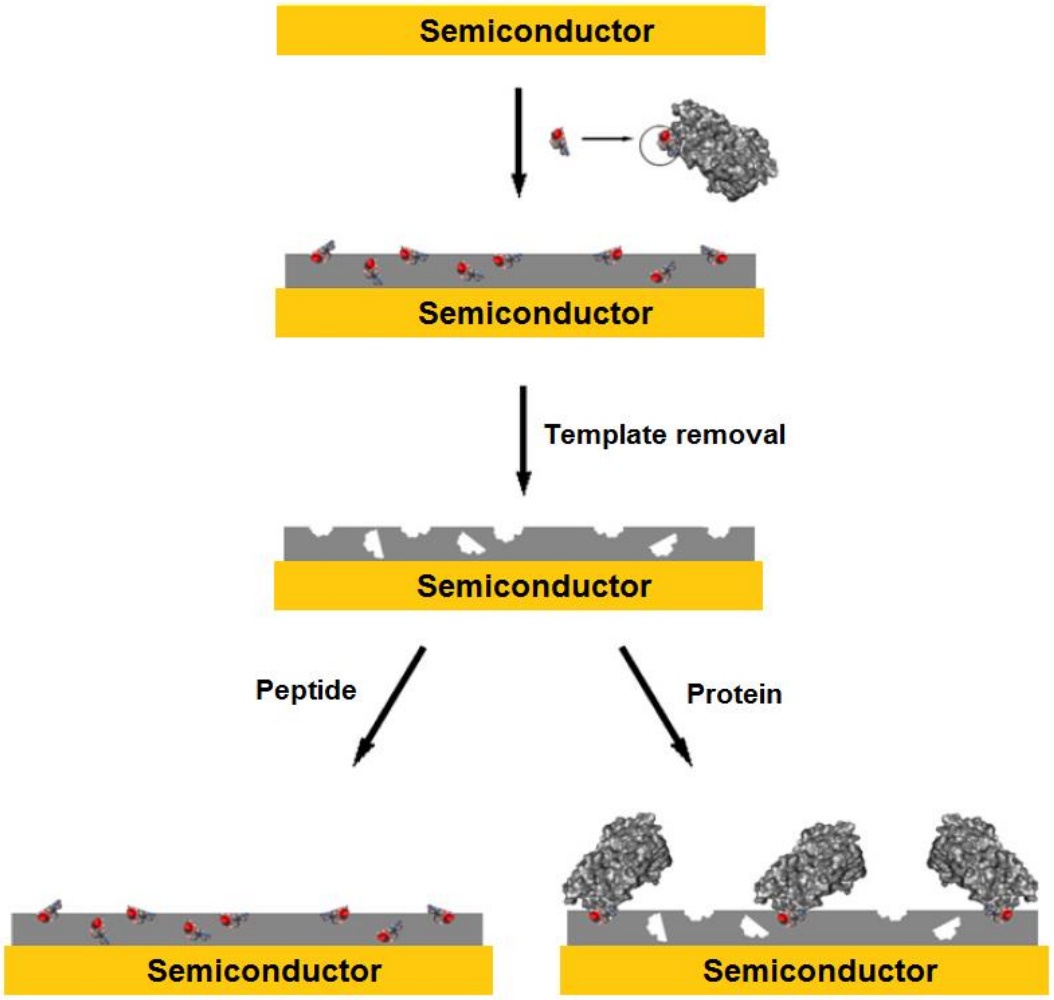

Scheme 5-1. Workflow of epitope-imprinted MIP-based chemosensor preparation (Adapted from[205]).

My future research is subdivided into four distinctive steps.

Step 1. **Biochemical insights into gluten in search of immunogenic gluten epitopes**. At first, I will earn biochemical and biological-databases knowledge by in silico digestion of gluten proteins, mostly of prolamins, which are the main gluten components. Focus will be on those epitopes that are reported as harmful for CS patients. Immunogenic epitopes will be selected to play the role of templates ready for imprinting. After literature survey, I have already chosen one of such epitopes, PQQPFPQQ, and imprinted it. The result of this project was submitted to the Polish Patent Office.[199] These preliminary results served as the prove of concept convincingly indicating that the future investigations will be successful.

Step 2. **Modeling tools for the identification of suitable monomer-template interactions**. We will characterize and select functional monomers containing sites

capable of forming complexes with the gluten epitope templates, and suitable for electrochemical polymerization. Both functional monomers and cross-linking monomers will be carefully selected. Suitable monomers will either be ordered if commercially available or if not, then custom designed and synthesized. *Bis*(2,2'-bithienyl)methane can readily be polymerized under oxidative electrochemical conditions. Moreover, it can relatively easily be derivatized with different receptor-type substituents at the methane carbon position to result in a range of useful functional monomers, each featuring different recognition site. Epitopes will be custom prepared by specialized suppliers, so to ensure the required level of purity. Quantum-chemistry calculations will be performed in order to optimize structures of complexes of gluten epitope templates with functional monomers. Most stable complexes will then be selected for the polymerization. These studies will be focused on determination of stability in solution of the pre-polymerization complex. The NMR spectroscopy, fluorescent spectroscopy, or isothermal titration calorimetry will be used for that purpose.

Step 3. **Chemosensors preparation**. After deposition of MIP films, they will be characterized by surface techniques including SEM, AFM, and XPS among others. Film wettability and thickness, as well as preparation of the chemosensors for determination of the previously chosen gluten epitopes, and pure gluten itself, will be investigated. Moreover, procedures of template removal from the MIP networks will be developed. Deposition of the MIP films onto chosen transduction structures, e.g., EG-FETs, will be performed.

Step 4. **Chemosensors performance evaluation and validation**. Further work will involve the possibility of the fabricated chemical sensors to respond selectively to the gluten epitopes. At first, analytes will be tested under laboratory conditions, and then the chemosensors will be tested with real food samples. In this step, analytical performance of the chemosensors will be characterized. We expect that these investigations will lead us to optimization of the conditions of MIP deposition and integration within the chemosensors. This step will include assessment of detectability and sensitivity of the MIP chemosensors, their selectivity with respect to mismatched epitope interferences. At the end of this step, a laboratory model of a gluten

chemosensor will be proposed. This model will be useful to devise a prototype of a gluten detector ready for commercialization.

Future research concerning the development of gluten chemosensor, in a form of the proposal, has already been submitted, together with Prof. Alessandra Maria Bossi of the Department of Biotechnology of the University of Verona, to the European Commission. After positive evaluation, European Commission awarded this proposal with Maria Curie Individual Fellowship (H2020-MSCA-IF-2016, type of action MSCA-IF-EF-ST) with a grant entitled “Gluten Epitope Molecularly imprinted polymer Sensor (GEMS)”, No. 752438.

Prof. Alessandra Maria Bossi leads the Group of Polymers Recognition and Biomimesis at the Department of Biotechnology of the Verona University. The group has an international reputation and a focal point for biomimesis, imprinted nanomaterials, and methodological biochemistry developments.

References

1. G. Hasko, M. V. Sitkovsky, C. Szabo, Immunomodulatory and neuroprotective effects of inosine, *Trends Pharmacol. Sci.,* **2004,** *25*, 152.

2. J.-F. Xia, Q.-L. Liang, X.-P. Liang, P. H. Yi-Ming Wang, P. Li, G.-A. Luo, Ultraviolet and tandem mass spectrometry for simultaneous quantification of 21 pivotal metabolites in plasma from patients with diabetic nephropathy., *J. Chromatogr.B,* **2009,** *877*, 1930.

3. J. Y. Zhao, Q. Liang, G. Luo, Y. Wang, Y. Zuo, M. Jiang, G. Yu, T. Zhang, Purine metabolites in gout and asymptomatic hyperuricemia: analysis by HPLC – electrospray tandem mass spectrometry, *Clin. Chem.,* **2005,** *51*, 1742.

4. C. M. Grum, R. H. Simon, D. R. Dantzker, I. H. Fox, Evidence for adenosine triphosphate degradation in critically-ill patients., *Chest J.,* **1985,** *88*, 763.

5. A. M. Amorini, A. Petzold, B. Tavazzi, J. Eikelenboom, G. Keir, A. Belli, G. Giovannoni, V. D. Pietro, C. Polman, S. D'Urso, R. Vagnozzi, B. Uitdehaa, G. Lazzarino, Increase of uric acid and purine compounds in biological fluids of multiple sclerosis patients, *Clin. Biochem.,* **2009,** *42*, 1001.

6. S. Buckley, L. Barsky, K. Weinberg, D. Warburton, In vivo inosine protects alveolar epithelial type 2 cells against hyperoxia-induced DNA damage through MAP kinase signaling, *Am. J. Physiol. – Lung Cell. Mol. Physiol.,* **2005,** *288*, L569.

7. S. Schneider, H. H. Klein, Inosine improves islet xenograft survival in immuncompetent diabetic mice, *Eur. J. Med. Res.,* **2005,** *10*, 283.

8. K. Susztak, E. P. Bottinger, Diabetic nephropathy: a frontier for personalized medicine, *J. Am. Soc. Nephrol.,* **2006,** *17*, 361.

9. C. G. Stathis, M. F. Carey, R. J. Snow, The influence of all opurinolonurinary purine loss after repeated sprint exercise in man, *Metab. Clin. Exp.,* **2005,** *54*, 1269.

10. Y. Kong, N. Zheng, Z. Zhang, R. Gao, High-performance capillary zone electrophoretic assay for markers of diabetic nephropathy in plasma and urine, *J. Chromatogr.A,* **2003,** *987*, 477.

11. L. Terzuoli, B. Porcelli, C. Setacci, M. Giubbolini, G. Cinci, F. Carlucci, R. Pagani, E. Marinello, Comparative determination of purine compounds in carotid plaque by capillary zone electrophoresis and high-performance liquid chromatography, *J. Chromatogr.B,* **1999,** *728*, 185.

12. D. A. Mei, G. J. Gross, K. Nithipatikom, Simultaneous determination of adenosine, inosine,hypoxanthine, xanthine, and uric acid in microdialysis samples using microbore column high-performance liquid chromatography with a diode array detector, *Anal. Biochem.,* **1996,** *238*, 34.

13. I.-S. Park, N. Kim, Simultaneous determination of hypoxanthine, inosine and inosine 5'-monophosphate with serially connected three enzyme reactors, *Anal. Chim. Acta,* **1999,** *394*, 201.

14. E. Watanabe, H. Endo, T. Hayashi, K. Toyama, Simultaneous determination of hypoxanthine and inosine with an enzyme sensor, *Biosensors,* **1986,** *2*, 235.

15. T. Yao, Enzyme electrode for the successive detection of hypoxanthine and inosine *Anal. Chim. Acta,* **1993,** *281*, 323.

16. E. Watanabe, S. Tokimatsu, K. Toyama, Simultaneous determination of hypoxanthine, inosine, inosine-5′-phosphate and adenosine-5′-phosphate with a multielectrode enzymesensor, *Anal. Chim. Acta,* **1984,** *164*, 139.

17. E.T.G. Cavalheiro, K.A. El-Noura, A. Brajter-Toth, Possibilities of the use of fast scan voltammetry in simultaneous determination of purines at carbon fiber ultramicroelectrodes, *J. Braz. Chem. Soc.,* **2000,** *11*, 512.

18. L. Liu, J.-f Song, P.-f Yu, B. Cui, A novel electrochemical sensing system for inosine and its application for inosine determination in pharmaceuticals and human serum, *Electrochem. Commun.,* **2006,** *8*, 1521.

19. R. N. Goyal, V.K. Gupta, S. Chatterjee, Simultaneous determination of adenosine and inosine using single-wall carbon nanotubes modified pyrolytic graphite electrode, *Talanta,* **2008,** *76*, 662.

20. S. B. Revin, S. A. John, Selective determination of inosine in the presence of uric acid and hypoxanthine using modified electrode, *Anal. Biochem.,* **2012,** *421*, 278.

21. A. M. Oliveira-Brett, Ls. A. Silva, G. Farace, P. Vadgama, C. M. A. Brett, Voltammetric and impedance studies of inosine-5′-monophosphate and hypoxanthine, *Bioelectrochemistry,* **2003,** *59*, 49.

22. J. A. Gwira, F. Wei, S. Ishibe, J. M. Ueland, J. Barasch, L. G. Cantley, Expression of neutrophil gelatinase-associated lipocalin regulates epithelial morphogenesis in vitro., *J. Biol. Chem.,* **2005,** *280*, 7875.

23. J. Mishra, C. Dent, R. Tarabishi, M. M. Mitsnefes, Q. Ma, C. Kelly, S. M. Ruff, K. Zahedi, M. Shao, J. Bean, K. Mori, J. Barasch, P. Devarajan, Neutrophil gelatinase-associated lipocalin (NGAL) as a biomarker for acute renal injury after cardiac surgery., *Lancet,* **2005,** *365*, 1231.

24. J. Kanda, K. Mori, H. Kawabata, T. Kuwabara, K.P. Mori, H. Imamaki, M. Kasahara, H. Yokoi, C. Mizumoto, N.H. Thoennissen, H.P. Koeffler, J. Barasch, A. Takaori-Kondo, M. Mukoyama, K. Nakao, An AKI biomarker lipocalin-2 in the blood derives from the kidney in renal injury but from neutrophils in normal and infected conditions., *Clin. Exp. Nephrol.,* **2015,** *19*, 99.

25. A. Abbas, L. M. Tian, J. J. Morrissey, E. D. Kharasch, S. Singamaneni, Hot spot-localized artificial antibodies for label-free plasmonic biosensing, *Adv. Funct. Mater. ,* **2013,** *23*, 1789.

26. L. M. Tian, K. K. Liu, J. J. Morrissey, N. Gandra, E. D. Kharasch, S. Singamaneni, Gold nanocages with built-in artificial antibodies for label-free plasmonic biosensing, *J. Mater. Chem. B,* **2014,** *2*, 167.

27. P. S. Sharma, A. Pietrzyk-Le, F. D'Souza, W. Kutner, Electrochemically synthesized polymers in molecular imprinting for chemical sensing., *Anal. Bioanal. Chem.,* **2012,** *402*, 3177.

28. C. M. Hangarter, M. Bangar, A. Mulchandani, N. V. Myung, Conducting polymer nanowires for chemiresistive and FET-based bio/chemical sensors, *J. Mater. Chem.,* **2010,** *20*, 3131.

29. Matthews, D. E., An overview of phenylalanine and tyrosine kinetics in humans., *J. Nutr.,* **2007,** *137*, 1549S.

30. N. E. Walsh, S. Ramamurthy, L. Schoenfeld, J. Hoffman, Analgesic effectiveness of D-phenylalanine in chronic pain patients, *Arch. Phys. Med. Rehabil.,* **1986,** *67*, 436.

31. H. Khan, J. K. Park, The preparation of D-phenylalanine imprinted microbeads by a novel method of modified suspension polymerization., *Biotechnol. Bioprocess Eng.,* **2006,** *11*, 503.

32. L. Wu, Y. Gao, J. Wang, Synthesis, application, and molecular recognition mechanism study of phenylalanine molecularly imprinted polymer., *Anal. Lett.,* **2007,** *40*, 3129.

33. A. Mirmohseni, M. Shojaei, M. Farbodi, Application of a quartz crystal nanobalance to the molecularly imprinted recognition of phenylalanine in solution., *Biotechnol. Bioprocess Eng.,* **2008,** *13*, 592.

34. C. N. Casey, S. E. Campbell, U. J. Gibson, T. School, Phenylalanine detection using matrix assisted pulsed laser evaporation of molecularly imprinted amphiphilic block copolymer films., *Biosens. Bioelectron.,* **2010,** *26*, 703.

35. H. Qiu, Y. Xi, F. Lu, L. Fan, C. Luo, Determination of L-phenylalanine on-line based on molecularly imprinted polymeric microspheres and flow injection chemiluminescence, *Spectrochim. Acta, Part A,* **2012,** *86*, 456.

36. X.-Y. Liu, H.-X. Fang, L.-P. Yu, Molecularly imprinted photonic polymer based on β-cyclodextrin for amino acid sensing., *Talanta,* **2013,** *116*, 283.

37. C.-Y. Hsu, M.-H. Lee, J. L. Thomas, C.-P. Shih, T.-L. Hung, T.-J. Whang, H.-Y. Lin, Optical sensing of phenylalanine in urine via extraction with magnetic molecularly imprinted poly(ethylene-co-vinyl alcohol) nanoparticles, *Nanotechnology,* **2015,** *26*, 305502.

38. A. P. F. Turner, Biosensors: sense and sensibility, *Chem. Soc. Rev.,* **2013,** *42*, 3184.

39. Q. Liu, C. Wu, H. Cai, N. Hu, J. Zhou, P. Wang, Cell-based biosensors and their application in biomedicine, *Chem. Rev.,* **2014,** *114*, 6423.

40. R. Martınez-Manez, F. Sancenon, M. Biyikal, M. Hechtd, K. Rurack, Mimicking tricks from nature with sensory organic–inorganic hybrid materials, *J. Mater. Chem.,* **2011,** *21*, 12588.

41. M. J. Whitcombe, I. Chianella, L. Larcombe, S. A. Piletsky, J. Noble, R. Porter, A. Horgan, The rational development of molecularly imprinted polymer-based sensors for protein detection, *Chem. Soc. Rev.,* **2011,** *40*, 1547.

42. M. J. Whitcombe, N. Kirsch, I. A. Nicholls, Molecular imprinting science and technology: a survey of the literature for the years 2004–2011, *J. Mol. Recognit.,* **2014,** *27*, 297.

43. B. T. S. Bui, K. Haupt, Preparation and evaluation of a molecularly imprinted polymer for the selective recognition of testosterone-application tomolecularly imprinted sorbent assays, *J. Mol. Recognit.,* **2011,** *24*, 1123.

44. Z. Iskierko, P. S. Sharma, K. Bartold, A. Pietrzyk-Le, K. Noworyta, Kutner, W., Molecularly imprinted polymers for separating and sensing of macromolecular compounds and microorganisms, *Biotechnol. Adv.,* **2016,** *34*, 30.

45. M. Dabrowski, P. S. Sharma, Z. Iskierko, K. Noworyta, M. Cieplak, W. Lisowski, S. Oborska, A. Kuhn, W. Kutner, Early diagnosis of fungal infections using piezomicrogravimetric and electric chemosensors based on polymers molecularly imprinted with D-arabitol, *Biosens. Bioelectron.,* **2016,** *79*, 627.

46. W. J. Cheong, S. H. Yang, F. Ali, Molecular imprinted polymers for separation science: a review of reviews, *J. Sep. Sci.,* **2013,** *36*, 609.

47. A. C. Dias, E. C. Figueiredo, V. Grassi, E. A. Zagatto, M. A. Arruda, Molecularly imprinted polymer as a solid phase extractor in flow analysis, *Talanta,* **2008,** *76*, 988.

48. E. Hedborg, F. Winquist, I. Lundström, L. I. Andersson, K. Mosbach, Some studies of molecularly-imprinted polymer membranes in combination with field-effect devices, *Sens. Actuators A,* **1993,** *37-38*, 796.

49. D. Kriz, M. Kempe, K. Mosbach, Introduction of molecularly imprinted polymers as recognition elements in conductometric chemical sensors, *Sens. Actuators B,* **1996,** *33*, 178.

50. D. Kriz, K. Mosbach, Competitive amperometricmorphine sensor based on an agarose immobilised molecularly imprinted polymer, *Anal. Chim. Acta.,* **1995,** *300*, 71.

51. D. Kriz, O. Ramstrum, A. Svensron, K. Mosbach, Introducing biomimetic sensors based on molecularly imprinted polymers as recognition elements, *Anal. Chem.,* **1995,** *67*, 2142.

52. X.-F. Zheng, Q. Lian, H. Yang, X. Wang, Surface molecularly imprinted polymer of chitosan grafted poly(methyl methacrylate) for 5-fluorouracil and controlled release., *Sci. Rep.,* **2016,** *6*, 21409.

53. Y.-Q. Xia, T.-Y. Guo, H.-L. Zhao, M.-D. Song, B.-H. Zhang, B.-L. Zhang, Protein recognition onto silica particles using chitosan as intermedium substrate, *J. Biomed. Mat. Res. A,* **2009,** *90A*, 326.

54. K.-C. Ho, W.-M. Yeh, T.-S. Tung, J.-Y. Liao, Amperometric detection of morphine based on poly(3,4-ethylenedioxythiophene) immobilized molecularly imprinted polymer particles prepared by precipitation polymerization, *Anal. Chim. Acta.,* **2005,** *542*, 90.

55. L. D. Spurlock, A. Jaramillo, A. Praserthdam, J. Lewis, A. Brajter-Toth, Selectivity and sensitivity of ultrathin purine-ternplated overoxidized polypyrrole film electrodes, *Anal. Chim. Acta* **1996,** *336*, 37.

56 E. L. Holthoff, F. V. Bright, Molecularly templated materials in chemical sensing, *Anal. Chim. Acta.,* **2007,** *594*, 147.

57. P. S. Sharma, Z. Iskierko, A. Pietrzyk-Le, F. D'Souza, W. Kutner, Bioinspired intelligent molecularly imprinted polymers for chemosensing: A mini review, *Electrochem. Commun.,* **2015,** *50*, 81.

58. M. J. Whitcombe http://www.mipdatabase.com/.

59. D. Lakshmi, A. M. Bossi, M. J. Whitcombe, I. Chianella, S. A. Fowler, S. Subrahmanyam, E. V. Piletska, S. A. Piletsky, Electrochemical sensor for catechol and dopamine based on a catalytic molecularly imprinted polymer-conducting polymer hybrid recognition element, *Anal. Chem.,* **2009,** *81*, 3576.

60. T. S. C. R. Rebelo, C. Santos, J. Costa-Rodrigues, M. H. Fernandes, J. P. Noronha, M G F. Sales, Novel prostate specific antigen plastic antibody designed with charged binding sites for an improved protein binding and its application in a biosensor of potentiometric transduction, *Electrochim. Acta,* **2014,** *132*, 142.

61. Y. Zeng, Y. Zhou, T. Zhou, G. Shi, A novel composite of reduced graphene oxide and molecularlyimprinted polymer for electrochemical sensing 4-nitrophenol, *Electrochim. Acta,* **2014,** *130* 504.

62. S. Wei, Y. Liu, T. Hua, L. Liu, H. Wang, Molecularly imprinted electrochemical sensor for the determination of ampicillin based on a gold nanoparticle and multiwalled carbon nanotube-coated Pt electrode, *J. Appl. Polym. Sci.,* **2014,** *131*, 40613.

63. T. S. Anirudhan, S. Alexander, Multiwalled carbon nanotube based molecular imprinted polymer fortrace determination of 2,4-dichlorophenoxyaceticacid in naturalwater samples using a potentiometric method, *Appl. Surf. Sci.,* **2014,** *303*, 180.

64. Y. Liu, L. Zhu, Z. Luo, H. Tang, Fabrication of molecular imprinted polymer sensor for chlortetracycline based on controlled electrochemical reduction of graphene oxide, *Sens. Actuators B,* **2013,** *185*, 438.

65. G. Ertürk, D. Berillo, M. Hedström, B. Mattiasson, Microcontact-BSA imprinted capacitive biosensor for real-time, sensitive and selective detection of BSA, *Biotechnol. Rep.,* **2014,** *3*, 65.

66. A. Pietrzyk, S. Suriyanarayanan, W. Kutner, R. Chitta, F. D'Souza, Selective histamine piezoelectric chemosensor using a recognition film of the molecularly imprinted polymer of bis(bithiophene) derivatives, *Anal. Chem.,* **2009,** *81*, 2633.

67. T.-P. Huynh, C. Bikram K.C., W. Lisowski, F. D'Souza, W. Kutner, Molecularly imprinted polymer of bis(2,2′-bithienyl)methanes for selective determination of adrenaline, *Bioelectrochemistry,* **2013,** *93*, 37.

68. T.-P. Huynh, P. Pieta, F. D'Souza, W. Kutner, Molecularly imprinted polymer for recognition of 5-fluorouracil by RNA-type nucleobase pairing, *Anal. Chem.,* **2013,** *85*, 8304.

69. K. Bartold, A. Pietrzyk-Le, T.-P. Huynh, Z. Iskierko, M. Sosnowska, K. Noworyta, W. Lisowski, F. Sannicolò, S. Cauteruccio, E. Licandro, F. D'Souza, W. Kutner, Programmed transfer of sequence information into a molecularly imprinted polymer for hexakis(2,2′-bithien-5-yl) DNA analogue formation toward single-nucleotide-polymorphism detection, *ACS Appl. Mater. Interfaces,* **2017,** *9*, 3948.

70. P. S. Sharma, M. Dabrowski, F. D'Souza, W. Kutner, Surface development of molecularly imprinted polymer films to enhance sensing signals, *TrAC Trends Anal. Chem.,* **2013,** *51*, 146.

71. M. Cieplak, K. Szwabinska, M. Sosnowska, C. Bikram K.C., P. Borowicz, K. Noworyta, F. D'Souza, Kutner, W., Selective electrochemical sensing of human serum albumin by semi-covalent molecular imprinting, *Biosens. Bioelectron.,* **2015,** *74*, 960.

72. D. Batra, K. J. Shea, Combinatorial methods in molecular imprinting, *Curr. Opin. Chem. Biol.,* **2003,** *7*, 434.

73. I. A. Nicholls, H. S. Andersson, K. Golker, H. Henschel, B. C. G. Karlsson, G. D. Olsson, A. M. Rosengren, S. Shoravi, S. Suriyanarayanan, J. G. Wiklander, S. Wikman, Rational design of biomimetic molecularly imprinted materials: theoretical and computational strategies for guiding nanoscale structured polymer development, *Anal. Bioanal. Chem.,* **2011,** *400*, 1771.

74. C. Malitesta, E. Mazzotta, R. A. Picca, A. Poma, I. Chianella, S. A. Piletsky, MIP sensors - the electrochemical approach, *Anal. Bioanal. Chem.,* **2012,** *402*, 1827.

75. G. Wulff, Enzyme-like catalysis by molecularly imprinted polymers., *Chem. Rev.,* **2002,** *102*, 1.

76. T.-P. Huynh, P. S. Sharma, M. Sosnowska, F. D'Souza, W. Kutner, Functionalized polythiophenes: Recognition materials for chemosensors and biosensors of superior sensitivity, selectivity, and detectability, *Prog. Polym. Sci.,* **2015,** *47*, 1.

77. J. P. Rosengren, J. G. Karlsson, I. A. Nicholls, Enantioselective synthetic thalidomide receptors based upon DNA binding motifs, *Org. Biomol. Chem.,* **2004,** *2*, 3374.

78. T. A. Sergeyeva, O. A. Slinchenko, L. A. Gorbach, V. F. Matyushov, O. O. Brovko, S. A. Piletsky, L. M. Sergeeva, G. V. Elska, Catalytic molecularly imprinted polymer membranes: development of the biomimetic sensor for phenols detection, *Anal. Chim. Acta.,* **2010,** *659* 274.

79. B. C. Tripp, K. Smith, J. G. Ferry, Carbonic anhydrase: new insights for an ancient enzyme, *J. Biol. Chem.,* **2001,** *276*, 48615.

80. A. Ribeiro, F. Veiga, D. Santos, J. J. Torres-Labandeira, A. Concheiro, C. Alvarez-Lorenzo, Bioinspired imprinted PHEMA-hydrogels for ocular delivery of carbonic anhydrase inhibitor drugs, *Biomacromolecules,* **2011,** *12*, 701.

81. M. J. Whitcombe, Molecularly imprinted polymers: Smart hydrogel crystal gardens., *Nature Chem.,* **2011,** *3*, 657.

82. A. Cumbo, B. Lorber, P. F.-X. Corvini, W. Meier, P. Shahgaldian, A synthetic nanomaterial for virus recognition produced by surface imprinting., *Nature Comm.,* **2013,** *4*, Art. No. 1503.

83. A. M. Bossi, F. Bonini, A. P. F. Turner, S. A. Piletsky, Molecularly imprinted polymers for the recognition of proteins: The state of the art, **2007,** *22*, 1131.

84. S. Li, S. Cao, M. J. Whitcombe, S. A. Piletsky, Size matters: challenges in imprinting macromolecules, *Prog. Polym. Sci.,* **2014,** *39*, 145.

85. M. Kempe, K. Mosbach, Separation of amino acids, peptides and proteins on molecularly imprinted stationary phases, *J. Chromatogr. A,* **1995,** *691*, 317.

86. C.-H. Lu, Y. Zhang, S.-F. Tang, Z.-B. Fang, H.-H. Yang, X. Chen, G.-N. Chen, Sensing HIV related protein using epitope imprinted hydrophilic polymer coated quartz crystal microbalance, *Biosens. Bioelectron.,* **2012,** *31*, 439.

87. K. Fukazawa, K. Ishihara, Fabrication of a cell-adhesive protein imprinting surface with an artificial cell membrane structure for cell capturing, *Biosens. Bioelectron.,* **2009,** *25*, 609.

88. G. Pan, Q. Guo, Y. Ma, H. Yang, B. Li, Thermo-responsive hydrogel layers imprinted with RGDS peptide: a system for harvesting cell sheets, *Angew. Chem. Int. Ed.,* **2013,** *52*, 6907.

89. A. Rechichi, C. Cristallini, U. Vitale, G. Ciardelli, N. Barbani, G. Vozzi, Giusti, P., New biomedical devices with selective peptide recognition properties. Part 1: Characterization and cytotoxicity of molecularly imprinted polymers, *J. Cell. Mol. Med.,* **2007,** *11*, 1367.

90. A. M. Bossi, P. S. Sharma, L. Montana, G. Zoccatelli, O. Laub, R. Levi, Fingerprint imprinted polymer (FIP): Rational selection of peptide epitope templates for the determination of proteins by molecularly imprinted polymers, *Anal. Chem.,* **2012,** *84*, 4036.

91. A. Rachkov, N. J. Minoura, Recognition of oxytocin and oxytocin-related peptides in aqueous media using a molecularly imprinted polymer synthesized by epitope approach, *J. Chromatogr. A,* **2000,** *899*, 111.

92. M. Mahmoudi, S. Bonakdar, M. A. Shokrgozar, H. Aghaverdi, R. Hartmann, A. Pick, G. Witte, W. J. Parak, Cell-imprinted substrates direct the fate of stem cells, *ACS Nano,* **2013,** *7*, 8379.

93. O. Mashinchian, S. Bonakdar, H. Taghinejad, V. Satarifard, M. Heidari, M. Majidi, S. Sharifi, A. Peirovi, S. Saffar, M. Taghinejad, M. Abdolahad, S. Mohajerzadeh, M. A. Shokrgozar, S. M. Rezayat, M. R. Ejtehadi, M. J. Dalby, M. Mahmoudi, Cell-imprinted substrates act as an artificial niche for skin regeneration, *ACS Appl. Mater. Interfaces,* **2014,** *6*, 13280.

94. K. Ren, N. Banaei, R. N. Zare, Sorting inactivated cells using cell-imprinted polymer thin films, *ACS Nano,* **2013**, *7*, 6031.

95. Y. Hu, L. Xie, Y. Lu, X. Ren, Isolation of viable type I and II methanotrophs using cell-imprinted polyurethane thin films, *ACS Appl. Mater. Interfaces,* **2014,** *6*, 20550.

96. F. T. C. Moreira, S. Sharma, R. A. F. Dutra, J. P. C. Noronha, A. E. G. Cass, M. G. F. Sales, Smart plastic antibody material (SPAM) tailored on disposable screen printed electrodes for protein recognition: application to myoglobin detection, *Biosens. Bioelectron.,* **2013,** *45*, 237.

97. H.-J. Chen, Z.-H. Zhang, L.-J. Luo, S.-Z. Yao, Surface-imprinted chitosan-coated magnetic nanoparticles modified multi-walled carbon nanotubes biosensor for detection of bovine serum albumin, *Sens. Actuators B,* **2012,** *163*, 76.

98. H.-J. Chen, Z.-H. Zhang, D. Xie, R. Cai, X. Chen, Y.-N. Liu, S.-Z. Yao, Surface-imprinting sensor based on carbon nanotubes/graphene composite for determination of bovine serum albumin, *Electroanalysis,* **2012,** *24*, 2109.

99. I. Heller, A. M. Janssens, J. Mannik, E. D. Minot, S. G. Lemay, C. Dekker, Identifying the mechanism of biosensing with carbon nanotube transistors, *Nano Lett.,* **2008,** *8*, 591.

100. M.-H. Do, A. Florea, C. Farre, A. Bonhomme, F. Bessueille, F. Vocanson, N.-T. Tran-Thi, N. Jaffrezic-Renault, Molecularly imprinted polymer-based electrochemical sensor for the sensitive detection of glyphosate herbicide, *Int. J. Environ. Anal. Chem.,* **2015,** *95*, 1489.

101. M. Jiang, M. Braiek, A. Florea, A. Chrouda, C. Farre, A. Bonhomme, F. Bessueille, F. Vocanson, A. Zhang, N. Jaffrezic-Renault, Aflatoxin B1 detection using a highly-sensitive molecularly-imprinted electrochemical sensor based on an electropolymerized metal organic framework, *Toxins,* **2015,** *7*, 3540.

102. T. Guo, Q. Deng, G. Fang, D. Gu, Y. Yang, S. Wang, Upconversion fluorescence metal-organic frameworks thermo-sensitive imprinted polymer for enrichment and sensing protein, *Biosens. Bioelectron.,* **2016,** *79*, 341.

103. S. M. Reddy, G. Sette, Q. Phan, Electrochemical probing of selective haemoglobin binding in hydrogel-based molecularly imprinted polymers, *Electrochim. Acta,* **2011,** *56*, 9203.

104. F. T. C. Moreira, R. A. F. Dutra, J. P. C. Noronha, A. L. Cunha, M. G. F. Sales, Artificial antibodies for troponin T by its imprinting on the surface of multiwalled carbon nanotubes: its use as sensory surfaces, *Biosens. Bioelectron.,* **2011,** *28*, 243.

105. N. Karimian, M. Vagin, M. H. A. Zavar, M. Chamsaz, A. P. F. Turner, A. Tiwari, An ultrasensitive molecularly-imprinted human cardiac troponin sensor, *Biosens. Bioelectron.,* **2013,** *50*, 492.

106. X. Zhou, W. Li, X. He, L. Chen, Y. Zhang, Recent advances in the study of protein imprinting, *Sep. Purif. Rev.,* **2007,** *36*, 257.

107. K. M. Mayer, S. Lee, H. Liao, B. C. Rostro, A. Fuentes, P. T. Scully, C. L. Nehl, J. H. Hafner, A label-free immunoassay based upon localized surface plasmon resonance of gold nanorods., *ACS Nano,* **2008,** *2*, 687.

108. A. Betatache, F. Lagarde, C. Sanglar, A. Bonhomme, D. Leonard, N. Jaffrezic-Renault, Gold electrodes modified with molecular imprinted acrylate polymer for impedimetric determination of testosterone, *Sens. Transducers,* **2014,** *27*, 92.

109. R. Tucceri, Non-conducting poly(o-aminophenol) films in the field of the bioelectrochemistry, *Am. J. Anal. Chem.,* **2013,** *4*, 13.

110. Y. Yang, C. Yi, J. Luo, R. Liu, J. Liu, J. Jiang, X. Liu, Glucose sensors based on electrodeposition of molecularly imprinted polymeric micelles: a novel strategy for MIP sensors, *Biosens. Bioelectron.,* **2011,** *26*, 2607.

111. C. Fang, C. Yi, Y.Wang, Y. Cao, X. Liu, Electrochemical sensor based on molecular imprinting by photo-sensitive polymers, *Biosens. Bioelectron.,* **2009,** *24*, 3164.

112. J. Wang, S. Banerji, N. Menegazzo, W. Peng, Q. Zou, K. S. Booksh, Glucose detection with surface plasmon resonance spectroscopy and molecularly imprinted hydrogel coatings, *Talanta,* **2011,** *86*, 133.

113. K. Pal, K. Melcher, H. E. Xu, Structure and mechanism for recognition of peptide hormones by Class B G-protein-coupled receptors, *Acta Pharmacol. Sin.,* **2012,** *33*, 300.

114. I. Basozabal, A. Guerreiro, A. Gomez-Caballero, M. A. Goicolea, R. J. Barrio, Direct potentiometric quantification of histamine using solid-phase imprinted nanoparticles as recognition elements, *Biosens. Bioelectron.,* **2014,** *58*, 138.

115. M. Peeters, S. Kobben, K. L. Jiménez-Monroy, L. Modesto, M. Kraus, T. Vandenryt, A. Gaulke, B. V. Grinsvena, S. Ingebrandt, T. Junkers, P. Wagn, Thermal detection of histamine with a graphene oxide based molecularly imprinted polymer platform prepared by reversible addition–fragmentation chain transfer polymerization, *Sens. Actuators B,* **2014,** *203*, 527.

116. Z. Iskierko, M. Sosnowska, P. S. Sharma, T. Benincori, F. D'Souza, I. Kaminska, K. Fronc, K. Noworyta, Extended-gate field-effect transistor (EG-FET) with molecularly imprinted polymer (MIP) film for selective inosine determination, *Biosens. Bioelectron.,* **2015,** *74*, 526.

117. M. C. Cela-Pérez, L. Barbosa-Pereira, X. Vecino, M. Pérez-Ameneiro, A. L. Latorre, J. M. López-Vilariño, M. V. González Rodríguez, A. B. Moldes, J. M. Cruz, Selective removal of ATP degradation products from food matrices II: Rapid screening of hypoxanthine and inosine by molecularly imprinted matrix solid-phase dispersion for evaluation of fish freshness., *Talanta,* **2015,** *135*, 58.

118. S. Suriyanarayanan, P. J. Cywinski, A. J. Moro, G. J. Mohr, W. Kutner, Chemosensors based on molecularly imprinted polymers, *Top Curr. Chem.,* **2012,** *325*, 165.

119. A. Hulanicki, S. Glab, F. Ingman, Chemical sensors. Definitions and classification., *Pure Appl. Chem.,* **1991,** *63*, 1247.

120. D. R. Theavenot, T. K. Toth, R. A. Durst, G. S. Wilson, Electrochemical biosensors: Recommended definitions and classification., *Pure Appl. Chem.,* **1999,** *71*, 2333.

121. L. Torsi, M. Magliulo, K. Manoli, G. Palazzo, Organic field-effect transistor sensors: a tutorial review, *Chem. Soc. Rev.,* **2013,** *42*, 8612.

122. H. Nakamura, I. Karube, Current research activity in biosensors., *Anal. Bioanal. Chem.,* **2003,** *377*, 446.

123. M. Cieplak, R. Weglowski, Z. Iskierko, D. Weglowska, P. S. Sharma, K. Noworyta, F. D'Souza, W. Kutner, Optical chemosensor for protein determination with molecularly imprinted polymer recognition and birefringence liquid crystal detection, *submitted manuscript,* **2017**.

124. K. Haupt, K. Noworyta, W. Kutner, Imprinted polymer-based enantioselective acoustic sensor using a quartz crystal microbalance., *Anal. Commun.,* **1999,** *36*, 391.

125. Z. Iskierko, A. Checinska, P. S. Sharma, K. Golebiewska, K. Noworyta, P. Borowicz, K. Fronc, V. Bandi, F. D'Souza, W. Kutner, Molecularly imprinted polymer based extended-gate field-effect transistor chemosensors for phenylalanine enantioselective sensing, *J. Mater. Chem. C,* **2017,** *5*, 969.

126. A. Merkoci, S. Alegret, New materials for electrochemical sensing IV. Molecular imprinted polymers., *Trends Anal. Chem.,* **2002,** *21*, 717.

127. R. G. Smith, N. D'Souza, S. Nicklin, A review of biosensors and biologicallyinspired systems for explosives detection, *Analyst,* **2008,** *133*, 571.

128. B. V. Dorst, J. Mehta, K. Bekaert, E. Rouah-Martin, W. D. Coen, P. Dubruel, R. Blust, J. Robbens, Recent advances in recognition elements of food and environmental biosensors: a review, *Biosens. Bioelectron.,* **2010,** *26*, 1178.

129. A. K. Wanekaya, W. Chen, A. Mulchandani, Recent biosensing developments in environmental security, *J. Environ. Monit.,* **2008,** *10*, 703.

130. E. C. Alocilja, S. M. Radke, Market analysis of biosensors for food safety, *Biosens. Bioelectron.,* **2003,** *18*, 841.

131. J. Janata, Thirty years of CHEMFETs – a personal view., *Electroanalysis,* **2004,** *16*, 1831.

132. P. Bergveld, Development of anion-sensitive solid-state device for neuro-physiological measurements, *IEEE Trans. Biomed. Eng.,* **1970,** *17*, 70.

133. C. Jimenez-Jorquera, J. Orozco, A. Baldi, ISFET based microsensors for environmental monitoring, *Sensors,* **2010,** *10*, 61.

134. C.-S. Lee, S. K. Kim, M. Kim, Ion-sensitive field-effect transistor for biological sensing, *Sensors,* **2009,** *9*, 7111.

135. P. Bergveld, Thirty years of ISFETOLOGY what happened in the past 30 years and what may happen in the next 30 years, *Sens. Actuators B,* **2003,** *88*, 1.

136. P. D. Batista, M. Mulato, C. Fd. O. Graeff, F. J. R. Fernandez, Fd. C. Marques, SnO_2 extended gate field-effect transistors pH sensor, *Braz. J. Phys.,* **2006,** *36*, 478.

137. C.-P. Chen, A. Ganguly, C.-Y. Lu, T.-Y. Chen, C.-C. Kuo, R.-S. Chen, W.-H. Tu, W. B. Fischer, K.-H. Chen, L.-C. Chen, Ultrasensitive in situ label-free DNA detection using a GaN nanowire-based extended-gate field-effect-transistor sensor, *Anal. Chem.,* **2011,** *83*, 1938.

138. L.-T. Yin, J.-C. Chou, W.-Y. Chung, T.-P. Sun, S.-K. Hsiung, Separate structure extended-gate H^+-ion sensitive field effect transistor on a glass substrate, *Sens. Actuators B,* **2000,** *71*, 106.

139. F.-G. Banica, *Chemical sensors and biosensors, fundamentals and applications.* John Wiley & Sons Ltd,: The Atrium, Southern Gate, Chichester, West Sussex, PO19 8SQ, United Kingdom, **2012**.

140. Y. L. Khung, D. Narducci, Synergizing nucleic acid aptamers with 1-dimensional nanostructures as label-free field-effect transistor biosensors, *Biosens. Bioelectron.,* **2013,** *50*, 278.

141. O. S. Kwon, S. J. Park, J. Jang, A high-performance VEGF aptamer functionalized polypyrrole nanotube biosensor, *Biomaterials,* **2010**, *31*, 4740.

142. S. Casalini, F. Leonardi, T. Cramer, F. Biscarini, Organic field-effect transistor for label-free dopamine sensing, *Org. Electron.,* **2013,** *14*, 156.

143. S. A. Piletsky, A. P. F. Turner, Electrochemical sensors based on molecularly imprinted polymers., *Electroanalysis,* **2002,** *14*, 317.

144. M. F. Frasco, L. A. A. N. A. Truta, M. G. F. Sales, F. T. C. Moreira, Imprinting technology in electrochemical biomimetic sensors, *Sensors,* **2017,** *17*, 523.

145. M. Lahav, A. B. Kharitonov, O. Katz, T. Kunitake, I. Willner, Tailored chemosensors for chloroaromatic acids using molecular Imprinted TiO2 thin films on Ion-sensitive field-effect transistors, *Anal. Chem.,* **2001,** *73*, 720.

146. N. Sallacan, M. Zayats, T. Bourenko, A. B. Kharitonov, I. Willner, Imprinting of nucleotide and monosaccharide recognition sites in acrylamidephenylboronic acid-acrylamide copolymer membranes associated with electronic transducers, *Anal. Chem.,* **2002,** *74*, 702.

147. S. P. Pogorelova, M. Zayats, T. Bourenko, A. B. Kharitonov, O. Lioubashevski, E. Katz, I. Willner, Analysis of $NAD(P)^+$/NAD(P)H cofactors by imprinted polymer membranes associated with ion-sensitive field-effect transistor devices and Au-quartz crystals, *Anal. Chem.,* **2003,** *75*, 509.

148. O. M. Petrukhin, S. P. Pogorelova, A. B. Kharitonov, E. V. Shipulo, Molecularly selective field-effect transistors for determining nicotinamide adenine dinucleotide and its phosphates, *J. Anal. Chem.,* **2007,** *62*, 894.

149. A. Kugimiya, K. Kohara, Biomimetic sensor for cAMP using an ion-sensitive field-effect transistor, *Mater. Sci. Eng. C,* **2009,** *29*, 959.

150. H.-Y. Lee, B. S. Kim, Grafting of molecularly imprinted polymers on iniferter-modified carbon nanotube, *Biosens. Bioelectron.,* **2009,** *25*, 587.

151. H.-H. Tsai, C.-F. Lin, Y.-Z. Juang, I.-L. Wang, Y.-C. Lin, R.-L. Wang, H.-Y. Lin, Multiple type biosensors fabricated using the CMOS BioMEMS platform, *Sens. Actuators B,* **2010,** *144*, 407.

152. A. Kugimiya, F. Babe, Phosphate ion sensing using molecularly imprinted artificial polymer receptor, *Polym. Bull.,* **2011,** *67*, 2017.

153. T. Alizadeh, F. Rezaloo, A new chemiresistor sensor based on a blend of carbon nanotube, nano-sized molecularly imprinted polymer and poly methyl methacrylate for the selective and sensitive determination of ethanol vapor, *Sens. Actuators B,* **2013,** *176*, 28.

154. Z. Iskierko, P. S. Sharma, D. Prochowicz, K. Fronc, F. D'Souza, D. Toczydłowska, F. Stefaniak, Noworyta, K., Molecularly imprinted polymer (MIP) film with improved surface area developed by using metal–organic framework (MOF) for sensitive lipocalin (NGAL) determination, *ACS Appl. Mater. Interfaces,* **2016,** *8*, 19860.

155. F. Sannicolo, P. R. Mussini, T. Benincori, R. Martinazzo, S. Arnaboldi, G. Appoloni, M. Panigati, E. Q. Procopio, V. Marino, R. Cirilli, S. Casolo, W. Kutner, K. Noworyta, A. Pietrzyk-Le, Z. Iskierko, K. Bartold, Inherently chiral spider-like oligothiophenes, *Chem. Eur. J.,* **2016,** *22*, 10839.

156. X. Jia, D. Chen, L. Bin, H. Lu, R. Zhang, Y. Zheng, Highly selective and sensitive phosphate anion sensors based on AlGaN/GaN high electron mobility transistors functionalized by ion imprinted polymer, *Sci. Rep.,* **2016,** *6*, 27728.

157. Y. Rayanasukha, S. Pratontep, S. Porntheeraphat, W. Bunjongpru, J. Nukeaw, Non-enzymatic urea sensor using molecularly imprinted polymers surfacemodified based-on ion-sensitive field effect transistor (ISFET), *Surf. Coat. Technol.,* **2016,** *306*, 147.

158. V. K. Tamboli, N. Bhalla, P. Jolly, C. R. Bowen, J. T. Taylor, J. L. Bowen, C. J. Allender, P. Estrela, Hybrid synthetic receptors on MOSFET devices for detection of prostate specific antigen in human plasma, *Anal. Chem.,* **2016,** *88*, 11486.

159. P. S. Sharma, A. Wojnarowicz, M. Sosnowska, T. Benincori, K. Noworyta, F. D'Souza, W. Kutner, Potentiometric chemosensor for neopterin, a cancer biomarker, using an electrochemically synthesized molecularly imprinted polymer as the recognition unit, *Biosens. Bioelectron.,* **2016,** *77*, 565.

160. L.-L. Chi, J.-C. Chou, W.-Y. Chung, T.-P. Sun, S.-K. Hsiung, Study on extended-gate field-effect transistor with tinoxide sensing membrane *Mater. Chem. Phys.,* **2000,** *63*, 19.

161. X. L. Jia, X. Y. Huang, T. Yin, L. H. Yang, D. J. Chen, H. Lu, R. Zhang, Y. D. Zheng, Ultrasensitive detection of phosphate using ion-imprinted polymer functionalized AlInN/GaN high electron mobility transistors, *IEEE Electron Device Lett.,* **2016,** *37*, 913.

162. B. H. Chu, C. Y. Chang, K. Kroll, N. Denslow, Y.-L. Wang, S. J. Pearton, A. M. Dabiran, A. M. Wowchak, B. Cui, P. P. Chow, F. Ren, AlGaN/GaN high electron mobility transistor based sensors for environmental and bio-applications, *Appl. Phys. Lett.,* **2010,** *96*, 013701.

163. S. C. Hung, Y. L. Wang, B. Hicks, S. J. Pearton, D. M. Dennis, Detection of chloride ions using an integrated Ag/AgCl electrode with AlGaN/GaN high electron mobility transistors., *Appl. Phys. Lett.,* **2008,** *92*, 193903.

164. T. Ito, S. M. Forman, C. Cao, F. Li, C. R. Eddy Jr., M. A. Mastro, R. T. Holm, R. L. Henry, K. L. Hohn, J. H. Edgar, Self-assembled monolayers of alkylphosphonic acid on GaN substrates., *Langmuir* **2008,** *24*, 6630.

165. A. Pietrzyk, S. Suriyanarayanan, W. Kutner, M. E. Zandler, F. D'Souza, Molecularly imprinted poly[*bis*(2,2'-bithienyl)methane] film with built-in molecular recognition sites for a piezoelectric microgravimetry chemosensor for selective determination of dopamine, *Bioelectrochemistry,* **2010,** *80*, 62.

166. M. J. Frisch, G. W. Trucks, H. B. Schlegel, G. E. Scuseria, M. A. Robb, J. R. Cheeseman, G. Scalmani, V. Barone, B. Mennucci, G. A. Petersson, H. Nakatsuji, M. Caricato, X. Li, H. P. Hratchian, A. F. Izmaylov, J. Bloino, G. Zheng, J. L. Sonnenberg, M. Hada, M. Ehara, K. Toyota, R. Fukuda, J. Hasegawa, M. Ishida, T. Nakajima, Y. Honda, O. Kitao, H. Nakai, T. Vreven, J. A. Montgomery, J., J. E. Peralta, F. Ogliaro, M. Bearpark, J. J. Heyd, E. Brothers, K. N. Kudin, V. N. Staroverov, R. Kobayashi, J. Normand, K. Raghavachari, A. Rendell, J. C. Burant, S. S. Iyengar, J. Tomasi, M. Cossi, N. Rega, J. M. Millam, M. Klene, J. E. Knox, J. B. Cross, V. Bakken, C. Adamo, J. Jaramillo, R. Gomperts, R. E. Stratmann, O. Yazyev, A. J. Austin, R. Cammi, C. Pomelli, J. W. Ochterski, R. L. Martin, K. Morokuma, V. G. Zakrzewski, G. A. Voth, P. Salvador, J. J. Dannenberg, S. Dapprich, A. D. Daniels, O. Farkas, J. B. Foresman, J. V. Ortiz, J. Cioslowski, D. J. Fox, Gaussian 09, Revision A.02, *Gaussian, Inc.: Wallingford CT,* **2009**.

167. A. Volkamer, A. Griewel, T. Grombacher, M. Rarey, Analyzing the topology of active sites: on the prediction of pockets and subpockets., *J. Chem. Inf. Model.,* **2010,** *50*, 2041−2052.

168. H. Li, M. Eddaoudl, M. O'Keeffe, O. M. Yaghi, Design and synthesis of an exceptionally stable and highly porous metal-organic framework, *Nature,* **1999,** *402*, 276.

169. W. Koh, W. Kutner, M. T. Jones, K. M. Kadish, An improved holder for the electrochemical quartz crystal microbalance and its cyclic voltammetry characteristics., *Electroanalysis* **1993,** *5*, 209.

170. A. Kochman, A., A. Krupka, A., J. Grissbach, W. Kutner, B. Gniewinska, L. Nafalski, Design and performance of a new thin-layer radial-flow holder for a quartz crystal resonator of an electrochemical quartz crystal microbalance., *Electroanalysis* **2006,** *18*, 2168.

171. M. H. Jamroz, Vibrational energy distribution analysis (VEDA): Scopes and limitations., *Spectrochim. Acta, Part A: Molecular and Biomolecular Spectroscopy,* **2013,** *114*, 220.

172. M. H. Jamroz, *Vibrational energy distribution analysis*. Spectroscopy and molecular modeling group, Institute of Nuclear Chemistry and Technology, Warsaw, Poland, **2004–2010**.

173. M. H. Jamroz, SPESCA, Spectroscopy and molecular modeling group,, *Institute of Nuclear Chemistry and Technology, Warsaw, Poland,* **2014**.

174. Z. Galus, *Fundamentals of electrochemical analysis*. Polish Scientific Publishers PWN: Warsaw, **1994**.

175. A. Cyganski, *Podstawy metod elektroanalitycznych*. Wydawnictwa Naukowo Techniczne: Warszawa, **1999**.

176. A. J. Bard, L. R. Faulkner, *Electrochemical methods: Fundamentals and Applications. 2nd ed.* John Wiley & Sons: New Jersey, **2001**.

177. J. Wang, *Analytical Electrochemistry. 3rd ed.* John Wiley & Sons, Inc.: New Jersey, USA, **2006**.

178. R. P. Buck, E. Lindner, W. Kutner, G. Inzelt, Piezoelectric chemical sensors (IUPAC Technical Report). *Pure Appl. Chem.,* **2004,** *76*, 1139.

179. G. Sauerbrey, The use of quartz oscillators for weighing thin layers and for microweighing., *Z. Phys.,* **1959,** *155*, 206.

180. J. McMurry, R. C. Fay, *Chemistry*. Prentice Hall: New Jersey, USA, 2003.

181. Cepheiden, Pronciple of PM-IRRAS., **2011**.

182. G. K. Binnig, C. F. Quate, *Phys. Rev. Lett.,* **1986,** *56*, 930.

183. Barret, C. J., www.barret-group.mcgill.ca.

184. G. K. Binnig, *Phys. Scr.,* **1987,** *T19*, 53.

185. D. McMullan, Scanning electron microscopy 1928–1965, *Scanning,* **1995,** *17*, 175.

186. Erni, R., Rossell, M. D., Kisielowski, C., Dahmen, U., Atomic-resolution imaging with a sub-50-pm electron probe., *Phys. Rev. Lett.,* **2009,** *102*.

187. Kelsall, R. W., Hamley, I. W., Geoghegan, M., *Nanotechnologie*. Wydawnictwo Naukowe PWN: Warszawa, **2008**.

188. B. D. Cullity, *Elements of X-ray Diffraction Addison Wesley Mass*. **1978**.

189. Chan, C. D. N., Diagram illustrating Bragg's Law angle of deviation 2 theta. Law.png, B., Ed. **2011**.

190. V. Tsionsky, L. Daikhin, M. Urbakh, E. Gileadi, *Looking at the metal/solution interface with the electrochemical quartz crystal microbalance: theory and experiment.* Marcel Dekker: New York, **2004**.

191. T. Madej, K. J. Addess, J. H. Fong, L. Y. Geer, R. C. Geer, C. J. Lanczycki, C. Liu, S. Lu, A. Marchler-Bauer, A. R. Panchenko, J. Chen, P. A. Thiessen, Y. Wang, D. Zhang, S. H. Bryant, MMDB: 3D structures and macromolecular interactions., *Nucleic Acids Res.,* **2012,** *40*, D461.

192. O. Trott, A. J. Olson, AutoDock Vina: Improving the speed and accuracy of docking with a new scoring function, efficient optimization and multithreading, *J. Comput. Chem.,* **2010**, 455.

193. M. T. Conato, A. J. Jacobson, Control of nucleation and crystal growth kinetics of MOF-5 on functionalized gold surfaces, *Microporous Mesoporous Mater.,* **2013,** *175*, 107.

194. W.-L. Liu, S.-H. Lo, B. Singco, C.-C. Yang, H.-Y. Huang, C.-H. Lin, Novel trypsin−FITC MOF bioreactor efficiently catalyzes protein digestion, *J. Mater. Chem. B,* **2013,** *1*, 928.

195. X. Wu, M. Hou, J. Ge, Metal−organic frameworks and inorganic nanoflowers: a type of emerging inorganic crystal nanocarrier for enzyme immobilization, *Catal. Sci. Technol.,* **2015,** *5*, 5077.

196. S. Y. Venyaminov, N. N. Kalnin, Quantitative IR Spectrophotometry of Peptide Compounds in Water (H2O) Solutions. II. Amide Absorption Bands of Polypeptides and Fibrous Proteins in *α*-, *β*-, and Random Coil Conformations. *Biopolymers* **1990,** *30*, 1259.

197. D. K. Yadav, V. Ganesan, P. K. Sonkar, R. Gupta, P. Rastogi, Electrochemical Investigation of Gold Nanoparticles Incorporated Zinc Based Metal-Organic Framework for Selective Recognition of Nitrite and Nitrobenzene, *Electrochim. Acta,* **2016,** *200*, 276.

198. J. Heinze, B. A. Frontana-Uribe, S. Ludwigs, Electrochemistry of conducting polymers-persistent models and new concepts., *Chem. Rev.,* **2010,** *110*, 4724.

199. Z. Iskierko, M. Sosnowska, P. S. Sharma, K. Noworyta, F. D'Souza, V. Bandi, T. Benincori, G. Appoloni, W. Kutner Warstwa rozpoznająca epitop glutenu i jej otrzymywanie metodą wdrukowywania molekularnego z zastosowaniem pochodnych tiofenu, oraz zastosowanie tej warstwy do selektywnego wykrywania i/lub oznaczania glutenu występującego w zbożowych produktach spożywczych. 24 May 2016, **2016**.

200. K. H. Long, A. Rubio-Tapia, A. E. Wagie, L. J. 3rd Melton, B. D. Lahr, C. T. Van Dyke, J. A. Murray, The economics of coeliac disease: a population-based study., *Aliment. Pharmacol. Ther.,* **2010,** *32*, 261.

201. G. Corrao, G. R. Corazza, V. Bagnardi, G. Brusco, C. Ciacci, M. Cottone, C. Sategna Guidetti, P. Usai, P. Cesari, M. A. Pelli, S. Loperfido, U. Volta, A. Calabró, M. Certo, Mortality in patients with coeliac disease and their relatives: a cohort study., *Lancet,* **2001,** *358*, 356.

202. M. J. Llorente-Alonso, M. J. Fernández-Aceñero, M. Sebastián, Gluten intolerance: Sex-and age-related features, *Can. J. Gastroenterol.,* **2006,** *20*, 719.

203. C. W. Wrigley, J. A. Bietz, *Proteins and aminoacids. Wheat – Chemistry and Technology,*. St. Paul American Association of Cereal Chemistry: **1988**; Vol. 1.

204. H. Wieser, Chemistry of gluten proteins., *Food Microbiology,* **2007,** *24*, 115.

205. C. H. Lu, Y. Zhang, S.-F. Tang, Z.-B. Fang, H.-H. Yang, X. Chen, G.-N. Chen, Sensing HIV related protein using epitope imprinted hydrophilic polymer coated quartz crystal microbalance, *Biosens. Bioelectron.,* **2012,** *31*, 439.

206. D. F. Tai, C. Y. Lin, T. Z. Wu, L. K. Chen, Recognition of dengue virus proteinusing epitope-mediated molecularly imprinted film., *Anal. Chem.,* **2005,** *77*, 5140.